1-1-2015

Recovery Techniques For Finite Element Methods And Their Applications

Hailong Guo
Wayne State University,

RECOVERY TECHNIQUES FOR FINITE ELEMENT METHODS AND THEIR APPLICATIONS

by

HAILONG GUO

DISSERTATION

Submitted to the Graduate School

of Wayne State University,

Detroit, Michigan

in partial fulfillment of the requirements

for the degree of

DOCTOR OF PHILOSOPHY

2015

MAJOR: MATHEMATICS

Approved by:

____

Advisor Date

____

____

____

____

DEDICATION

To My Parents

ACKNOWLEDGEMENTS

I must first express my deepest gratitude to my advisor Prof. Zhimin Zhang for his inspiring guidance, constant support, great patient, and endless caring. This work could not have been possible without his supervision and encouragement.

I would like to thank Prof. Fatih Celiker, Prof. Weisong Shi, Prof. Peiyong Wang, and Prof. Sheng Zhang for serving my dissertation committee.

I also want to thank my colleagues and friends Dr. Amhed Naga, Dr. Runchang Lin, Dr. Can Huang, Dr. Li Fan, and Ren Zhao for their kindly help and invaluable suggestions.

In addition, I am in debt to Prof. Ziqing Xie for her long time support and help since I was a undergraduate student.

Special thanks go to my family for their unconditional and unlimited love and support since I was born.

Finally, I wish to thank all people in the mathematics department for their co-operation and generous assistance. I enjoyed the warm and friendly atmosphere in the department and I appreciate the support I received during my stay at Wayne State University.

TABLE OF CONTENTS

CHAPTER 1 Introduction

Post-processing is an important technique in scientific computing, where it is necessary to draw some useful information that have physical meanings such as velocity, flux, stress, etc., from the primary results of the computing. These quantities of interest usually involve derivatives of the primary data. This type of post-processing methods are called recovery techniques. Typical recovery techniques include gradient recovery and Hessian recovery.

As for gradient recovery, it is extensive studied in the literature. Most of them are based on averaging methods [19, 63], local or global projections [12, 52, 90], or local least square fittings [58, 79, 107, 110, 111, 112]. However, all the methods above are only limited to C^0 finite element methods. According to [4], a good recovery operator should satisfy consistency condition, localization condition, and boundedness and linearity condition. For conforming elements, it is well known that polynomial preserving recovery (PPR) [107] satisfies all the above conditions. Unfortunately, there is no such type gradient recovery for the Crouzeix-Raviart element in the literature. To bridge the gap, we propose and analyze a gradient recovery method for the Crouzeix-Raviart element in this work.

Hessian matrix is particularly significant in adaptive mesh design, since it can indicate the direction where the function changes the most and guide us to construct anisotropic meshes to cope with the anisotropic properties of the solution of the underlying partial differential equation [59]. It also plays an important role in finite element approximation of second order non-variational elliptic problems [65], numerical solution of some fully nonlinear equations such as Monge-Ampère equation [66, 83], and designing nonlocal finite element technique [45]. There have been some works in literature on this subject. In 1998, Lakhany-Whiteman used a simple averaging method twice at edge centers of the regular uniform triangular mesh to produce a superconvergent Hessian [64]. Later, some other reseachers such as Agouzal et al.[2], Bank et al.[13] and Ovall [88] also studied Hessian recovery. Comparsion studies of existing Hessian recovery techniques can be found in Vallet et al. [94] and Picasso et al. [89]. However, there is no systematic theory guaranteeing convergence under general circumstances. Moreover, there are certain technical difficulties in obtaining rigorous convergence proof for meshes other than the regular pattern triangular mesh. In a very recent work, Kamenski-Huang argued that it is not necessary to have very accurate or even convergent Hessian in order to obtain a good mesh [61]. Our goal is not targeted on the direction of adaptive mesh refinement; instead, we emphasize on obtaining accurate Hessian matrices via recovery techniques. We propose an effective Hessian recovery method and establish a solid theoretical analysis for such method.

The applications of recovery techniques include adaptive finite element methods and eigenvalue problems. In this work, we discuss the application of the proposed gradient recovery for the Crouzeix-Raviart element into adaptive nonconforming finite element method. Also, we apply the polynomial preserving recovery into efficient eigenvalue computation to propose several superconvergent two-grid schemes and multilevel adaptive methods for elliptic eigenvalue problems.

The rest of this dissertation is organized as follows:

Chapter 2 begins with introducing some basic notation of Soboleve spaces and model problems. Then we review some preliminary knowledges of finite element methods and their approximations of the model problems.

Chapter 3 focuses on recovery of the first order derivative for the Crouzeix-Raviart element. In this chapter, we propose and analyze a gradient recovery method for the Crouzeix-Raviart element. The proposed method is proved to preserving quadratic polynomials and to be a bounded linear operator. Its application in adaptive nonconforming finite element is also discussed. This chapter is based on our published paper [49].

Chapter 4 is devoted to recovery of the second order derivative of Lagrange element of arbitrary order. A new Hessian recovery strategy is proposed and its mathematical theory is established. This chapter is based on our submitted paper [50].

Chapter 5 concentrates on application of recovery technique. In partial, we employ polynomial preserving recovery to design some fast and efficient algorithms for eigenvalue problems. Our new algorithms compare favorably with some existing algorithms and enjoy superconvergence property. This chapter is based on our submitted paper [51].

CHAPTER 2 Preliminaries

2.1 Sobolev spaces

In this work, we assume $\Omega \subset \mathbb{R}^2$ is a bounded polygonal domain with Lipschitz continuous boundary $\partial\Omega$. Let $\int_\Omega f(z)dz$ denote the Lebesgue integral [1, 25, 35] for some Lebegue measure function f on the domain Ω. For $1 \le p \le \infty$, let

$$\|f\|_{p,\Omega} = \left(\int_\Omega |f(z)|^p dz\right)^{1/p},$$

and for the case $p = \infty$,

$$\|f\|_{0,\infty,\Omega} = \operatorname{ess\,sup}\{|f(z)| : z \in \Omega\}.$$

Define the Lebesgue spaces

$$L^p(\Omega) = \{f : \|f\|_{p,\Omega} < \infty\}.$$

A multi-index is a 2-tuple of non-negative integers α_i, $i = 1, 2$. The length of α of is given by

$$|\alpha| = \sum_{i=1}^{2} \alpha_i.$$

The weak partial derivative $D^\alpha v$, see [1, 25, 35], is then defined as

$$D^\alpha v = \left(\frac{\partial}{\partial x}\right)^{\alpha_1} \left(\frac{\partial}{\partial y}\right)^{\alpha_2}.$$

Also, $D^k u$ with $|\alpha| = k$ is the vector of all partial derivatives of order k. Let $W^{k,p}(\Omega) = \{v :$

$D^\alpha v \in L^p(\Omega), |\alpha| \leq k\}$ be the classical Sobolev spaces with norms

$$\|v\|_{k,p,\Omega} = \left(\sum_{|\alpha|\leq k} \int_\Omega |D^\alpha v(z)|^p dz \right)^{\frac{1}{p}}, \quad 1 \leq p < \infty,$$

$$\|v\|_{k,\infty,\Omega} = \operatorname*{ess\,sup}_{|\alpha|\leq k, z\in\Omega} |D^\alpha v(z)|, \quad p = \infty;$$

and seminorms

$$|v|_{k,p,\Omega} = \left(\sum_{|\alpha|=k} \int_\Omega |D^\alpha v(z)|^p dz \right)^{\frac{1}{p}}, \quad 1 \leq p < \infty,$$

$$|v|_{k,\infty,\Omega} = \operatorname*{ess\,sup}_{|\alpha|=k, z\in\Omega} |D^\alpha v(z)|, \quad p = \infty.$$

When $p = 2$, let $H^k(\Omega) = W^{k,2}(\Omega)$ and the index p is omitted in their corresponding norms and seminorms.

For any positive integer n, we say a vector function $\vec{v} = (v_1, v_2, \cdots, v_n)^T \in W^{k,p}(\Omega)^n$ provided that $v_i \in W^{k,p}(\Omega)$ for $i = 1, 2, \cdots, n$. Its norm is defined as

$$\|\vec{v}\|_{k,p,\Omega} = \left(\sum_{i=1}^n \|v_i\|_{k,p,\Omega}^p \right)^{\frac{1}{p}}, \quad 1 \leq p < \infty,$$

$$\|\vec{v}\|_{k,\infty,\Omega} = \operatorname*{ess\,sup}_{|\alpha|\leq k, z\in\Omega, 1\leq i\leq n} |D^\alpha v_i(z)|, \quad p = \infty;$$

and similarly the seminorm of $\vec{v}$ is defined as

$$|\vec{v}|_{k,p,\Omega} = \left(\sum_{i=1}^n |v_i|_{k,p,\Omega}^p \right)^{\frac{1}{p}}, \quad 1 \leq p < \infty,$$

$$|\vec{v}|_{k,\infty,\Omega} = \operatorname*{ess\,sup}_{|\alpha|=k, z\in\Omega, 1\leq i\leq n} |D^\alpha v_i(z)|, \quad p = \infty.$$

The subscript p is omitted in case of $p = 2$.

For a subdomain $\mathcal{A}$ of Ω, let $\mathbb{P}_m(\mathcal{A})$ be the space of polynomials of degree less than or equal to m over $\mathcal{A}$ and n_m be the dimension of $\mathbb{P}_m(\mathcal{A})$ with $n_m = \frac{1}{2}(m+1)(m+2)$. Similarly, we use $W^{k,p}(\mathcal{A})$ to denote the restriction of classical Sobolev space on $\mathcal{A}$ with norm $\|\cdot\|_{k,p,\mathcal{A}}$ and seminorm $|\cdot|_{k,p,\mathcal{A}}$. When $p = 2$, we simply denote $H^k(\mathcal{A}) = W^{k,2}(\mathcal{A})$ and the subscript p is omitted.

Throughout this article, the letter C or c, with or without subscript, denotes a generic constant which is independent of h and may not be the same at each occurrence. To simplify notation, we denote $x \leq Cy$ by $x \lesssim y$.

2.2 Model problems and their variation problems

In the work, we consider both second order elliptic equation and Stokes equation.

2.2.1 Elliptic equation

Our first model problem will be the following homogeneous elliptic equation

$$\begin{cases} -\nabla(\mathcal{D}\nabla u) + cu = f, & \text{in } \Omega, \\ u = 0, & \text{on } \partial\Omega; \end{cases} \tag{2.1}$$

where D is a 2×2 symmetric positive definite matrix and c as well as f are scalars.

The variational form is to find $u \in H_0^1(\Omega)$ such that

$$\mathcal{B}(u, v) = L(v), \quad \forall v \in H_0^1(\Omega). \tag{2.2}$$

where

$$\mathcal{B}(u,v) = \int_\Omega [(\mathcal{D}\nabla u)\nabla v + cuv]dz,$$
$$L(v) = \int_\Omega fvdz.$$

We assume that $\mathcal{D}$ and f in $L^\infty(\Omega)$. In addition, assume there exist two constant $\overline{c}$ and $\underline{c}$ such that $0 < \underline{c} \leq c(z) \leq \overline{c} < \infty$. Then it is to check that the bilinear form $\mathcal{B}$ and linear functional L satisfies the following three conditions:

1. $\mathcal{B}$ is continuous, i.e.

$$\mathcal{B}(u,v) \lesssim ||u||_{1,\Omega}||v||_{1,\Omega}, \quad \forall u,v \in H_0^1(\Omega);$$

2. $\mathcal{B}$ is coercive, i.e.

$$||u||_{1,\Omega}^2 \lesssim \mathcal{B}(u,u), \quad \forall u \in H_0^1(\Omega);$$

3. L is continuous, i.e.

$$|L(v)| \lesssim ||v||_{1,\Omega}, \quad \forall v \in H_0^1(\Omega).$$

According to Lax-Milgram Lemma [25, 35], variational problem (2.2) has an unique solution. Furthermore, the above conditions 1 and 2 implies $\mathcal{B}$ is an inner production on $H_0^1(\Omega)$. Define the energy norm as $|||\cdot|||_\Omega = \sqrt{\mathcal{B}(\cdot,\cdot)}$. Then $|||\cdot|||_\Omega$ and $||\cdot||_{1,\Omega}$ are two equivalent norms in $H_0^1(\Omega)$.

2.2.2 Stokes equation

Our second model problem is the following Stokes equation

$$\begin{cases} -\Delta\vec{u} + \nabla p = \vec{f}, & \text{in } \Omega, \\ \text{div}\vec{u} = 0, & \text{in } \Omega, \\ \vec{u} = 0, & \text{on } \partial\Omega; \end{cases} \tag{2.3}$$

which describes the motion of an incompressible viscous fluid in Ω [17, 41]. Here $\vec{u} : \Omega \to \mathbb{R}^2$ is the velocity field and $p : \Omega \to \mathbb{R}$ is the pressure.

Let $V = H_0^1(\Omega)^2$ and $M = L_0^2(\Omega) = \{q \in L^2(\Omega) : \int_\Omega q dx = 0\}$. Then the variational formulation of (2.3) reads as: Find $(\vec{u}, p) \in V \times M$ such that

$$\begin{cases} a(\vec{u}, \vec{v}) + \quad b(\vec{v}, p) = (\vec{f}, \vec{v}), & \forall \vec{v} \in V, \\ \qquad\qquad b(\vec{u}, q) = 0, & \forall q \in M; \end{cases} \tag{2.4}$$

where

$$a(\vec{v}, \vec{w}) = \int_\Omega \nabla\vec{v} : \nabla\vec{w} dz, \quad \forall \vec{v} \in V,$$
$$b(\vec{v}, q) = \int_\Omega \text{div}\vec{v}\, q dz \quad \forall q \in M;$$

with $\nabla\vec{v} : \nabla\vec{w} = \sum_{i=1}^2 \frac{\partial v_i}{\partial x_j} \frac{\partial w_i}{\partial x_j}$.

Suppose $\vec{f} \in L^2(\Omega)^2$, then it easy to see that $|(\vec{f}, \vec{v})| \leq \|\vec{f}\|_{0,\Omega} \|\vec{v}\|_{1,\Omega}$ for any $\vec{v} \in V$. In addition, one can prove the following coercive condition

$$\|v\|_{1,\Omega} \lesssim a(\vec{v}, \vec{v}) \quad \forall \vec{v} \in V, \tag{2.5}$$

and Babuska-Brezzi condition (or inf-sup condition) [18, 26, 36]

$$\inf_{q \in M} \sup_{\vec{v} \in V} \frac{(\text{div}\vec{v}, q)}{||\vec{v}||_{1,\Omega}||q||_{0,\Omega}} \geq C. \tag{2.6}$$

Thus, the variational problem (2.4) exists an unique solution $(\vec{u}, p)$.

2.3 Finite element spaces

The finite element methods solve variational problems associated with boundary value problem on some finite dimensional spaces, which are called the finite element spaces. To construct a finite element space, first, a triangulation $\mathcal{T}_h$ is established on $\bar{\Omega}$; second, we define a finite element on element T for each $T \in \mathcal{T}_h$. According to [35], a finite element in $\mathbb{R}^2$ is a triple (T, P, Σ) where

1. T is a close subset of $\mathbb{R}^2$ with non empty interior and Lipschitz-continuous boundary;

2. P is a space of real-valued functions defined over the set T;

3. Σ is a finite set of linearly independent linear forms which is P-unisolvent defined over the space P. Those linear forms are called degrees of freedom.

There are many different finite elements. In this work, we concentrate on C^0 Lagrange elements and the Crouzeix-Raviart element.

2.3.1 Finite Element meshes

A finite element mesh (or triangulation) $\mathcal{T}_h$ is a partition of Ω into finitely many subdomains, called elements. Elements can be triangles or quadrilaterals. In this work, we restrict our discussion on conforming meshes consisting of simplexs, i.e. triangles. Here, a conforming mesh means that the intersection of any two elements is empty, a common vertex, or a common edge.

For any $T \in \mathcal{T}_h$, let h_T denote the diameter of T and ρ_T denote the supremum of the diameter of the spheres inscribed in T. The mesh size of $\mathcal{T}_h$ is denoted by $h = \max\{h_T : T \in \mathcal{T}_h\}$. We say $\mathcal{T}_h$ is regular if there exists a constant σ such that

$$\frac{h_T}{\rho_T} \leq \sigma, \quad \forall T \in \mathcal{T}_h.$$

In the sequel, we always assume mesh $\mathcal{T}_h$ is regular.

A mesh $\mathcal{T}_h$ is called quasi-uniform mesh if there exists a constant $\nu \geq 0$ such that

$$\frac{h}{h_T} \leq \nu, \quad \forall T \in \mathcal{T}_h.$$

A very important type of quasi-uniform mesh is uniform mesh. Uniform mesh plays an important role in superconvergence analysis [32, 71, 109]. Meshes can also be categorized as structured or unstructured. Structured meshes have a uniform topological structure that unstructured meshes lack. In this work, we shall consider both structured meshes and unstructured meshes.

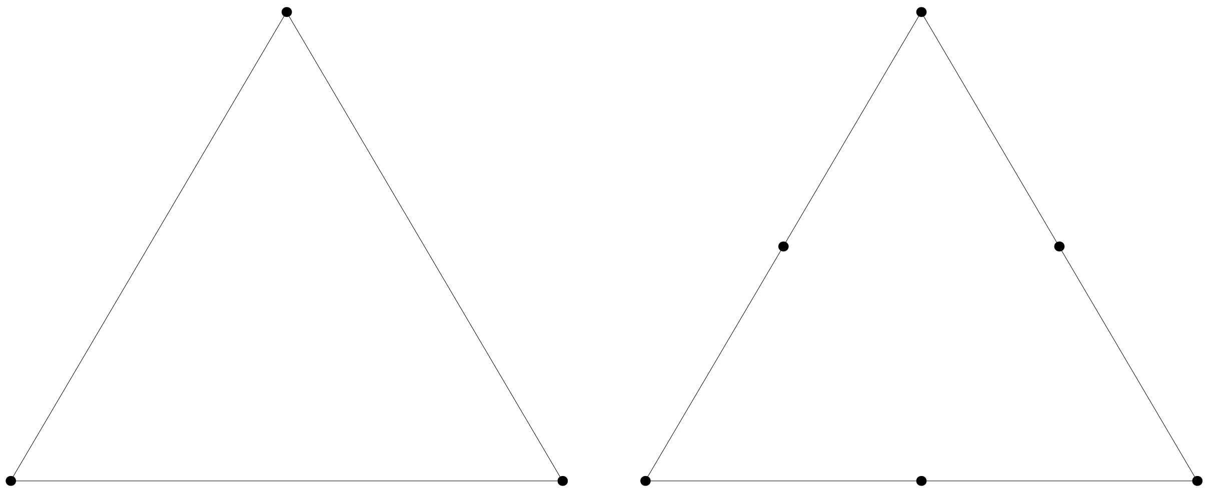

(a) Linear element (b) Quadratic element

Figure 1: C_0 Lagrange element

2.3.2 C^0 Lagrange Elements

For any $T \in \mathfrak{T}$, let $a_j, 1 \leq j \leq 3$, be the vertices of T. For any $r > 0$, let

$$\Sigma_r(T) = \left\{ x = \sum_{j=1}^{3} \lambda_j a_j ; \sum_{j=1}^{3} \lambda_j = 1, \lambda_j \in \{0, \frac{1}{r}, \dots, , \frac{r-1}{r}, 1\}, 1 \leq j \leq 3 \right\}.$$

Then the C^0 Lagrange element of degree r is defined as $(T, \mathbb{P}_r(T), \Sigma_r(T))$. Typical examples of C^0 Lagrange elements include linear element and quadratic element, see Fig 1. For linear element, degrees of freedom only contains vertices. However, for quadratic element, degrees of freedom includes both vertices and edge centers.

The C^0 finite element space of order r associated with mesh $\mathfrak{T}_h$ is defined as

$$S^{h,r} = \{v \in C(\bar{\Omega}) : v|_T \in \mathbb{P}_r(T), \forall T \in \mathfrak{T}_h\}.$$

Note that the choice of $\Sigma_r(T)$ guarantees the continuity of v across the boundaries of elements in $\mathcal{T}_h$. Let $\mathcal{N}_h$ denote the the set of all mesh nodes. Then for any function $v \in S^{h,r}$, it can be written as

$$v = \sum_{z \in \mathcal{N}_h} v(z)\phi_z$$

where ϕ_z is called the nodes shape function associated with z is defined by

$$\phi_z(z') = \begin{cases} 1 & \text{if} z' = z; \\ 0 & \text{if} z' \in \mathcal{N}_h \setminus \{z\}. \end{cases}$$

It is easy to see that the set $\{\phi_z : z \in \mathcal{N}_h\}$ forms a basis of $S^{h,r}$, which is called nodal basis. Let $I_h : C(\bar{\Omega}) \to S^{h,r}$ denote the standard Lagrange interpolation operator, i.e.

$$I_h u = \sum_{z \in \mathcal{N}_h} u(z)\phi_z, \tag{2.7}$$

for any $u \in C(\bar{\Omega})$.

For piecewise defined function, [25, 33, 35] prove the following smooth result:

Theorem 2.1. *Let $\mathcal{T}_h$ be a mesh of Ω. Let $k \geq 1$. Then a piecewise infinitely differentiable function $v : \bar{\Omega} \to \mathbb{R}$ over the mesh $\mathcal{T}_h$ belongs to $H^k(\Omega)$ if and only if $v \in C^{k-1}(\Omega)$.*

Theorem 2.1 implies $S^{h,r} \subset H^1$. In addition, let $S_0^{h,r} = S^{h,r} \cap H_0^1(\Omega)$. It means that the finite element space $S_0^{h,r}$ is a subspace of H_0^1 where the model problem (2.1) is posed. For this reason, the C^0 Lagrange elements are often referred to as conforming elements.

2.3.3 The Crouzeix-Raviart element

For the conforming finite elements, it is assumed that the finite element spaces lie in the function space in which the variational problem is posed. However, there are too many limitation of conforming finite elements. For example, for fourth order elliptic differential equations, conforming finite element require C^1 elements, and this leads to extremely large systems of equations. Thus, people try to relax the condition by not requiring finite element spaces to be subspaces of corresponding function spaces. Those types of finite elements are called nonconfomring elements.

In this work, we consider the simplest nonconforming element, i.e. the Crouzeix-Ravirat element. It is also referred as the nonconforming P_1 element. Differentiating from the conforming linear element, the degrees of freedom are on edge centers; see Fig 2.

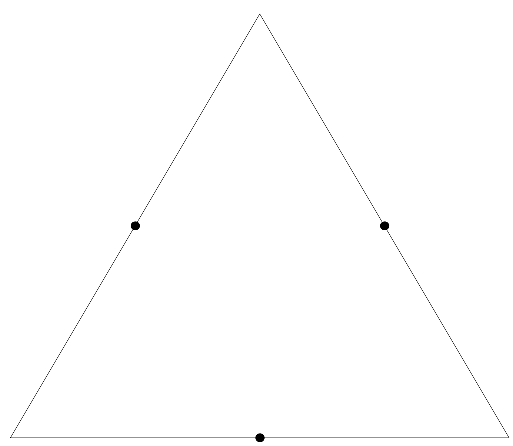

Figure 2: The Crouzeix Raviart element

Let $\mathcal{T}_h$ be a shape regular triangulation of Ω. Denote the set of all edges and edge centers by $\mathcal{E}_h$ and $\mathcal{M}_h$, respectively. For any edge $e \in \mathcal{E}$, let $\mathcal{M}(e)$ be the middle point of edge e.

Define the Crouzeix-Raviart finite element space as follows:

$$X^{\mathrm{nc}} := \{v \in L_2(\Omega) : v|_T \in \mathbb{P}_1(T) \text{ and } v \text{ is continous at } \mathcal{M}_h\}\,,$$

$$X_0^{\mathrm{nc}} := \{v \in X^{\mathrm{nc}} : v(\mathcal{M}(e)) = 0 \text{ for all } e \in \mathcal{E}_h \cap \partial\Omega\}\,.$$

2.4 Finite element approximation of model problems

In the subsection, we firstly introduce the finite element approximation for second order elliptic problem (2.2) using both C^0 Lagrange elements and the Crouzeix-Raviart element. Then we discretize the Stokes equation with stable nonconforming finite element.

2.4.1 Conforming finite element approximation of elliptic equation

The conforming finite element approximation of the model problem (2.2) is to find $u_h \in S_0^{h,r}$ such that

$$\mathcal{B}(u_h, v_h) = L(v_h), \quad \forall v_h \in S_0^{h,r}. \tag{2.8}$$

Note that $S_0^{h,r}$ is a subspace of $H_0^1(\Omega)$. Then equations (2.2) and (2.8) implies the following Theorem:

Theorem 2.2. **(Céa's Lemma)** *There exist a constant $C > 0$, independent of the $S_0^{h,r}$, such that*

$$||u - u_h||_{1,\Omega} \le C \inf_{v \in S_0^{h,r}} \|u - v\|_{1,\Omega}.$$

Taking v as the Lagrange interpolation of u, see (2.7), we can get the following H^1 error estimate:

Theorem 2.3. *If the solution u of* (2.2) *is in the space $H^{r+1}(\Omega) \cap H_0^1(\Omega)$ and $u_h \in S_0^{h,r}$ is* *the solution of* (2.8)*, then*

$$\|u - u_h\|_{1,\Omega} \lesssim h^r |u|_{r+1,\Omega}.$$

Using the duality argument (or Nitsche' Trick) [17, 25, 35], we can prove the following L^2 error estimate:

Theorem 2.4. *Under the same hypothesis of Theorem 2.3, we have the following error estimate:*

$$\|u - u_h\|_{0,\Omega} \lesssim h^{r+1} |u|_{r+1,\Omega}.$$

Remark. Theorems 2.3 and 2.4 imply that the optimal convergence rate of L^2 Error is two, the optimal convergence rate of H^1 is one and hence the optimal convergence rate of piecewise H^2 error is zero when we using linear element. It means an approximation of second order derivatives using piecewise linear element should not converge. In chapter 4, we will propose an effective post-processing method which can produce superconvergent or even ultraconvergent Hessian matrix.

2.4.2 Nonconforming finite element approximation of elliptic equation

The nonconforming finite element approximation of (2.2) consists of finding $u_h \in X_0^{\mathrm{nc}}$ such that

$$\mathcal{B}_h(u_h, v_h) = (f, v_h) \quad \forall v_h \in X_0^{\mathrm{nc}}, \tag{2.9}$$

where

$$\mathcal{B}_h(w, v) := \sum_{T \in \mathcal{T}_h} \int_T (\mathcal{D}\nabla w \cdot \nabla v + cuv) dx,$$

for all $w, v \in X^{\mathrm{nc}}$. For a subdomain $\mathcal{A}$ of Ω, define the broken semi-norm on $\mathcal{A}$ as $||v||^2_{1,h,\mathcal{A}} := \sum_{T\in\mathcal{T}_h\cap\mathcal{A}} |v|^2_{1,T}$. Using the second Strang Lemma [17, 25, 35], we can prove the following error estimate

Theorem 2.5. *If the solution u of* (2.2) *is in the space $H^2(\Omega)\cap H^1_0(\Omega)$ and $u_h \in X_0^{nc}$ is the solution of* (2.9), *then*

$$\|u - u_h\|_{1,h,\Omega} \lesssim h|u|_{2,\Omega}.$$

Remark. Theorem 2.5 implies that the optimal convergence rate in discrete H^1 norm is 1. In the chapter 3, we will propose a gradient recovery operator for the Crouzeix-Raviart element which is numerically verified to be superconvegent to the exact gradient.

2.4.3 Nonconforming finite element approximation of Stokes Equation

In this subsection, we restrict our discussion on nonconforming finite element approximation of Stokes equation. Define $\widetilde{M}^h = \{q \in L^2(\Omega) : q|_T \in \mathbb{P}_0, T \in \mathcal{T}\}$ and $M^h = \widetilde{M}_h \cap L^2_0(\Omega)$. Let $V^h = X^{\mathrm{nc}} \times X^{\mathrm{nc}}$ and $V_0^h = X_0^{\mathrm{nc}} \times X_0^{\mathrm{nc}}$. The nonconforming finite element approximation reads as finding $(\vec{u}_h, p_h) \in V_0^h \times M^h$ such that

$$\begin{cases} a_h(\vec{u}_h, \vec{v}_h) + & b_h(\vec{v}_h, p_h) = (\vec{f}, \vec{v}_h), \quad \forall \vec{v}_h \in V_0^h, \\ & b_h(\vec{u}_h, q_h) = 0, \qquad \forall q_\in M^h; \end{cases} \tag{2.10}$$

where

$$a_h(\vec{v}_h, \vec{w}_h) = \int_\Omega \nabla_h \vec{v}_h : \nabla_h \vec{w}_h dx = \sum_{T\in\mathcal{T}_h} \int_T \nabla \vec{v}_h : \nabla \vec{w}_h dx,$$

$$b(\vec{v}_h, q_h) = \int_\Omega \nabla_h \cdot \vec{v}_h \, q_h dx = \sum_{T\in\mathcal{T}_h} \int_T \nabla \cdot \vec{v}_h \, q_h dx;$$

for any $\vec{v}_h, \vec{w}_h \in V^h$ and $q_h \in M^h$. Here ∇_h is called broken gradient operator. [16] prove the following discrete inf-sup condition

$$\inf_{q_h \in M^h} \sup_{\vec{v}_h \in V_0^h} \frac{b_h(\vec{v}_h, q_h)}{\|\vec{v}_h\|_{1,h,\Omega} \|q_h\|_{0,\Omega}} \geq \beta \geq 0, \tag{2.11}$$

where the constant β is independent of h and $\|\vec{v}_h\|^2_{1,h,\mathcal{A}} = \|v_1\|^2_{1,h,\mathcal{A}} + \|v_2\|^2_{1,h,\mathcal{A}}$ for any $\mathcal{A} \subset \Omega$. Therefore the discrete variational problem (2.10) is well posed and the following discrete H^1 error estimate holds:

Theorem 2.6. *Let the solution* $(\vec{u}, p)$ *of the Stokes problem* (2.4) *satisfy*

$$\vec{u} \in \left(H^2(\Omega) \cap H_0^1(\Omega)\right)^2, \quad p \in H^1(\Omega) \cap L_0^2(\Omega).$$

Then

$$\|\vec{u} - \vec{u}_h\|_{1,h,\Omega} + \|p - p_h\|_{0,\Omega} \leq h(|u|_{2,\Omega} + |p|_{1,\Omega}).$$

Remark. Theorem 2.6 implies that H^1 error of velocity filed is of order $O(h)$. Our numerical experiments in Chapter 3 indicates that the gradient recovery method proposed in Chapter 3 can also applies to each component of velocity to get superconvergent gradient.

CHAPTER 3 Gradient recovery for the Crouzeix-Raviart element

The Crouzeix-Raviart element was first proposed in [37] to solve stationary Stokes problem. It has many useful properties [21], such as commutative relations with respect to the gradient, divergence, and curl operators, and the existence of an interpolation operator that can be defined on $H^s(\Omega)$ for $s \geq \frac{1}{2}$. The applications of the Crouzeix-Raviart element can be found in solids [24, 43], fluids[37] and electromagnets [22, 23], which can be called as a universal element [21].

In this chapter, we concentrate on post-processing of the Crouzeix-Raviart element and its application. Specifically speaking, we propose a good gradient recovery method for the Crouzeix-Raviart element, which is based on the standard of [4], and apply it to a posteriori error estimates for adaptive nonconforming finite element method.

We provide the main definition of the gradient recovery operator in Section 3.1. Some illustrations of the proposed gradient recovery operator are given in Section 3.2. The properties are investigated in Section 3.3. Two numerical examples are presented to illustrate superconvergence of the proposed gradient recovery method in Section 3.4 and its application to adaptive finite element method will be discussed in Section 3.5. Finally, some conclusions will be drawn in Section 3.6.

3.1 Definition of Gradient Recovery Operator

Gradient recovery is a method providing a better approximation of ∇u. We introduce a new gradient recovery operator $G_h : X^{\mathrm{nc}} \to X^{\mathrm{nc}} \times X^{\mathrm{nc}}$. The structure of $G_h u_h$ relies on the fact that every function in X^{nc} is uniquely defined by its values at edge centers. Given a finite element solution $u_h \in X^{\text{nc}}$, we only need to define $G_h u_h$ at edge centers. After determining values of $G_h u_h$ at all edge centers, we obtain $G_h u_h \in X^{\text{nc}} \times X^{\text{nc}}$ on the whole domain by interpolation, i.e.

$$G_h u_h := \sum_{z \in \mathcal{M}} (G_h u_h)(z) \phi_z,$$

where $\{\phi_z : z \in \mathcal{M}_h\}$ is nodal basis of X^{nc}.

For any edge center $z = (x, y)$ and $1 \leq n \in \mathbb{N}$, define the union of elements around z in the first n layers as follows

$$\mathcal{L}(z, n) := \cup\{T : T \in \mathcal{T}_h, T \cap \mathcal{L}(z, n-1) = e \text{ for some } e \in \mathcal{E}_h\},$$

with $\mathcal{L}(z, 0) := \{e \in \mathcal{E}_h : z \text{ is the middle point of } e\}$.

Let z be the middle point of some interior edge e, i.e. $z = \mathcal{M}(e)$. Intuitively, it is natural to use information on triangle T_1 and T_2 to recover gradient at z where $T_1 \cap T_2 = e$, i.e. $T_1, T_2 \in \mathcal{L}(z, 1)$. Let $|T_i|$ be the area of T_i $(i = 1, 2)$ and $|\omega|$ be the sum of $|T_1|$ and $|T_2|$. There are several possible ways to define $(G_h u_h)(z)$.

1. Simple averaging:

$$(G_h u_h)(z) = \frac{1}{2}(\nabla u_h|_{T_1} + \nabla u_h|_{T_2}).$$

2. Weighted averaging:

$$(G_h u_h)(z) = (\frac{|T_1|}{|\omega|}\nabla u_h|_{T_1} + \frac{|T_2|}{|\omega|}\nabla u_h|_{T_2}).$$

3. Fitting a linear polynomial:

$$(G_h u_h)(z) = \nabla p_z(z)$$

where

$$p_z = \arg \min_{p \in \mathbb{P}_1(L(z,1))} \sum_{\widetilde{z} \in \mathcal{M} \cap L(z,1)} |(u_h - p)(\widetilde{z})|^2;$$

and $\mathcal{M}_h$ is the set of edge centers.

Remark. Method 3 can be viewed as nonconforming counterpart of SCR proposed in [58]. On regular pattern uniform mesh, the above three methods give the same result.

Remark. Hu and Ma prove $O(h^{1.5})$ superconvergence for the simple averaging method on uniform mesh of regular pattern in [54] by using the equivalence between the Crouzeix-Ravart element and Raviart-Thomas element [76] and the superconvergence result of Raviart-Thomas element [20].

However, just as we know for C^0 Lagrange elements, the approximation property of the above three methods depends heavily on symmetry of local element patch $L(z,1)$ with respect to z. Simple calculation combined with Taylor expansion reveals that they exhibit superconvergence only on regular pattern uniform meshes.

Inspired by the idea of Polynomial Preserving Recovery (PPR) [79, 80, 107], the new gradient recovery method fits a quadratic polynomial at every edge center. Let $z_i = (x_i, y_i) \in \mathcal{M}_h$ be an edge center and $\mathcal{K}_{z_i}$ denote a patch of elements around z_i. Let $p_{z_i} \in \mathbb{P}_2(\mathcal{K}_{z_i})$ be the quadratic polynomial that best fits u_h at the edge centers in $\mathcal{K}_{z_i}$ in discrete least-squares sense, i.e.,

$$p_{z_i} = \arg \min_{p \in \mathbb{P}_2(K_{z_i})} \sum_{\widetilde{z} \in \mathcal{M}_h \cap K_{z_i}} |(u_h - p)(\widetilde{z})|^2,$$

and define the recovered gradient at z_i as

$$(G_h u_h)(z_i) = \nabla p_{z_i}(x_i, y_i).$$

Let $z_{i_0}, z_{i_1}, \ldots, z_{i_m}$ denote all the edge centers in $\mathcal{K}_{z_i}$. Without loss of generality, let $z_i = z_{i_0}$ and $h_i = \max\{|z_{i_j} - z_i| : 1 \leq j \leq m\}$. To avoid the computational instability resulting from small h_i, we introduce coordinate transformation

$$F : (x, y) \to (\xi, \eta) = \frac{(x, y) - (x_i, y_i)}{h_i},$$

All computations are carried out on the local element patch $\widehat{K}_{z_i} = F(K_{z_i})$. Then we can rewrite the fitting polynomial as

$$p_{z_i}(x, y) = P^T a = \widehat{P}^T \widehat{a}.$$

with

$$P^T = (1, x, y, x^2, xy, y^2), \quad \widehat{P}^T = (1, \xi, \eta, \xi^2, \xi\eta, \eta^2);$$

$$a^T = (a_0, a_1, a_2, a_3, a_4, a_5), \quad \widehat{a}^T = (a_0, h_i a_1, h_i a_2, h_i^2 a_3, h_i^2 a_4, h_i^2 a_5).$$

The coefficient vector $\widehat{a}$ can be obtained by solving

$$A^T A \widehat{a} = A^T b.$$

with $b^T = (u_h(z_{i_0}), u_h(z_{i_1}), \ldots, u_h(z_{i_m}))$ and

$$A = \begin{pmatrix} 1 & \xi_0 & \eta_0 & \xi_0^2 & \xi_0\eta_0 & \eta_0^2 \\ 1 & \xi_1 & \eta_1 & \xi_1^2 & \xi_1\eta_1 & \eta_1^2 \\ 1 & \xi_2 & \eta_2 & \xi_2^2 & \xi_2\eta_2 & \eta_2^2 \\ \vdots & \vdots & \vdots & \vdots & \vdots & \vdots \\ 1 & \xi_m & \eta_m & \xi_m^2 & \xi_m\eta_m & \eta_m^2 \end{pmatrix}.$$

Then the recovered gradient at z_i is defined as

$$(G_h u_h)(z_i) = \nabla p_{z_i}(0,0) = \begin{pmatrix} a_1 \\ a_2 \end{pmatrix} = \frac{1}{h_i} \begin{pmatrix} \widehat{a}_1 \\ \widehat{a}_2 \end{pmatrix} \tag{3.1}$$

Since p_{z_i} has 6 unknowns, it requires that $\mathcal{K}_{z_i}$ contains at least 6 edge centers. This naturally leads to $\mathcal{K}_{z_i} = \mathcal{L}(z_i, 2)$. Also, notice that $\mathcal{K}_{z_i}$ containing more than 6 middle points can not guarantee the uniqueness of p_{z_i}. If p_{z_i} is not unique and $\mathcal{L}(z_i, n) = \mathcal{K}_{z_i} \subsetneq \mathcal{L}(z_i, n+1)$, then set $\mathcal{K}$ equal $\mathcal{L}(z_i, n+1)$ and recompute p_{z_i}. The patch $\mathcal{K}_{z_i}$ is defined to be the first $\mathcal{L}(z_i, n)$ such that p_{z_i} is unique.

Remark. In superconvergent patch recovery (SPR) [111, 112] and PPR, if z_i lies on an edge between two vertices z_{i_1} and z_{i_2}, then recovered gradient is defined at z_i as $(G_h u_h)(z_i) = \beta \nabla p_{z_{i_1}}(z_i) + (1-\beta)\nabla p_{z_{i_2}}(z_i)$ where β is determined by the ratio of distances of z_i to z_{i_1} and z_{i_2}.

Remark. For the most usual cases, $\mathcal{K}_{z_i} = \mathcal{L}_{z_i,2}$ can guarantee the uniqueness of p_{z_i}. However, we can use a slightly large patch to get an litter improved results. For the numerical results in the chapter, we use $\mathcal{K}_{z_i} = \mathcal{L}_{z_i,2}$ for elliptic equation and $\mathcal{K}_{z_i} = \mathcal{L}_{z_i,3}$ for stokes equation.

Remark. From the above definition, we can see that the proposed gradient recovery method is problem independent. In the following sections, we will apply the gradient recovery to second order elliptic problem (2.1) and Stokes equation (2.3) to show that it can produce superconvergent post-processing gradients.

3.2 Illustrations of the Proposed Gradient Recovery Method

To illustrate the essential idea of the above gradient recovery operator, we study regular pattern and chevron pattern uniform meshes in detail. Note that G_h is a linear operator from X^{nc} to $X^{\mathrm{nc}} \times X^{\mathrm{nc}}$. To simplify notation, sometimes G_h is rewritten as the following component form

$$G_h = \begin{pmatrix} G_h^x \\ \\ G_h^y \end{pmatrix}, \tag{3.2}$$

where G_h^x and G_h^y are linear operators from X^{nc} to X^{nc}.

3.2.1 Regular Pattern

All edge centers can be classified into three cases: vertical edge center, horizontal edge center and diagonal edge center. We select two typical cases as showed in Figure 3 and 4. Other cases can be treated as an orthogonal rotation of the above two cases.

First, consider the case that z is a vertical edge center, i.e. the dotted point in Figure 3. In order to investigate the approximation property of recovery operator, we replace the

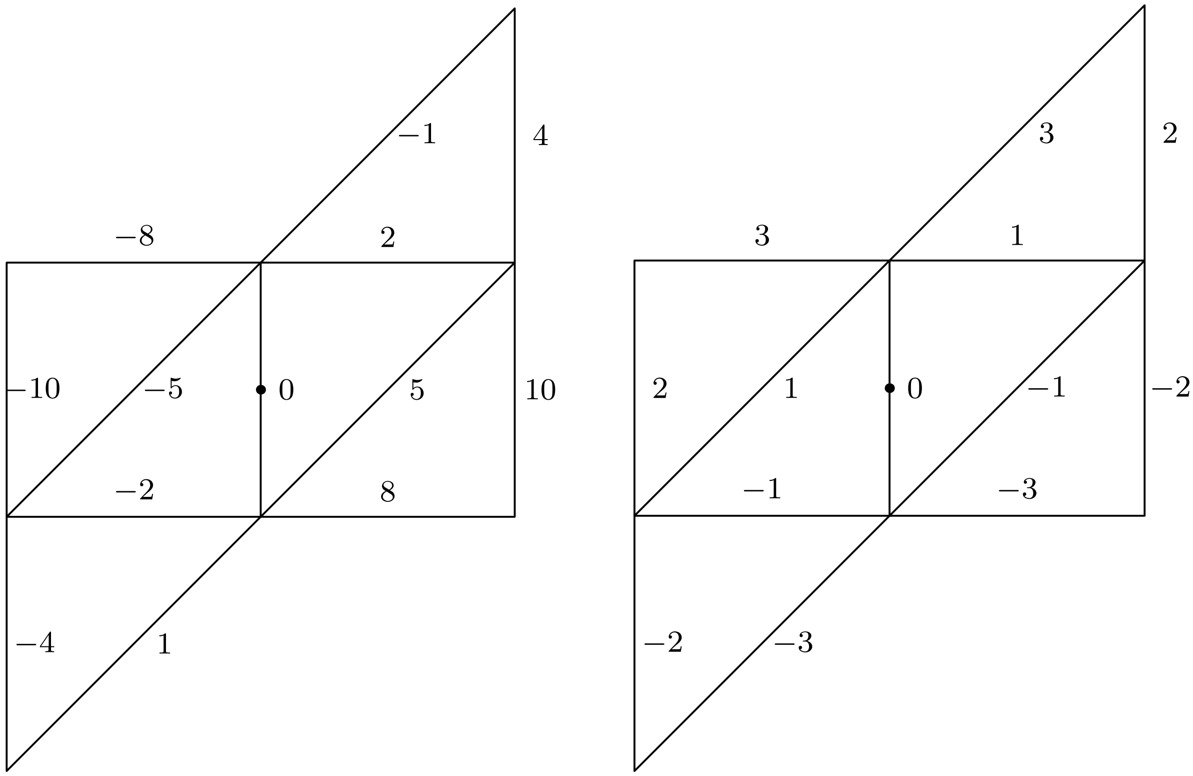

(a) $G_h^x u$: denominator $84h$ (b) $G_h^y u$: denominator $28h$

Figure 3: Recovery at vertical edge center of Regular Pattern

finite element solution u_h by the exact solution u in the sequel. Given

$$\vec{\xi} = (0, 1, 2, 1, -1, -2, -1, -1, 1, 2, 1, -2, -1)^T,$$

$$\vec{\eta} = (0, 0, 0, 1, 1, 0, 0, -1, -1, 2, 2, -2, -2)^T,$$

$$b = (u_0, u_1, u_2, u_3, u_4, u_5, u_6, u_7, u_8, u_9, u_{10}, u_{11}, u_{12})^T,$$

where $u_i = u(F^{-1}(\xi_i, \eta_i))$ for $0 \leq i \leq 12$, we want to fit a polynomial

$$\widehat{p}_2(\xi, \eta) = (1, \xi, \eta, \xi^2, \xi\eta, \eta^2)(\widehat{a}_0, \widehat{a}_1, \widehat{a}_2, \widehat{a}_3, \widehat{a}_4, \widehat{a}_5)^T,$$

in the least square sense with respect to (ξ, η). Let $\vec{e} = (1,1,1,1,1,1,1,1,1,1,1,1,1)^T$ and

$$A = (\vec{e}, \vec{\xi}, \vec{\eta}, \vec{\xi} \circ \vec{\xi}, \vec{\xi} \circ \vec{\eta}, \vec{\eta} \circ \vec{\eta})$$

where $\circ$ is Hadamard product for matrices. Simple calculation shows that

$$B = \begin{pmatrix}
\frac{17}{53} & 0 & 0 & -\frac{5}{53} & \frac{6}{53} & -\frac{6}{53} \\
\frac{12}{53} & \frac{5}{84} & -\frac{1}{28} & -\frac{233}{5512} & \frac{375}{5512} & -\frac{37}{424} \\
-\frac{3}{53} & \frac{5}{42} & -\frac{1}{14} & \frac{157}{1378} & -\frac{93}{1378} & -\frac{1}{106} \\
\frac{12}{53} & \frac{1}{42} & \frac{1}{28} & -\frac{339}{5512} & \frac{587}{5512} & -\frac{37}{424} \\
0 & -\frac{2}{21} & \frac{3}{28} & \frac{3}{104} & -\frac{19}{104} & \frac{1}{8} \\
-\frac{3}{53} & -\frac{5}{42} & \frac{1}{14} & \frac{157}{1378} & -\frac{93}{1378} & -\frac{1}{106} \\
\frac{12}{53} & -\frac{5}{84} & \frac{1}{28} & -\frac{233}{5512} & \frac{375}{5512} & -\frac{37}{424} \\
\frac{12}{53} & -\frac{1}{42} & -\frac{1}{28} & -\frac{339}{5512} & \frac{587}{5512} & -\frac{37}{424} \\
0 & \frac{2}{21} & -\frac{3}{28} & \frac{3}{104} & -\frac{19}{104} & \frac{1}{8} \\
-\frac{3}{53} & \frac{1}{21} & \frac{1}{14} & \frac{51}{1378} & \frac{119}{1378} & -\frac{1}{106} \\
0 & -\frac{1}{84} & \frac{3}{28} & -\frac{3}{104} & -\frac{7}{104} & \frac{1}{8} \\
-\frac{3}{53} & -\frac{1}{21} & -\frac{1}{14} & \frac{51}{1378} & \frac{119}{1378} & -\frac{1}{106} \\
0 & \frac{1}{84} & -\frac{3}{28} & -\frac{3}{104} & -\frac{7}{104} & \frac{1}{8}
\end{pmatrix}$$

where $B^T = (A^T A)^{-1} A^T$. Thus we have $\widehat{a} = B^T b$. Recall that

$$(\widehat{a}_0, \widehat{a}_1, \widehat{a}_2, \widehat{a}_3, \widehat{a}_4, \widehat{a}_5) = (a_0, ha_1, ha_2, h^2 a_3, h^2 a_4, h^2 a_5),$$

and hence it holds that

$$p_2(x,y) = \widehat{a}_0 + \frac{1}{h}(\widehat{a}_1 x + \widehat{a}_2 y) + \frac{1}{h^2}(\widehat{a}_3 x^2 + \widehat{a}_4 xy + \widehat{a}_5 y^2).$$

Differentiating with respect to x and y and evaluate at $(0,0)$, it follows that

$$\begin{aligned}(G_h^x u)(z) = \frac{1}{84h}(&5u_1 + 10u_2 + 2u_3 - 8u_4 - 10u_5 - 5u_6 - \\ &2u_7 + 8u_8 + 4u_9 - u_{10} - 4u_{11} + u_{12}),\end{aligned} \tag{3.3}$$

and

$$\begin{aligned}(G_h^y u)(z) = \frac{1}{28h}(&-u_1 - 2u_2 + u_3 + 3u_4 + 2u_5 + u_6 - \\ &u_7 - 3u_8 + 2u_9 + 3u_{10} - 2u_{11} - 3u_{12}).\end{aligned} \tag{3.4}$$

By using computer algebra system such as **Mathematica**, it is very easy to get the following Taylor expansion for $(G_h u)(z)$

$$(G_h u)(z) = \begin{pmatrix} u_x(z) + \frac{h^2}{42}(21u_{xxx}(z) + 12u_{xxy} + 19u_{xyy} + 3u_{yyy}(z)) + o(h^2) \\ u_y(z) + \frac{h^2}{42}(39u_{xxy} + 39u_{xyy}(z) + 22u_{yyy}(z)) + o(h^2) \end{pmatrix}.$$

It obviously demonstrates that $(G_h u)(z)$ provides a second order approximation to ∇u.

Then we consider that z is a diagonal edge center as seen in Figure 4. Repeating the same procedure as above, we obtain

$$\begin{aligned}(G_h^x u)(z) = \frac{1}{84h}(&5u_1 + 10u_2 + 8u_3 - 2u_4 - 10u_5 - 5u_6 - \\ &8u_7 + 2u_8 + u_9 - 4u_{10} - u_{11} + 4u_{12}),\end{aligned} \tag{3.5}$$

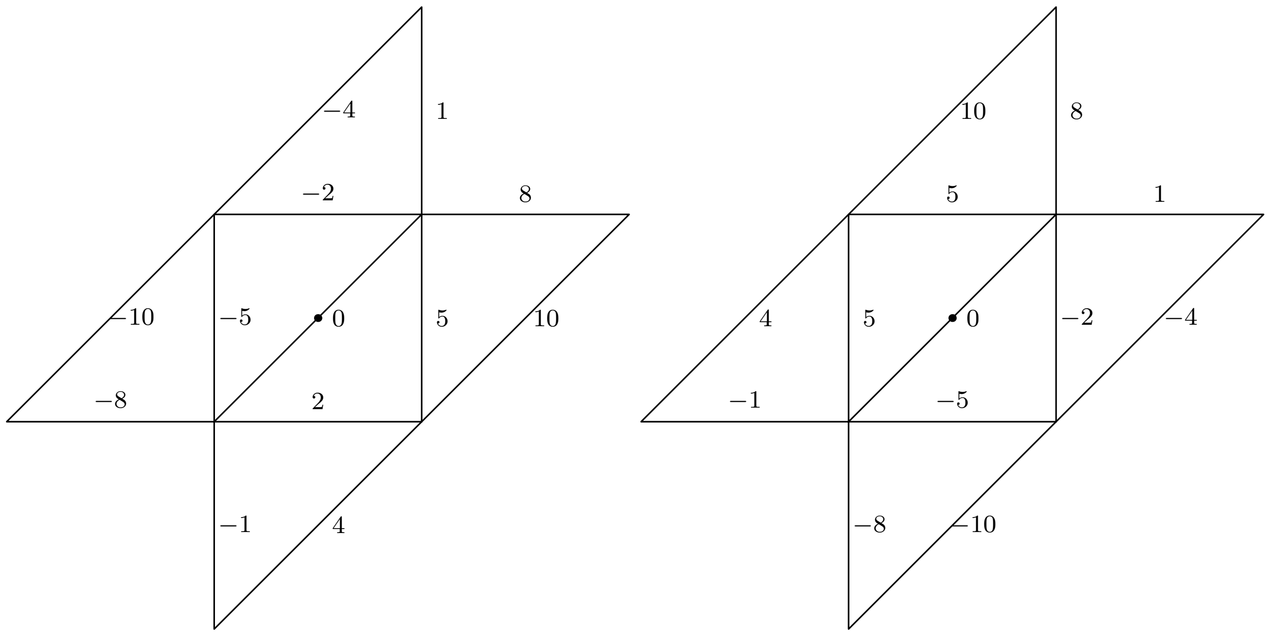

(a) $G_h^x u$: denominator $84h$ (b) $G_h^y u$: denominator $84h$

Figure 4: Recovery at diagonal edge center of Regular Pattern

and

$$(G_h^y u)(z) = \frac{1}{84h}(-2u_1 - 4u_2 + u_3 + 5u_4 + 4u_5 + 5u_6 - \\ u_7 - 5u_8 + 8u_9 + 10u_{10} - 8u_{11} - 10u_{12}). \tag{3.6}$$

Also, we have the following Taylor expansion

$$(G_h u)(z) = \begin{pmatrix} u_x(z) + \frac{h^2}{42}(25u_{xxx}(z) + 17u_{xxy} + 10u_{xyy} - 3u_{yyy}(z)) + o(h^2) \\ u_y(z) - \frac{h^2}{42}(3u_{xxx} - 10u_{xxy}(z) - 17u_{xxy} - 25u_{yyy}(z)) + o(h^2) \end{pmatrix}.$$

Again (3.5) and (3.6) provide a second order approximation to ∇u.

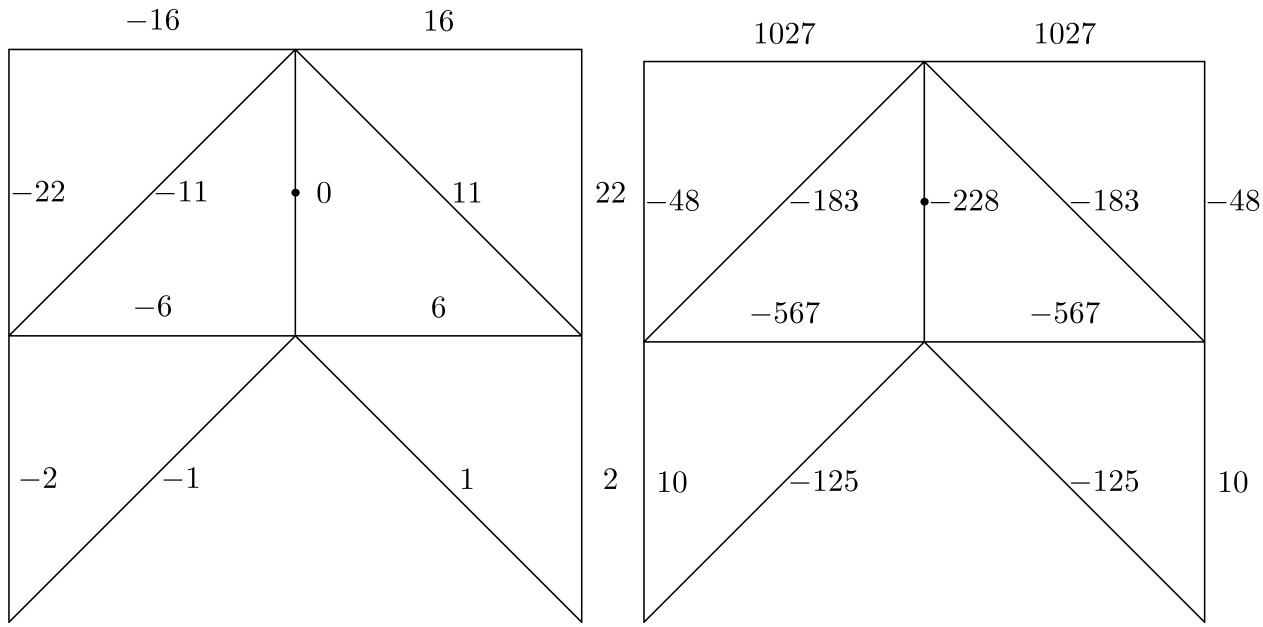

(a) $G_h^x u$: denominator $64h$

(b) $G_h^y u$: denominator $3648h$

Figure 5: Recovery at vertical edge center of Chevron Pattern

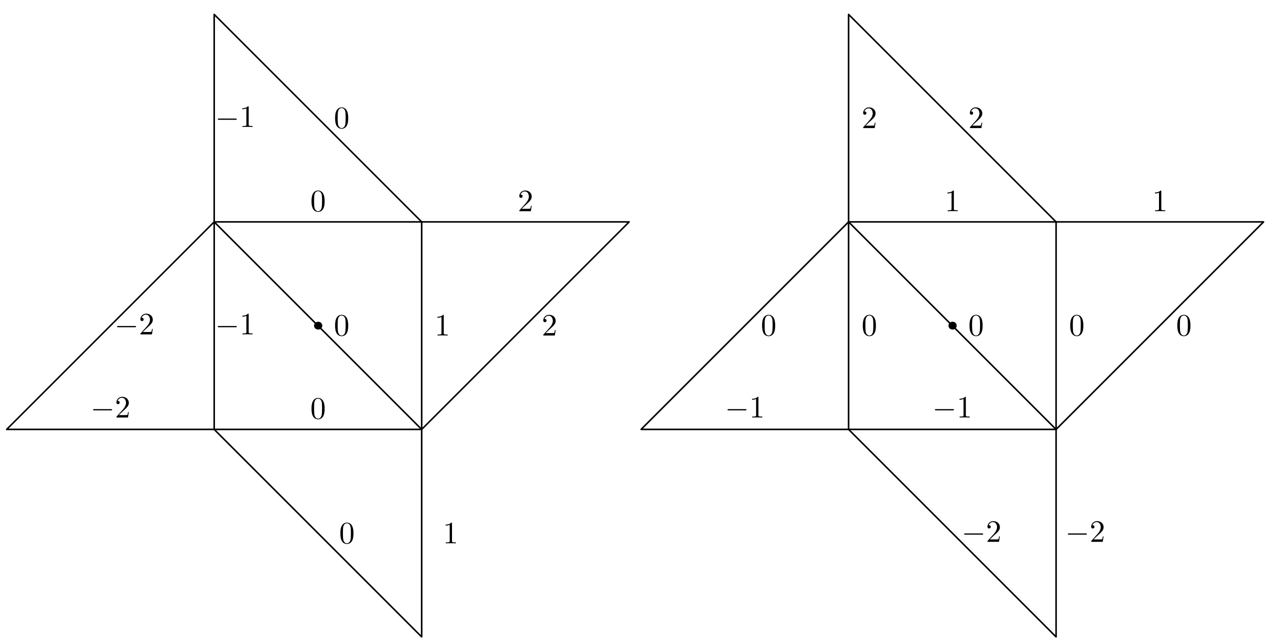

(a) $G_h^x u$: denominator $20h$

(b) $G_h^y u$: denominator $20h$

Figure 6: Recovery at diagonal edge center of Chevron Pattern

3.2.2 Chevron Pattern

Similar to Regular pattern, the gradient recovery operator are different when z are horizontal edge center, vertical edge center and diagonal edge center. Again, we choose two typical edge centers as depicted in Figure 5 and Figure 6. First, consider the case when z is a vertical edge center. Following the same procedure as regular pattern, we get

$$\begin{aligned}(G_h^x u)(z) = \frac{1}{164h}(&11u_1 - 11u_2 - 6u_3 + 6u_4 + 22u_5 + 16u_6 - \\ &16u_7 - 22u_8 - 2u_9 - u_{10} + u_{11} + 2u_{12}),\end{aligned} \tag{3.7}$$

and

$$\begin{aligned}(G_h^y u)(z) = \frac{1}{3648h}(&-228u_0 - 183u_1 - 183u_2 - 567u_3 - 567u_4 - 48u_5 + 1027u_6 \\ &+ 1027u_7 - 48u_8 + 10u_9 - 125u_{10} - 125u_{11} + 10u_{12}).\end{aligned} \tag{3.8}$$

It is straightforward to verify that

$$(G_h u)(z) = \begin{pmatrix} u_x(z) + \frac{h^2}{246}(113u_{xxx}(z) + 63u_{xyy}(z)) + o(h^2) \\ u_y(z) + \frac{h^2}{1824}(882u_{xxy}(z) + 419u_{yyy}(z)) + o(h^2) \end{pmatrix}.$$

which clearly indicates that $G_h u(z)$ converges to ∇u at rate of $O(h^2)$.

Then we consider z is diagonal edge center in Chevron pattern uniform mesh. The sampling points in patch K_z is displayed in Figure 6. Simple calculation verifies that

$$(G_h u)(z) = \frac{1}{20h}\begin{pmatrix} u_1 - u_3 + 2u_5 + 2u_6 - u_8 - 2u_9 - 2u_{10} + u_{12} \\ u_2 - u_4 + u_6 + 2u_7 + 2u_8 - u_{10} - 2u_{11} - 2u_{12} \end{pmatrix}. \tag{3.9}$$

Using Taylor expansion, we get

$$(G_h u)(z) = \begin{pmatrix} u_x(z) + \frac{h^2}{30}(17u_{xxx}(z) + 9u_{xxy}(z) + 12u_{xyy}(z) - 3u_{yyy}(z)) + o(h^2) \\ u_y(z) + \frac{h^2}{30}(3u_{xxx}(z) + 12u_{xxy}(z) - 9u_{xyy}(z) + 17u_{yyy}(z)) + o(h^2) \end{pmatrix}.$$

It approximates ∇u with second order accuracy.

3.3 Properties of the Gradient Recovery Operator

The two examples in previous section show that G_h provides a finite difference scheme with 2nd order accuracy. Moreover, we can show G_h has 2nd order accuracy in case of Criss-cross pattern and Unionjack pattern uniform meshes. In general, the following theorem holds.

Theorem 3.1. *The recovery operator G_h preserves polynomials of degree two on $\mathcal{K}_z$ for an arbitrary mesh.*

Proof. Suppose $u \in \mathbb{P}_2(\mathcal{K}_z)$. Then clearly the least square fitting of a polynomial of degree two will reproduce u, i.e. $p_z = u$ on K_z. Thus $G_h u = \nabla u$ on K_z. □

A direct application of Theorem 3.1 and Bramble-Hilbert Lemma implies the following superconvergence result.

Theorem 3.2. *Let $u \in W^3_\infty(K_z)$. Then*

$$\|\nabla u - G_h u\|_{0,\infty,\mathcal{K}_z} \leq Ch^2 |u|_{3,\infty,\mathcal{K}_z}.$$

Proof. It is similar to the proof of Theorem 2.2 in [107]. □

From now on, we assume $v \in X^{\mathrm{nc}}$ and z_i is the middle point of an arbitrary edge. By

(3.1), we know

$$(G_h v)(z_i) = \begin{pmatrix} (G_h^x v)(z_i) \\ \\ (G_h^y v)(z_i) \end{pmatrix} = \begin{pmatrix} a_1 \\ \\ a_2 \end{pmatrix} = \frac{1}{h_i} \begin{pmatrix} \widehat{a}_1 \\ \\ \widehat{a}_2 \end{pmatrix} = \frac{1}{h_i} \begin{pmatrix} \sum\limits_{j=0}^{m} b_j^1 v_{i_j} \\ \sum\limits_{j=0}^{m} b_j^2 v_{i_j} \end{pmatrix},$$

where $v_{i_j} = v(z_{i_j})$ and b_j^1 and b_j^2 are some constants that independent of h and h_i for $0 \le j \le m$. In addition, let z_{i_j} $(0 \le j \le m)$ be all edge centers in $\mathcal{K}_{z_i}$, $z_i = z_{i_1}$, and $v_i = v(z_i)$. By setting $u \equiv v_i$ in Theorem 3.1, we can conclude that

$$G_h v_i = \begin{pmatrix} 0 \\ \\ 0 \end{pmatrix}.$$

Thus, we can rewrite $(G_h v)(z_i)$ as

$$(G_h v)(z_i) = \begin{pmatrix} (G_h^x v)(z_i) \\ \\ (G_h^y v)(z_i) \end{pmatrix} = \frac{1}{h_i} \begin{pmatrix} \sum\limits_{j=1}^{m} b_j^1 (v_{i_j} - v_i) \\ \sum\limits_{j=1}^{m} b_j^2 (v_{i_j} - v_i) \end{pmatrix}.$$

Notice that for any z_{i_j}, we can find $z_i = z_{j_0}, \ldots, z_{j_{n_j}} = z_{i_j}$ such that z_{j_ℓ} and $z_{j_{\ell+1}}$ belong to the same triangle $T \in \mathcal{T}_h$ and $z_{j_\ell} \in \mathcal{K}_{z_i} \cap \mathcal{M}$. Then

$$(G_h^x v)(z_i) = \sum_{j=1}^{m} b_j^1 \sum_{\ell=0}^{n_j-1} \frac{(v_{j_\ell} - v_{j_{\ell+1}})}{h_i}.$$

Let e_{j_ℓ} denote the line segment connecting v_{j_ℓ} and $v_{j_{\ell+1}}$, and h_{j_ℓ} denote the length of e_{j_ℓ}. Then we have

$$(G_h^x v)(z_i) = \sum_{j=1}^{m} b_j^1 \sum_{\ell=0}^{n_j-1} \frac{h_{j_\ell}}{h_i} \frac{(v_{j_\ell} - v_{j_{\ell+1}})}{h_{j_\ell}}.$$

Since $v \in X^{\mathrm{nc}}$, it follows that $\frac{(v_{j_\ell} - v_{j_{\ell+1}})}{h_{j_\ell}} = \frac{\partial v}{\partial t_{j_\ell}}$, where t_j denotes the unit tangent vector of e_{k_j}. Notice that $\frac{h_{j_\ell}}{h_i}$ are bounded by a constant independent of h and h_i, then we get

$$|(G_h^x v)(z_i)| \lesssim |v|_{1,\infty,\mathcal{K}_{z_i}}.$$

The same argument yields that

$$|(G_h^y v)(z_i)| \lesssim |v|_{1,\infty,\mathcal{K}_{z_i}}.$$

For any triangle $T \in \mathcal{T}_h$, let z_1, z_2, z_3 be the three edge centers of T and $K = \mathcal{K}_{z_1} \cup \mathcal{K}_{z_2} \cup \mathcal{K}_{z_3}$. Then the above result can be summarized as the following theorem

Theorem 3.3. *$G_h : X^{nc} \to X^{nc} \times X^{nc}$ is a linear operator, and there exists a constant C independent of h such that*

$$\|G_h v\|_{0,\infty,T} \leq C|v|_{1,\infty,K} \quad \forall T \in \mathcal{T}_h,$$

for any $v \in X^{nc}$.

With aid of an inverse estimate, we can prove the following corollary

Corollary 3.4. *There is a constant C independent of h such that*

$$\|G_h v\|_{0,2,T} \leq C|v|_{1,2,K} \quad \forall T \in \mathcal{T}_h$$

for any $v \in X^{nc}$.

Let $G_X : X \to X \times X$ be any gradient recovery operator from $X \to X \times X$ satisfying consistency condition, localization condition, and boundness and linearity condition in [4] where X is some finite element space. A classical way to prove the superconvergence of gradient recovery operator is to rewrite $\nabla u - G_X(u_h)$ as

$$\nabla u - G_X(u_h) = \nabla u - G_X(u_I) + G_X(u_I - u_h) \tag{3.10}$$

where u_I is the interpolation of the exact solution u in the finite element space X. According to [4], we can prove $O(h^{(1+r)})$ superconvergence result provided that there is $O(h^{(1+r)})$ supercloseness [12, 71, 101] between the gradient of the finite element solution u_h and the gradient of the interpolation u_I. However, there is no such type supercloseness for the Crouzeix-Raviart element. Actually, [69] proved that the best convergence rate of $|u_h - u_I|_{1,h,\Omega}$ is at best of $O(h)$.

It is worth to point out that supercloseness between the gradient of the finite element solution u_h and the gradient of the interpolation u_I is only a sufficient condition. It is well known that there is no supercloseness for Lagrange linear element when the mesh is uniform mesh of Criss-cross pattern or Unionjack pattern. But PPR and SPR can still produce superconvergent approximate gradient on this two type of uniform meshes; see [107]. The same thing applies to the proposed gradient recovery method.

3.4 Numerical Experiment

In this section, we present numerical examples to demonstrate superconvergence of our gradient recovery method. First, we consider the second order elliptic problem (2.2) and its nonconforming finite element approximation (2.9). Then, we study the superconvergent property of gradient recovery operator G_h applied to each component of velocity filed for nonconforming finite element approximation (2.10) of Stokes equation (2.4).

In order to identify the performance of the gradient recovery operator, we split mesh vertices $\mathcal{N}$ into interior vertices $\mathcal{N}_{h,1}$ and near boundary vertices $\mathcal{N}_{h,2}$, where $\mathcal{N}_{h,2} = \{z \in \mathcal{N}_h : \text{dist}(z, \partial\Omega) \leq L\}$ and $\mathcal{N}_{h,1} = \mathcal{N}_h \setminus \mathcal{N}_{h,2}$. Let

$$\Omega_{h,1} = \bigcup \{T \in \mathcal{T}_h : T \text{ has all of its vertices in } \mathcal{N}_{h,1}\},$$

and $\Omega_{h,2} = \Omega \setminus \Omega_{h,1}$.

For elliptic equation, let u be solution of (2.2), u_h be the solution be the solution of (2.9), u_I is the interpolation of u in the Crouzeix-Raviart space X^{nc}. The notation used is the following:

$E_h = \|u - u_h\|_{1,h,\Omega}$ denotes broken H_1-semi error of finite element solution u_h;

$E_i = \|u_I - u_h\|_{1,h,\Omega}$ denotes broken H_1-semi error between u_h and u_I;

$E_r = ||\nabla u - G_h u_h||_{0,\Omega_{h,2}}$ denotes L_2 error of recovered gradient in the interior domain.

To make notation consist, we use the similar notation for Stokes equation without repeating the definition. In the following numerical test, we take $L = 0.1$.

3.4.1 Elliptic equation

Consider the following Poisson equation

$$-\Delta u = 2\pi^2 \sin \pi x \sin \pi y, \quad \text{in} \quad \Omega = (0,1)^2,$$

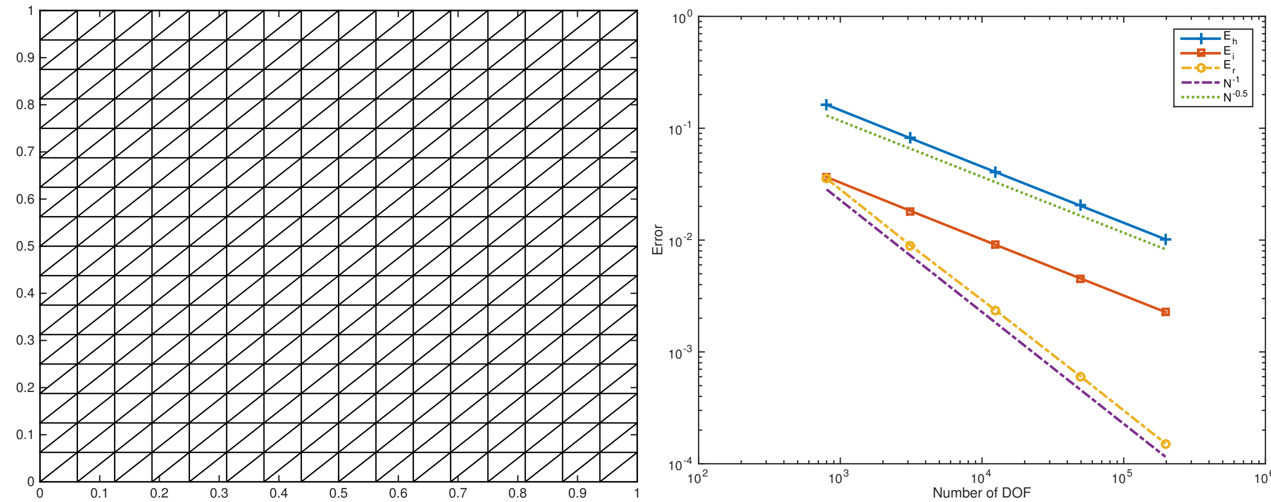

(a) Regular pattern mesh (b) Error

Figure 7: Numerical result of elliptic equation on regular pattern mesh

with $u = 0$ on $\partial\Omega$. The exact solution is

$$u(x, y) = \sin \pi x \sin \pi y.$$

First, uniform meshes are considered. In Figure 7, we report the numerical results for regular pattern uniform meshes. The meshes are obtained by decomposing the unit square into 16×16, 32×32, 64×64, and 128×128 subsquares and then dividing each subsquare into triangles with regulars pattern. We observe $\|u - u_h\|_{1,h,\Omega}$ is $O(h)$ as proved in Theorem 2.3. The recovered gradient superconverges at rate of $O(h^2)$ which doubles the convergence rate of finite element solution. Notice that $\|u_I - u_h\|_{1,h,\Omega}$ converge at the same order of $\|u-u_h\|_{1,h,\Omega}$, which means there is no supercloseness result for the Crouzeix-Raviart element, but it is much smaller than $\|u - u_h\|_{1,h,\Omega}$. The numerical results of Chevron, Criss-cross and Unionjack pattern are displayed in Figure 8, 9 and 10, respectively. $O(h^2)$ superconvergence of recovered gradient is also observed.

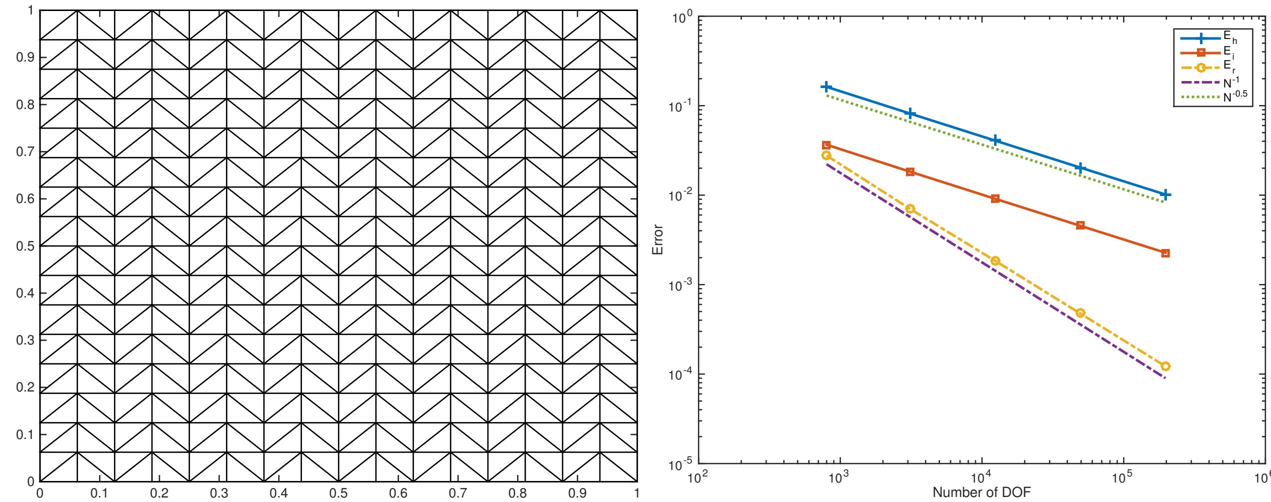

(a) Chevron pattern mesh (b) Error

Figure 8: Numerical result of elliptic equation on chevron pattern mesh

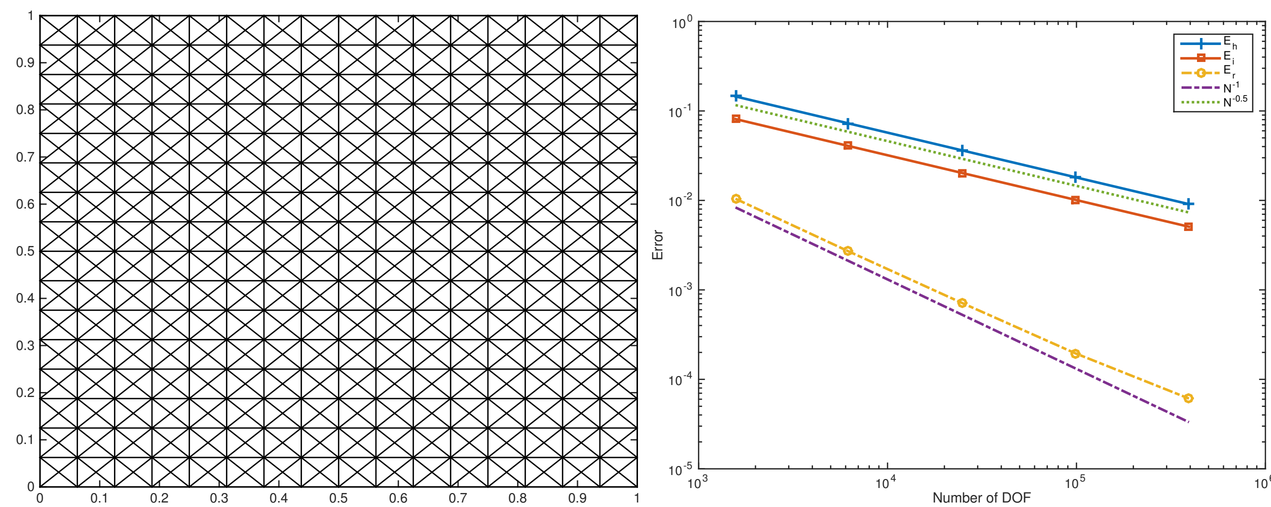

(a) Crisscross pattern mesh (b) Error

Figure 9: Numerical result of elliptic equation on crisscross pattern mesh

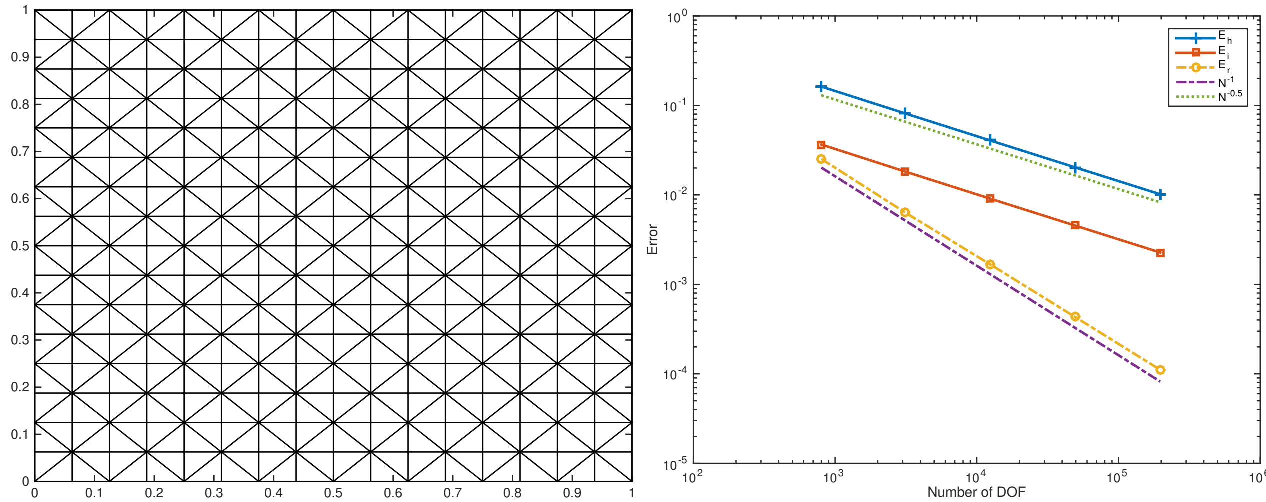

(a) Unionjack pattern mesh (b) Error

Figure 10: Numerical result of elliptic equation on unionjack pattern mesh

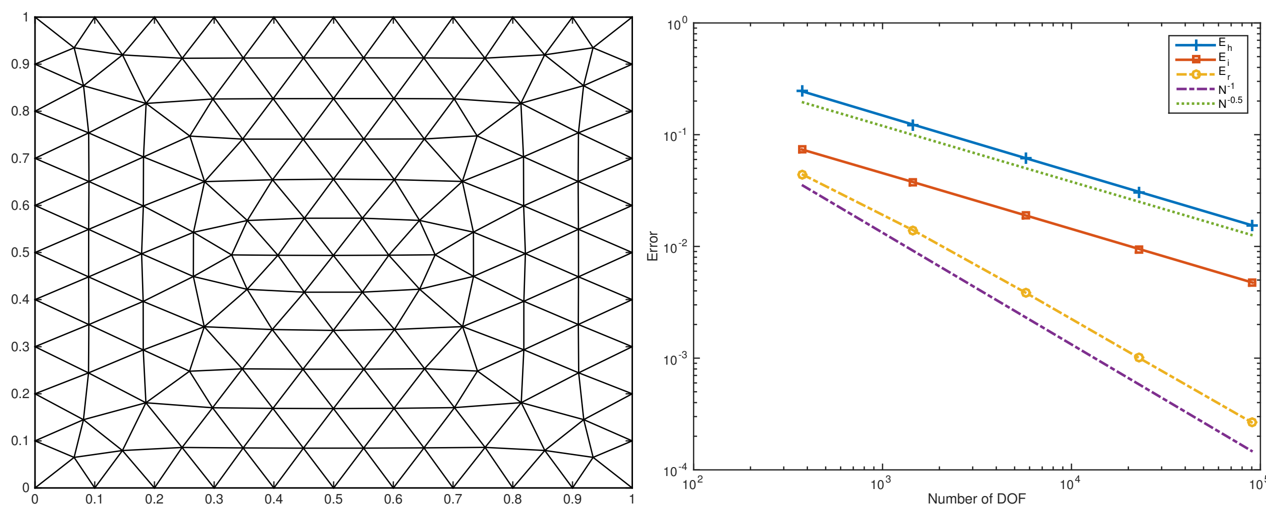

(a) Delaunay mesh (b) Error

Figure 11: Numerical result of elliptic equation on delaunay mesh

Then we turn to unstructured mesh. We start from an initial mesh generated by EasyMesh [84], followed by four levels of refinement using bisection. As we can see in Figure 11, the rate of convergence for the recovered gradient in the L^2 norm is very close to 2 and hence implies a superconvergent recovery.

From the above numerical results, we can observe the superconvergence for the proposed gradient recover operator on both structured meshes and unstructured mesh. Hence, it serves an asymptotically exact posteriori error estimators for adaptive finite element for the Crouzeix-Raviart element which will be studied at next section.

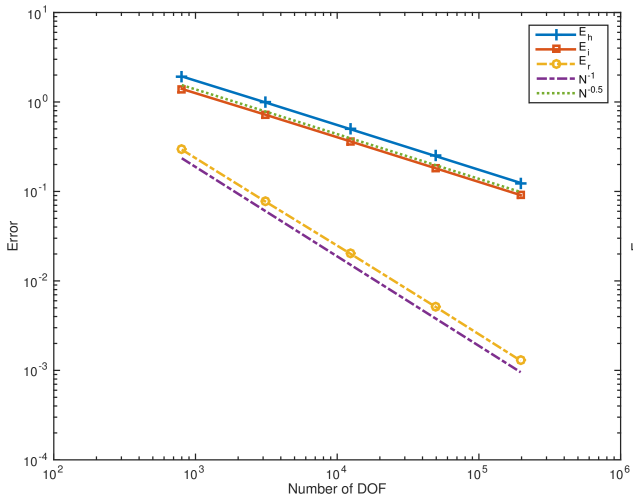

Figure 12: Numerical result of Stokes equation on regular pattern mesh

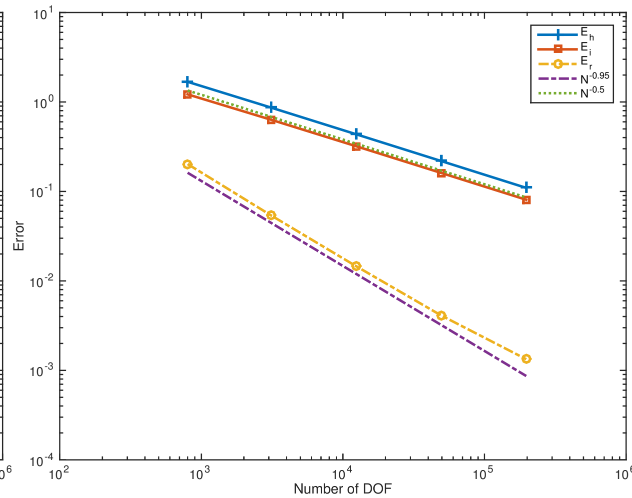

Figure 13: Numerical result of Stokes equation on chevron pattern mesh

3.4.2 Stokes equation

In the subsection, we consider the Stokes equation (2.3) on the unit square $\Omega = [0,1] \times [0,1]$ with exact solution

$$\vec{u}(x, y) = \begin{pmatrix} 20xy^3 \\ 5x^4 - 5y^4 \end{pmatrix},$$

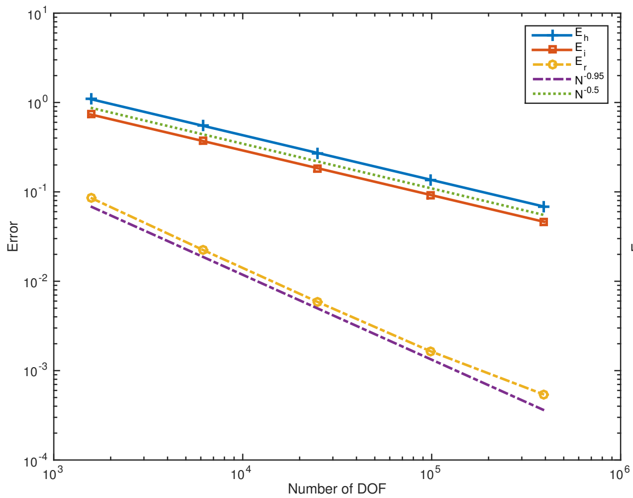

Figure 14: Numerical result of Stokes equation on crisscross pattern mesh

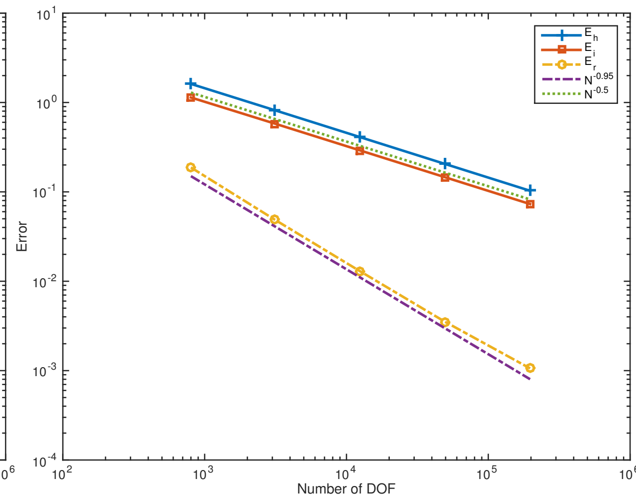

Figure 15: Numerical result of Stokes equation on unionjack pattern mesh

and $p(x, y) = 60x^2y - 20y^3 - 5$. Let $(\vec{u}_h, p_h)$ be the nonconforming finite element approximation of the variational problem (2.4), i.e. $(\vec{u}_h, p_h)$ is the solution of the discrete variational problem (2.10). Here we focus on the gradient recovery of velocity field $\vec{u}_h$. $G_h\vec{u}_h$ means that the gradient recovery operator G_h is applied to each component of $\vec{u}_h$. According to Theorem 2.6, the optimal convergence rate of $\|\vec{u}_h - \vec{u}\|_{1,h,\Omega}$ is $O(h)$. We can get superconvergence results by gradient recovery.

The numerical result for regular pattern uniform mesh is reported in Figure 12. $O(h)$ convergence are observed for $||\vec{u} - \vec{u}_h||_{1,h,\Omega}$ and $\|\vec{u}_I - \vec{u}_h\|_{1,h,\Omega}$ for all kinds of meshes while $O(h^2)$ superconvergence can be obersved for $\|G_h\vec{u}_h - \nabla\vec{u}\|_{0,\Omega_{h,1}}$.

Figure 13 listed the numerical result for chevron pattern uniform mesh. The discrete H^1 error and the disrecte H^1 norm of the difference between finite element solution $\vec{u}_h$ and the nonconforming finite element interpolation $\vec{u}_I$ of the exact solution $\vec{u}$ are both about $O(h)$. Concerning the performance of gradient recovery operator, $O(h^{1.9})$ superconvergence can be observed. Compared to the result on regular pattern uniform mesh, the superconvergence

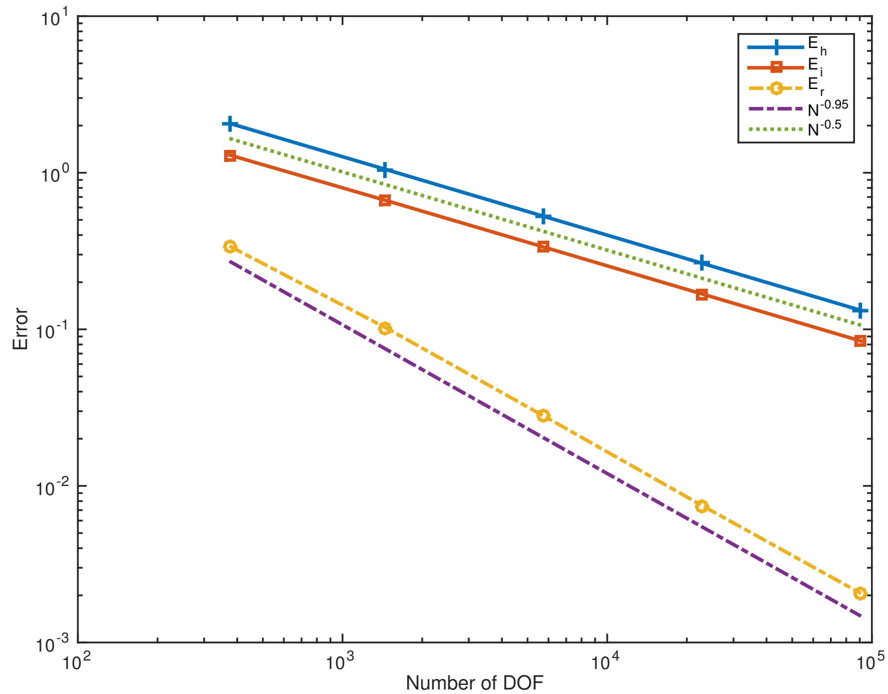

Figure 16: Numerical result of Stokes equation on Delaunay mesh

rate is a bit low.

Figure 14 and 15 present the numerical result for other two uniform meshes and Figure 16 shows the numerical result for Delaunay mesh. These numerical results are similar to chevron pattern uniform mesh. The recovered gradient superconverges at rate of $O(h^{1.9})$ in the interior of the domain.

It is worth to point that $\|\vec{u}_I - \vec{u}_h\|_{1,h,\Omega}$ is almost the same as $\|\vec{u} - \vec{u}_h\|_{1,h,\Omega}$ for Stokes equation. Thus, supercloseness result is not true for nonconforming finite element approximation Stokes equation (2.10). Even in this case, we can get a superconvergent gradient by post-processing.

3.5 Application to adaptive methods

One of the most important applications of gradient recovery is in adaptive finite element methods. Adaptive finite element method (AFEM) is characterized by the loop of the form [86, 87]

$$\mathbf{SOLVE} \rightarrow \mathbf{ESTIMATE} \rightarrow \mathbf{MARK} \rightarrow \mathbf{REFINE}$$

More precisely, given an initial mesh $\mathcal{T}_0$, set $k = 0$ and iterate

- **SOLVE.** Compute the solution u_k of discrete variational problem (2.9) on the Crouzeix-Raviart element space X^{nc} defined on the mesh $\mathcal{T}_k$.

- **ESTIMATE.** Compute the local error estimator $\{\eta(u_k, T)\}_{T\in\mathcal{T}_k}$ using u_k and (or) $\mathcal{T}_h$.

- **MARK.** Collect a subset $\mathcal{M}_k \subset \mathcal{T}_h$ of marked elements according the above posterior estimator and some marking strategy. In this work, only bulk marking strategy [38] is considered.

- **REFINE** Refine $\mathcal{T}_k$ into a shape regular mesh and conforming mesh $\mathcal{T}_{k+1}$ using bisection [15, 86, 87] in such a way that each element in $\mathcal{M}_k$ is bisected at least once and, finally, increment k.

The essential part of AFEM is the **ESTIMATE** step. A posterior error estimators can be categorized into two classes: residue type and recovery type. There are extensive investigations of residue type a posteriori error estimators including both conforming finite element [4, 9, 10, 11, 15, 86, 87, 95, 96] and the Crouzeix-Raviart element [3, 39]. Concerning recovery type a posteriori estimators for conforming finite element method, the theory is also relative mature, see [4, 29, 79, 98, 101, 110, 111, 112]. In particular, SPR and PPR become a standard part of several commercial finite element softwares. The study of recovery type a posteriori error estimator for nonconforming finite element methods is limited [27, 29, 42].

In this section, we apply the proposed gradient recovery technique to a recovery type posteriori error estimate. Define a local a posteriori error estimator on the element T as

$$\eta(u_h, T) = \|\mathcal{D}^{\frac{1}{2}}(G_h u_h - \nabla u_h)\|_{0,T}, \tag{3.11}$$

and a global error estimator as

$$\eta(u_h, \Omega) = \left(\sum_{T \in \mathcal{T}_h} \eta(u_h, T) \right)^{\frac{1}{2}}. \tag{3.12}$$

In the context of adaptive finite element methods for boundary value problems, the effectivity index κ is used to measure the quality of an error estimator [4, 11]. This index is defined by the ratio between the estimated error and the true error

$$\kappa = \frac{\|G_h u_h - \nabla_h u_h\|_{0,\Omega}}{\|\nabla u - \nabla_h u_h\|_{0,\Omega}} \tag{3.13}$$

where ∇_h is the broken gradient operator. To test the robustness of the error estimator (5.26), we use the first three examples in [30] as our benchmark problems. Readers are referred to [30] for computational comparison of several posteriori error estimators for the Crouzeix-Raviart element.

Example 2.5.1. Let us consider the Laplace equation on the L-shaped domain $\Omega = (-1,1) \times (-1,1) \setminus (0,1) \times (-1,0)$ with the Dirichlet boundary condition which is is chosen

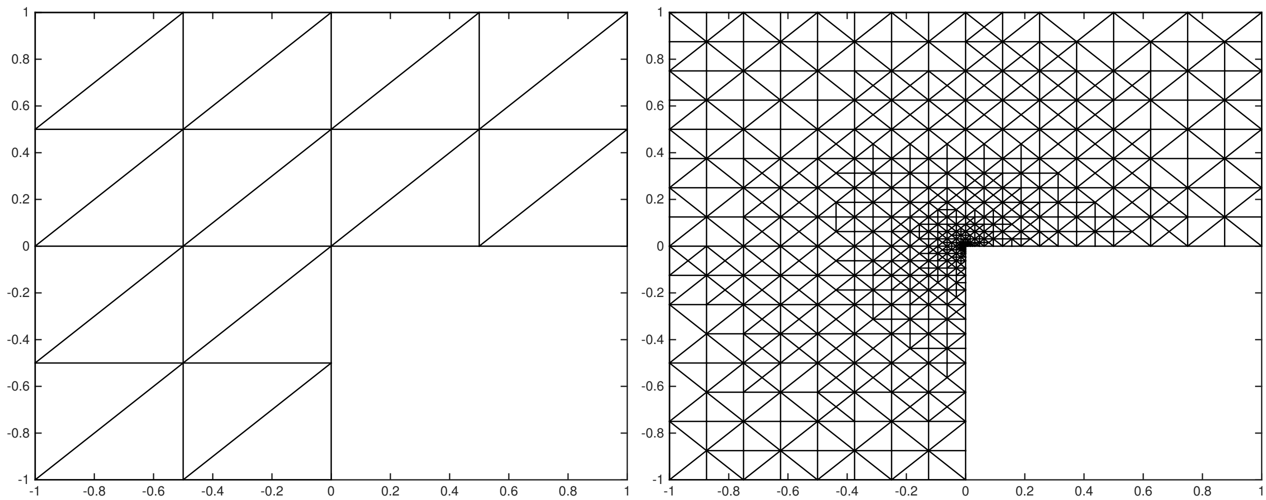

(a) Initial mesh (b) Adaptive refined mesh

Figure 17: Meshes of Poisson equation on L-shaped domain

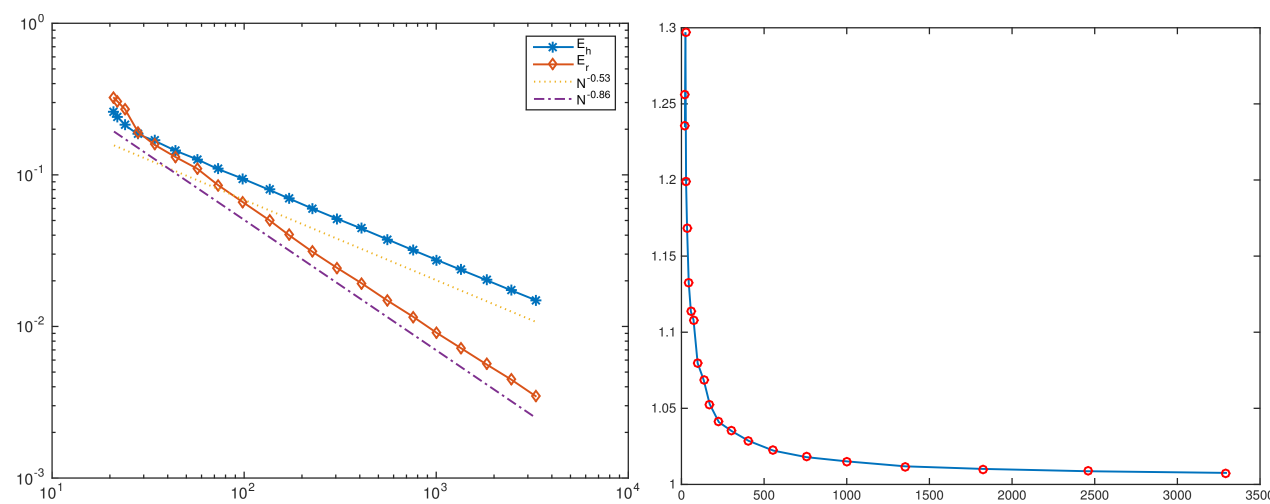

(a) Error (b) Effective index

Figure 18: Numerical results of Poisson equation on L-shape domain

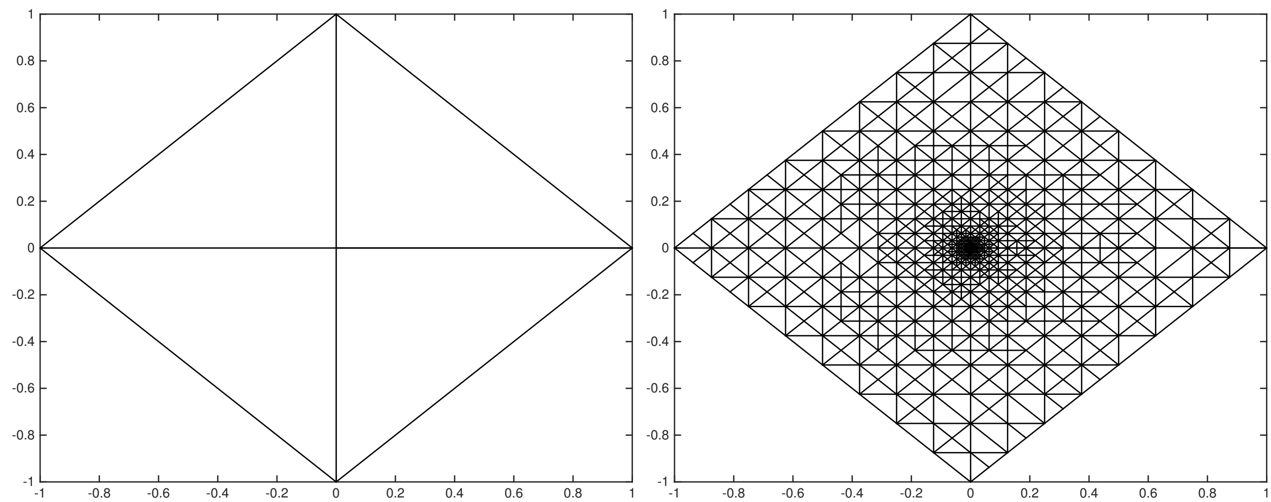

(a) Initial mesh (b) Adaptive refined mesh

Figure 19: Meshes of Poisson equation on Crack domain

so that the true solution is $r^{2/3}\sin(2\theta/3)$ in polar coordinates. The solution has a corner singularity at $(0,0)$. To obtain optimal convergence rate $O(h)$, we use adaptive finite element method. Fig 17(a) shows the initial mesh while Fig 17(b) plots the adaptive refined mesh. The mesh is locally refined at the singularity point. We numerically observed from Fig 18(a) that

$$||u - \nabla u_h||_{1,h,\Omega} \approx O(N^{-0.54}) \quad ||u - G_h u_h||_{0,\Omega} \approx O(N^{-0.86}).$$

Notice that $\|u - u_h\|_{1,h,\Omega}$ converges at optimal rate.

The effectivity index are plotted in Fig 18(b). We see that κ converges to 1 quickly after the first few iterations which indicates the posteriori error estimator (5.26) or (3.12) is asymptotically exact.

Example 2.5.2. The second benchmark problem is elliptic equation (2.1) with $\mathcal{D} = I$ and $c = 0$ on the crack domain $\Omega = \{|x| + |y| \leq 1\}\ \{0 \leq x \leq 1, y = 0\}$. The right hand side function is 1 and the exact solution is $u = \sqrt{\frac{1}{2}(r-x)} - \frac{1}{4}r^2$ with $r = \sqrt{x^2 + y^2}$. The

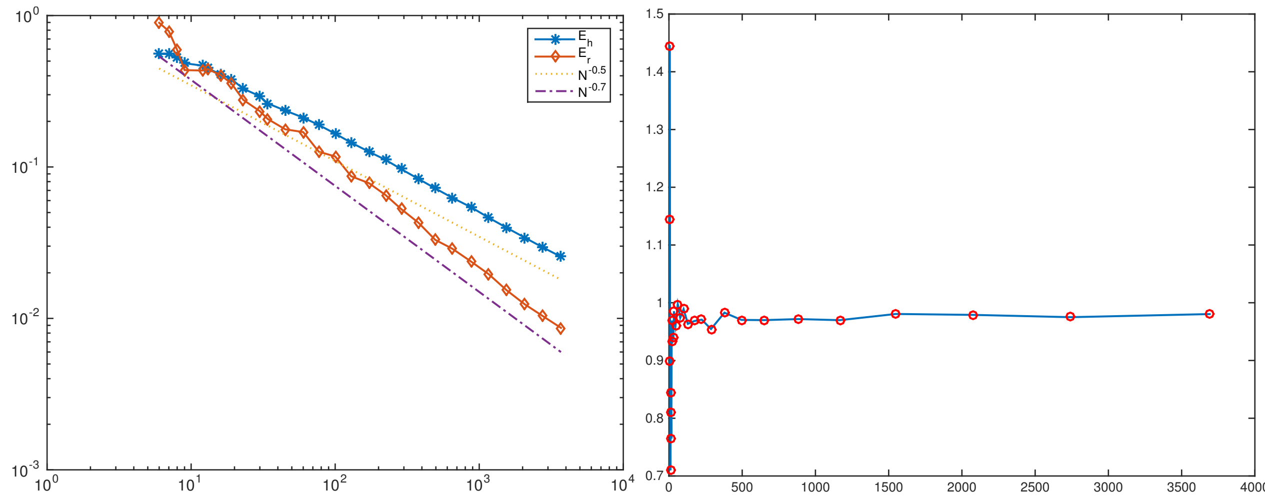

(a) Error

(b) Effective index

Figure 20: Numerical results of Poisson equation on Crack domain

initial mesh and the adaptive refined mesh is plotted in Fig 19. Fig 20(a) shows that H^1 error of numerical solution is optimal and the recovery gradient error superconverges at rate of $O(h^{1.4})$. Similarly to previous example, the error estimator is aymptotically exact which is indicated by the effective index closing to 1, see Figure 20(b).

Example 2.5.3. Our third benchmark problem employs homogeneous boundary data and an oscillation source term f that matches the exact solution $u(x, y) = x(x-1)y(y-1)\exp(-100(x-1/2)^2 - 100(y-117/1000)^2)$ on the square domain $\Omega = [0, 1]^2$, see[30, 74]. We use the initial mesh as in Figure 21(a) and the resulting adaptive refined mesh is in Figure 21(b) which is locally refined near the oscillation point. The numerical result is presented in Figure 22. Since the solution is smooth, we observe $O(h^2)$ superconvergence for gradient recovery error. The estimator is asymptotically exact.

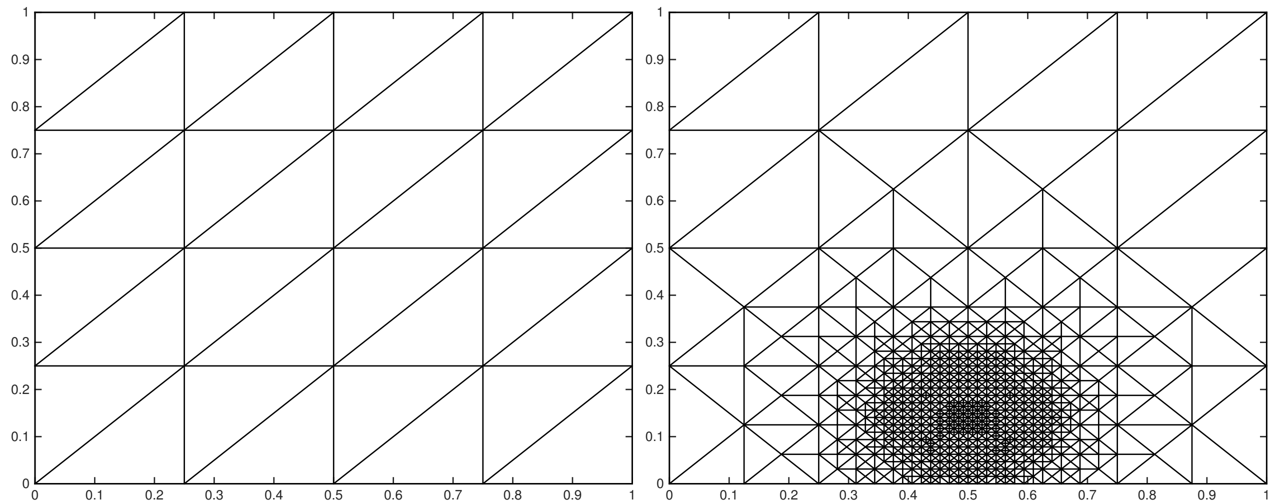

(a) Initial mesh (b) Adaptive refined mesh

Figure 21: Meshes of Poisson equation on square domain with ossilcatlions

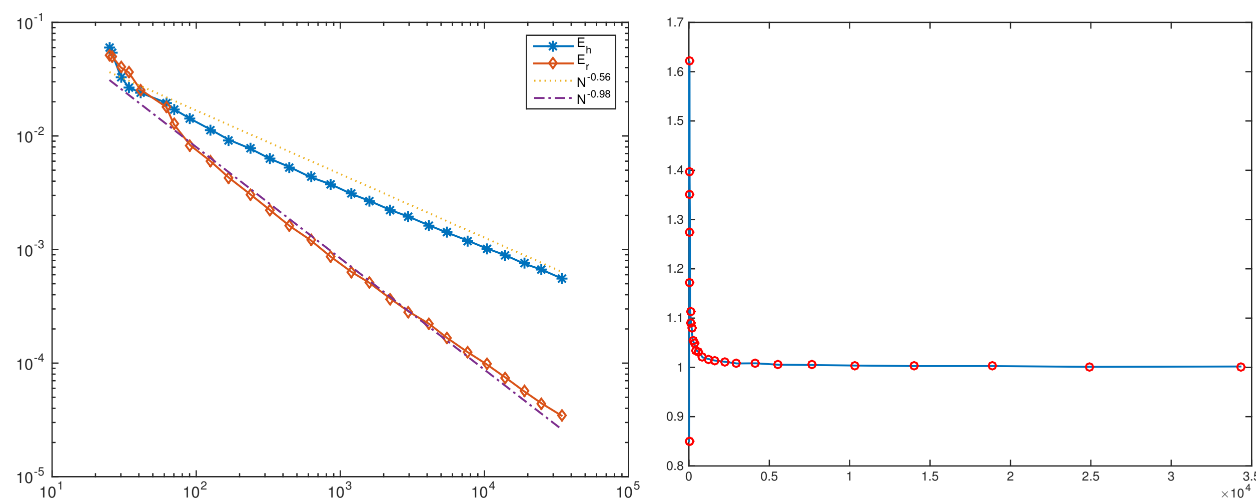

(a) Error (b) Effective index

Figure 22: Numerical Results of Poisson equation on square domain with ossilcatlions

3.6 Conclusion

We proposed a gradient recovery method for the Crouzeix-Raviart element. The proposed method fits a quadratic polynomial in least square sense at any edge center and then take derivative to get recovered gradient. We proved that it is polynomial preserving and is a bounded linear operator. Numerical experiment showed that it produces superconvergent recovered gradient and can serve as an asymptotically exact posteriori error estimator.

CHAPTER 4 Hessian recovery for finite element

Hessian matrix has many applications in scientific computing [61, 65, 66, 83, 45]. which is typically unavailable in a numerical simulation. A widely-used approach to avoid this difficulty in practical computation is to replace the information by one recovered from the obtained numerical approximation [60, 89, 94]. However, there is no general theory guaranteeing convergence for existing Hessian recovery methods.

In this chapter, we study Hessian recovery for C_0 finite element methods of arbitrary order. Our approach is to apply PPR twice to the primary computed data. We proved that the proposed Hessian recovery method preserves polynomials of degree $r + 1$ on general unstructured meshes and superconvergence at a rate of $o(h^r)$ on mildly structured meshes. In addition, the method is proved to be ultraconvergent (two order higher) for translation invariant finite element space of any order.

In Section 4.1, we introduce some notation. Since the building block of our Hessian recovery is polynomial preserving recovery (PPR), we describe the definition of PPR in Section 4.2. The formal definition of our Hessian recovery operator is provided in Section 4.3. This definition is illustrated with two examples on uniform meshes and followed by discussion of its properties. The main superconvergence analysis of the proposed Hessian recovery method is shown in Section 4.4. In Section 4.5, we use some numerical examples to verify our theoretical results. We end this chapter with some concluding remarks in Section 4.6.

4.1 Notation

To simplify notation, the Hessian operator H is denoted by

$$H = \begin{pmatrix} \partial_{xx} & \partial_{xy} \\ \partial_{yx} & \partial_{yy} \end{pmatrix}. \tag{4.1}$$

For any $0 < h < \frac{1}{2}$, let $\mathcal{T}_h$ be a shape regular triangulation of $\bar{\Omega}$ as defined in section 2.3.1. For any $r \in \mathbb{N}$, let $S^{h,r}$ be the continuous finite element space with piecewise polynomial of degree r, see section 2.3.2. In this section, we suppose $\mathcal{T}_h$ is quasi-uniform. Let $\mathcal{N}_h$ denote the set of mesh nodes, i.e. the dual space of $S^{h,r}$.

Then we talk about a special finite element space, which is widely used for superconvergence anaysis [97]. For $\mathcal{A} \subset \Omega \subset \mathbb{R}^2$, let $S^{h,r}(\mathcal{A})$ denote the restrictions of functions in $S^{h,r}$ to $\mathcal{A}$ and let $S^{h,r}_{00}(\mathcal{A})$ denote the set of those functions in $S^{h,r}(\mathcal{A})$ with compact support in the interior of $\mathcal{A}$ [97]. Let $\Omega_0 \subset\subset \Omega_1 \subset\subset \Omega_2 \subset\subset \Omega$ be separated by $d \geq c_o h$ and ℓ be a direction, i.e., a unit vector in $\mathbb{R}^2$. Let τ be a parameter, which will typically be a multiple of h. Let T^ℓ_τ denote translation by τ in the direction ℓ, i.e.,

$$T^\ell_\tau v(z) = v(z + \tau\ell), \tag{4.2}$$

and for an integer ν

$$T^\ell_{\nu\tau} v(z) = v(z + \nu\tau\ell). \tag{4.3}$$

Following the definition of [97], the finite element space $S^{h,r}$ is called translation invariant by τ in the direction ℓ if

$$T^{\ell}_{\nu\tau} v \in S^{h,r}_{00}(\Omega), \quad \forall v \in S^{h,r}_{00}(\Omega_1), \tag{4.4}$$

for some integer ν with $|\nu| < M$. Equivalently, $\mathcal{T}_h$ is called a translation invariant mesh. To clarify the matter, we consider five popular triangular mesh patterns: Regular, Chevron, Union-Jack, Criss-cross, and equilateral patterns, as shown in Figure 23.

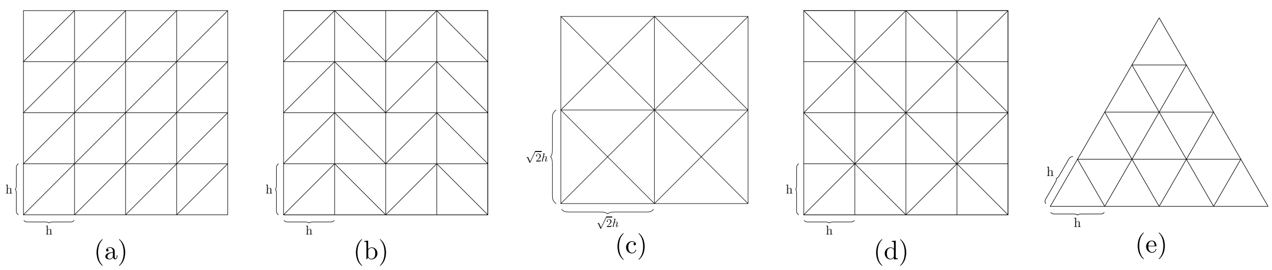

Figure 23: Five types of uniform meshes: (a) Regular pattern; (b) Chevron pattern; (c) Criss-cross pattern; (d) Union-Jack pattern; (e) Equilateral pattern

We see that:

1) Regular pattern is translation invariant by h in directions $(1, 0)$ and $(0, 1)$, by $2\sqrt{2}h$ in directions $(\pm\frac{\sqrt{2}}{2}, \frac{\sqrt{2}}{2})$, and by $\sqrt{5}h$ in directions $(\frac{2\sqrt{5}}{5}, \pm\frac{\sqrt{5}}{5})$ and $(\pm\frac{\sqrt{5}}{5}, \frac{2\sqrt{5}}{5})$, ...

2) Chevron pattern is translation invariant by h in the direction $(0, 1)$, by $2h$ in the direction $(1, 0)$, and by $2\sqrt{2}h$ in directions $(\pm\frac{\sqrt{2}}{2}, \frac{\sqrt{2}}{2})$, and by $\sqrt{5}h$ in directions $(\pm\frac{\sqrt{5}}{5}, \frac{2\sqrt{5}}{5})$, ...

3) Criss-cross pattern is translation invariant by $\sqrt{2}h$ in directions $(1, 0)$ and $(0, 1)$, and by $2h$ in directions $(\pm\frac{\sqrt{2}}{2}, \frac{\sqrt{2}}{2})$, ...

4) Union-Jack pattern is translation invariant by $2h$ in directions $(1, 0)$ and $(0, 1)$, and by $2\sqrt{2}h$ in directions $(\pm\frac{\sqrt{2}}{2}, \frac{\sqrt{2}}{2})$, ...

5) Equilateral pattern is translation invariant by h in directions $(1, 0)$ and $(\pm\frac{1}{2}, \frac{\sqrt{3}}{2})$, and

by $\sqrt{3}h$ in directions $(0,1)$ and $(\frac{\sqrt{3}}{2}, \pm\frac{1}{2})$, ...

4.2 Polynomial preserving recovery

Let $G_h : S^{h,r} \to \prod_{i=1}^{2} S^{h,r}$ denote the PPR gradient recovery operator [79, 80, 107]. Given a function $u_h \in S^{h,r}$, it suffices to define $(G_h u_h)(z)$ for all $z \in \mathcal{N}_h$. Let $z \in \mathcal{N}_h$ be a vertex and $\mathcal{K}_z$ be a patch of elements around z which is defined in [80, 107]. Select all nodes in $\mathcal{N}_h \cap \mathcal{K}_z$ as sampling points and fit a polynomial $p_z \in \mathbb{P}_{r+1}(\mathcal{K}_z)$ in the least squares sense at those sampling points, i.e.

$$p_z = \arg \min_{p \in \mathbb{P}_{r+1}(\mathcal{K}_z)} \sum_{\widetilde{z} \in \mathcal{N}_h \cap \mathcal{K}_z} (u_h - p)^2(\widetilde{z}). \tag{4.5}$$

We called p_z is the least-square polynomial approximation (LSPA) of u_h at z. The recovered gradient at z is defined as

$$(G_h u_h)(z) = \nabla p_z(z).$$

For linear element, all nodes in $\mathcal{N}_h$ are vertices and hence $G_h u_h$ is well defined. However, $\mathcal{N}_h$ may contain edge nodes or interior nodes for higher order elements. If z is an edge node which lies on an edge between two vertices z_1 and z_2, we define

$$(G_h u_h)(z) = \beta \nabla p_{z_1}(z) + (1-\beta) \nabla p_{z_2}(z)$$

where β is determined by the ratio of distances of z to z_1 and z_2. If z is an interior node which lies in a triangle formed by three vertices z_1, z_2, and z_3, we define

$$(G_h u_h)(z) = \sum_{j=1}^{3} \beta_j \nabla p_{z_j}(z),$$

where β_j is the barycentric coordinate of z.

Zhang and Naga proved the following properties of PPR in [79, 80, 107]:

1. G_h is linear.

2. G_h satisfied the consistency condition, i.e.

$$G_h(I_h p) = \nabla p, \forall p \in \mathbb{P}_{r+1}(\Omega). \tag{4.6}$$

3. G_h is bounded in the following sense:

$$\|G_h v\|_{0,T} \lesssim |v|_{1,\mathcal{K}_T}, \quad \forall T \in \mathcal{T}_h, \text{ and } \forall v \in S^{h,r} \tag{4.7}$$

   where

$$\mathcal{K}_T = \bigcup\{\mathcal{K}_z : z \text{ is a vertice of } T\}$$

   is the patch corresponding to T. This condition is called the boundedness condition.

Remark. It was proved in [79] that certain rank condition and geometric condition guarantee the uniqueness of p_z in (4.5).

Remark. In order to avoid numerical instability, a discrete least squares fitting process is carried out on a reference patch ω_z .

4.3 Hessian recovery method

Given $u \in S^{h,r}$, let $G_h u \in \prod_{i=1}^{2} S_h$ be the recovered gradient using PPR as defined in previous section. We rewrite $G_h u$ as

$$G_h u = \begin{pmatrix} G_h^x u \\ G_h^y u \end{pmatrix}. \tag{4.8}$$

In order to recover the Hessian matrix of u, we apply gradient recovery operator G_h to $G_h^x u$ and $G_h^y u$ one more time, respectively, and define the Hessian recovery operator H_h as follows

$$H_h u = \begin{pmatrix} G_h(G_h^x u), & G_h(G_h^y u) \end{pmatrix} = \begin{pmatrix} G_h^x(G_h^x u) & G_h^x(G_h^y u) \\ G_h^y(G_h^x u) & G_h^y(G_h^y u) \end{pmatrix}. \tag{4.9}$$

Just as PPR, we obtain $H_h : S^{h,r} \to \prod_{i=1}^{2} S^{h,r} \times \prod_{i=1}^{2} S^{h,r}$ on the whole domain Ω by interpolation after determining values of $H_h u$ at all nodes in $\mathcal{N}_h$.

Remark. The two gradient recovery operators in definition (4.9) of H_h can be different. Actually we can define the Hessian recovery operator H_h as following

$$H_h u = \begin{pmatrix} \widetilde{G}_h(G_h^x u), & \widetilde{G}_h(G_h^y u) \end{pmatrix}.$$

By choosing G_h and $\widetilde{G}_h$ as PPR or SPR operator, we obtain four different Hessian recovery operators, i.e., PPR-PPR, PPR-SPR, SPR-PPR, and SPR-SPR. However, numerical tests have shown that PPR-PPR is the best one.

In order to demonstrate our method, we shall discuss two examples in detail. For the sake of simplicity, only linear element on uniform mesh will be considered. In practice, the method can be applied to arbitrary mesh and higher order elements.

Example 4.1. Consider the regular pattern uniform mesh as in Figure 24(a). We want to recovery the Hessian matrix at z_0. As deduced in [107], the recovered gradient at z_0 is given by

$$(G_h u)(z_0) = \frac{1}{6h}\left(\begin{pmatrix} 2 \\ 1 \end{pmatrix} u_1 + \begin{pmatrix} 1 \\ 2 \end{pmatrix} u_2 + \begin{pmatrix} -1 \\ 1 \end{pmatrix} u_3 \right.$$
$$\left. - \begin{pmatrix} 2 \\ 1 \end{pmatrix} u_4 - \begin{pmatrix} 1 \\ 2 \end{pmatrix} u_5 + \begin{pmatrix} 1 \\ -1 \end{pmatrix} u_6 \right).$$

Here $u_i = u(z_i), (i = 0, 1, \ldots 18)$ represents function value of u at node z_i. Thus, according to the definition (4.9) of the Hessian recovery operator H_h, we have

$$\begin{pmatrix} H_h^{xx} u \\ H_h^{xy} u \end{pmatrix}(z_0) = \frac{1}{6h}\left(2(G_h u)(z_1) + (G_h u)(z_2) - (G_h u)(z_3) - \right.$$
$$\left. 2(G_h u)(z_4) - (G_h u)(z_5) + (G_h u)(z_6)\right), \tag{4.10}$$

and

$$\begin{pmatrix} H_h^{yx} u \\ H_h^{yy} u \end{pmatrix}(z_0) = \frac{1}{6h}\left((G_h u)(z_1) + 2(G_h u)(z_2) + (G_h u)(z_3) - \right.$$
$$\left. (G_h u)(z_4) - 2(G_h u)(z_5) - (G_h u)(z_6)\right), \tag{4.11}$$

where

$$(G_h u)(z_1) = \frac{1}{6h}\left(\begin{pmatrix}2\\1\end{pmatrix}u_7 + \begin{pmatrix}1\\2\end{pmatrix}u_8 + \begin{pmatrix}-1\\1\end{pmatrix}u_2 - \begin{pmatrix}2\\1\end{pmatrix}u_0 - \begin{pmatrix}1\\2\end{pmatrix}u_{18} + \begin{pmatrix}1\\-1\end{pmatrix}u_6\right),$$

and $(G_h u)(z_2), \ldots, (G_h u)(z_6)$ follow the similar pattern. Direct calculation reveals that

$$\begin{aligned}
(H_h^{xx}u)(z_0) = \frac{1}{36h^2}(&-12u_0 + 2u_1 - 4u_2 - 4u_3 + 2u_4 - 4u_5 - 4u_6 + 4u_7 + 4u_8 + u_9\\
&- 2u_{10} + u_{11} + 4u_{12} + 4u_{13} + 4u_{14} + u_{15} - 2u_{16} + u_{17} + 4u_{18}),\\
(H_h^{xy}u)(z_0) = \frac{1}{36h^2}(&6u_0 - u_1 + 5u_2 - u_3 - u_4 + 5u_5 - u_6 - 2u_7 + u_8 + u_9\\
&+ u_{10} - 2u_{11} - 5u_{12} - 2u_{13} + u_{14} + u_{15} + u_{16} - 2u_{17} - 5u_{18}),\\
(H_h^{yx}u)(z_0) = \frac{1}{36h^2}(&6u_0 - u_1 + 5u_2 - u_3 - u_4 + 5u_5 - u_6 - 2u_7 + u_8 + u_9\\
&+ u_{10} - 2u_{11} - 5u_{12} - 2u_{13} + u_{14} + u_{15} + u_{16} - 2u_{17} - 5u_{18}),\\
(H_h^{yy}u)(z_0) = \frac{1}{36h^2}(&-12u_0 - 4u_1 - 4u_2 + 2u_3 - 4u_4 - 4u_5 + 2u_6 + u_7 - 2u_8 + u_9\\
&+ 4u_{10} + 4u_{11} + 4u_{12} + u_{13} - 2u_{14} + u_{15} + 4u_{16} + 4u_{17} + 4u_{18}).
\end{aligned}$$

It is observed that $(H_h^{xy}u)(z_0) = (H_h^{yx}u)(z_0)$, which means the recovered Hessian matrix is symmetric, a property of the exact Hessian we would like to maintain.

Using Taylor expansion, we can show that

$$
\begin{aligned}
(H_h^{xx}u)(z_0) &= u_{xx}(z_0) + \frac{h^2}{3}(u_{xxxx}(z_0) + u_{xxxy}(z_0) + u_{xxyy}(z_0)) + O(h^4),\\
(H_h^{xy}u)(z_0) &= u_{xy}(z_0) + \frac{h^2}{3}(u_{xxxy}(z_0) + u_{xxyy}(z_0) + u_{xyyy}(z_0)) + O(h^4),\\
(H_h^{yx}u)(z_0) &= u_{yx}(z_0) + \frac{h^2}{3}(u_{xxxy}(z_0) + u_{xxyy}(z_0) + u_{xyyy}(z_0)) + O(h^4),\\
(H_h^{yy}u)(z_0) &= u_{yy}(z_0) + \frac{h^2}{3}(u_{xxyy}(z_0) + u_{xyyy}(z_0) + u_{yyyy}(z_0)) + O(h^4),
\end{aligned}
$$

which imply that $H_h u$ provides a second order approximation of Hu at z_0.

Example 4.2. Consider the Chevron pattern uniform mesh as shown in Figure 24(b). Repeating the procedure as in Example 4.1, we derive the recovered Hessian matrix at z_0 as

$$
\begin{aligned}
(H_h^{xx}u)(z_0) &= \frac{1}{144h^2}(-72u_0 + 36u_{13} + 36u_7),\\
(H_h^{xy}u)(z_0) &= \frac{1}{144h^2}(-12u_1 + 12u_3 + 24u_4 - 24u_6 + 6u_7 +\\
&\qquad + 36u_9 - 36u_{11} - 6u_{13} + 6u_{14} - 6u_{18}),\\
(H_h^{yx}u)(z_0) &= \frac{1}{144h^2}(12u_1 - 12u_3 + 36u_4 - 36u_6 - 6u_7 +\\
&\qquad 6u_8 + 24u_9 - 24u_{11} - 6u_{12} + 6u_{13}),\\
(H_h^{yy}u)(z_0) &= \frac{1}{144h^2}(-48u_0 - 10u_1 - 22u_2 - 10u_3 - 10u_4 + 18u_5 -\\
&\qquad 10u_6 - 2u_7 + u_8 + 10u_9 + 36u_{10} + 10u_{11} + u_{12} -\\
&\qquad 2u_{13} + u_{14} + 10u_{15} + 16u_{16} + 10u_{17} + u_{18}).
\end{aligned}
$$

In addition, we have the following Taylor expansion

$$
\begin{aligned}
(H_h^{xx}u)(z_0) &= u_{xx}(z_0) + \frac{h^2}{3}u_{xxxx}(z_0) + \frac{2h^4}{45}u_{xxxxxx}(z_0) + O(h^5),\\
(H_h^{xy}u)(z_0) &= u_{xy}(z_0) + \frac{h^2}{12}(3u_{xxxy}(z_0) + 2u_{xyyy}(z_0)) - \frac{h^3}{24}u_{xxxyy}(z_0) + O(h^4),\\
(H_h^{yx}u)(z_0) &= u_{yx}(z_0) + \frac{h^2}{12}(3u_{xxxy}(z_0) + 2u_{xyyy}(z_0)) + \frac{h^3}{24}u_{xxxyy}(z_0) + O(h^4),\\
(H_h^{yy}u)(z_0) &= u_{yy}(z_0) + \frac{h^2}{6}(u_{xxyy}(z_0) + 2u_{yyyy}(z_0)) - \frac{5h^3}{72}u_{xxyyy}(z_0) + O(h^4).
\end{aligned}
$$

We conclude that $H_h u$ is a second order approximation to the Hessian matrix. It is worth pointing out that, though $H_h^{xy} \neq H_h^{yx}$ for the Chevron pattern uniform mesh, they are both second order finite difference schemes at z_0.

Remark. PPR-PPR is the only one among the four Hessian recovery methods mentioned in Remark 4.3 that provides second order approximation for all five mesh patterns, especially the Chevron pattern.

Both Example 4.1 and 4.2 indicate that for linear element the PPR-PPR approach is equivalent to a finite difference scheme of second order accuracy at vertex z_0. In general, we can show that H_h preserves polynomials of degree up to $k+1$ for kth order element.

Consider P_k-element. Let u be a polynomial of degree $k+1$. Since G_h preserves polynomials of degree $k+1$, it follows that $G_h u = \nabla u$ which is a polynomial of degree k. Therefore, we have

$$
H_h u = (G_h(G_h^x u), G_h(G_h^y u)) = (G_h\frac{\partial u}{\partial x}, G_h\frac{\partial u}{\partial x}) = (\nabla\frac{\partial u}{\partial x}, \nabla\frac{\partial u}{\partial x}) = Hu. \tag{4.12}
$$

It means that H_h preserves polynomials of degree $k+1$ for arbitrary mesh.

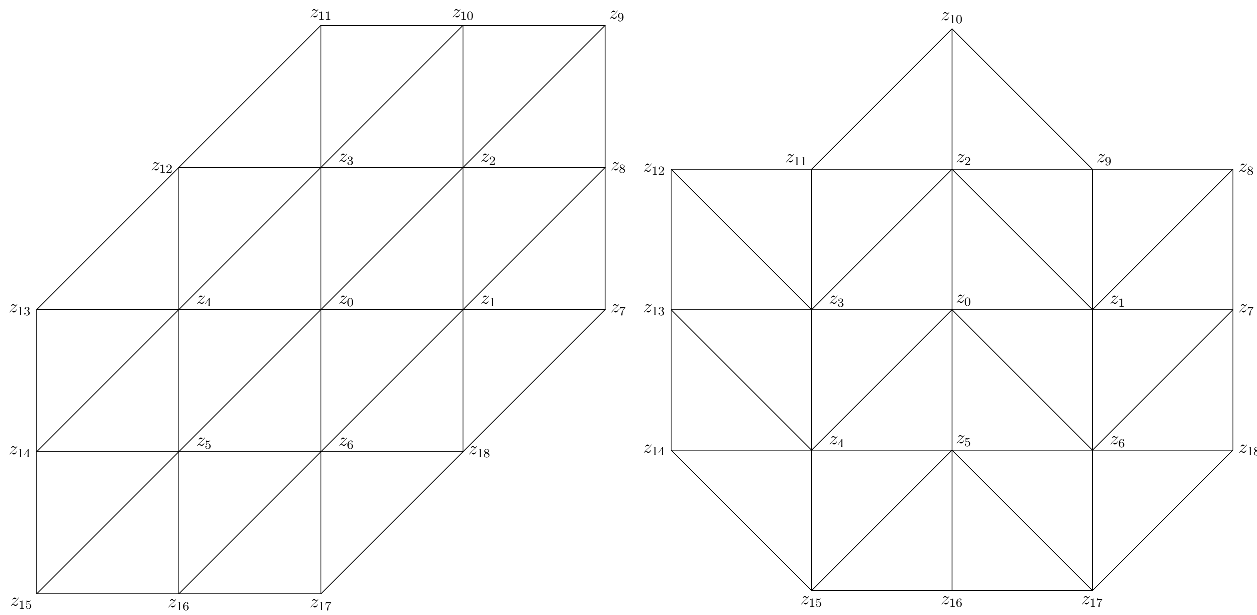

(a) Regular pattern

(b) Chevron pattern

Figure 24: Illustration on Hessian recovery on uniform mesh

Now we proceed to translation invariant mesh. According to the polynomial preserving property (4.6), the recovered gradient is exact for polynomials of degree $k+1$. Therefore

$$G_h^x u = D_x u + h^{k+1}\boldsymbol{a}^x \cdot D^{k+2}u + h^{k+2}\boldsymbol{b}^x \cdot D^{k+3}u + h^{k+3}\boldsymbol{c}^x \cdot D^{k+4}u + \cdots ; \tag{4.13}$$

$$G_h^y u = D_y u + h^{k+1}\boldsymbol{a}^y \cdot D^{k+2}u + h^{k+2}\boldsymbol{b}^y \cdot D^{k+3}u + h^{k+3}\boldsymbol{c}^y \cdot D^{k+4}u + \cdots . \tag{4.14}$$

Note that $\boldsymbol{a}^x, \boldsymbol{a}^y, \boldsymbol{b}^x, \boldsymbol{b}^y, \boldsymbol{c}^x, \boldsymbol{c}^y, \cdots$ are functions of (x, y) if $z = (x, y)$ a nodal point of arbitrary mesh.

Let $\boldsymbol{z} = (x, y)$ be any node on a translation invariant mesh. Notice that coefficients $\boldsymbol{a}^x$, $\boldsymbol{a}^y$, $\boldsymbol{b}^x$, $\boldsymbol{b}^y, \ldots$ depend only on the coordinates of nodes, since we recover gradient at nodes only. Thus for translation invariant meshes, $\boldsymbol{a}^x$, $\boldsymbol{a}^y$, $\boldsymbol{b}^x$, $\boldsymbol{b}^y, \ldots$ are constants. Note that

$$\begin{aligned}
&(H_h^{xy}u)(\boldsymbol{z}) = (G_h^y(G_h^x u))(\boldsymbol{z}) \\
=&G_h^y[D_x u(\boldsymbol{z}) + h^{k+1}\boldsymbol{a}^x \cdot D^{k+2}u(\boldsymbol{z}) + h^{k+2}\boldsymbol{b}^x \cdot D^{k+3}u(\boldsymbol{z}) + \cdots] \\
=&(G_h^y(D_x u))(\boldsymbol{z}) + h^{k+1}(\boldsymbol{a}^x \cdot G_h^y(D^{k+2}u))(\boldsymbol{z}) + h^{k+2}(\boldsymbol{b}^x \cdot G_h^y(D^{k+3}u))(\boldsymbol{z}) + \cdots \\
=&(D_y D_x u)(\boldsymbol{z}) + h^{k+1}(\boldsymbol{a}^y \cdot D^{k+2}D_x u)(\boldsymbol{z}) + h^{k+2}(\boldsymbol{b}^y \cdot D^{k+3}D_x u)(\boldsymbol{z}) \\
&+ h^{k+1}(\boldsymbol{a}^x \cdot D_y(D^{k+2}u))(\boldsymbol{z}) + h^{k+2}(\boldsymbol{b}^x \cdot D_y(D^{k+3}u))(\boldsymbol{z}) + O(h^{k+3}) \\
=&(D_y D_x u)(\boldsymbol{z}) + h^{k+1}[\boldsymbol{a}^y \cdot D^{k+2}D_x u + \boldsymbol{a}^x \cdot D_y(D^{k+2}u)](\boldsymbol{z}) + \\
&h^{k+2}[\boldsymbol{b}^y \cdot D^{k+3}D_x u + \boldsymbol{b}^x \cdot D_y(D^{k+3}u)](\boldsymbol{z}) + O(h^{k+3}).
\end{aligned} \tag{4.15}$$

Notice that (4.15) is valid only at nodal points. Similarly,

$$\begin{aligned}
(H_h^{yx}u)(\boldsymbol{z}) =&(D_x D_y u)(\boldsymbol{z}) + h^{k+1}[\boldsymbol{a}^x \cdot D^{k+2}D_y u + \boldsymbol{a}^y \cdot D_x(D^{k+2}u)](\boldsymbol{z}) + \\
&h^{k+2}[\boldsymbol{b}^x \cdot D^{k+3}D_y u + \boldsymbol{b}^y \cdot D_x(D^{k+3}u)](\boldsymbol{z}) + O(h^{k+3});
\end{aligned} \tag{4.16}$$

$$\begin{aligned}
(H_h^{xx}u)(\boldsymbol{z}) =&(D_x D_x u)(\boldsymbol{z}) + h^{k+1}[\boldsymbol{a}^x \cdot D^{k+2}D_x u + \boldsymbol{a}^x \cdot D_x(D^{k+2}u)](\boldsymbol{z}) + \\
&h^{k+2}[\boldsymbol{b}^x \cdot D^{k+3}D_x u + \boldsymbol{b}^x \cdot D_x(D^{k+3}u)](\boldsymbol{z}) + O(h^{k+3});
\end{aligned} \tag{4.17}$$

$$\begin{aligned}
(H_h^{yy}u)(\boldsymbol{z}) =&(D_y D_y u)(z) + h^{k+1}[\boldsymbol{a}^y \cdot D^{k+2}D_y u + \boldsymbol{a}^y \cdot D_y(D^{k+2}u)](\boldsymbol{z}) + \\
&h^{k+2}[\boldsymbol{b}^y \cdot D^{k+3}D_y u + \boldsymbol{b}^y \cdot D_y(D^{k+3}u)](\boldsymbol{z}) + O(h^{k+3}).
\end{aligned} \tag{4.18}$$

(4.15)–(4.18) imply that the Hessian recovery operator H_h is exact for polynomials of degree $k+2$ for translation invariant meshes. Also, we observe $H_h^{xy} = H_h^{yx}$ from (4.15) and (4.16) if z is a local symmetric center.

It is worth pointing out that, except for the Chevron pattern, (4.15)–(4.18) are valid for the other four patterns of uniform meshes, since the recovered gradient $G_h u$ produces the same stencil at each node.

Next we consider even order ($k = 2r$) element on translation invariant meshes and further assume that $\boldsymbol{z}$ is a local symmetry center for all sampling points involved, in which case

$$\boldsymbol{a}^x(\boldsymbol{z}) = \boldsymbol{0}, \quad \boldsymbol{c}^x(\boldsymbol{z}) = \boldsymbol{0}, \quad \boldsymbol{a}^y(\boldsymbol{z}) = \boldsymbol{0}, \quad \boldsymbol{c}^y(\boldsymbol{z}) = \boldsymbol{0}; \tag{4.19}$$

$$D\boldsymbol{a}^x(\boldsymbol{z}) = \boldsymbol{0}, \quad D\boldsymbol{c}^x(\boldsymbol{z}) = \boldsymbol{0}, \quad D\boldsymbol{a}^y(\boldsymbol{z}) = \boldsymbol{0}, \quad D\boldsymbol{c}^y(\boldsymbol{z}) = \boldsymbol{0}. \tag{4.20}$$

and $\boldsymbol{b}^x, \boldsymbol{b}^y, \cdots$ are constants in (4.14). Here the symbol D is understood as taking all partial derivatives to each entry of the vector. Consequently,

$$(G_h^y u)(\boldsymbol{z}) = (D_y u)(\boldsymbol{z}) + h^{k+2}(\boldsymbol{b}^y \cdot D^{k+3} u)(\boldsymbol{z}) + O(h^{k+4}), \tag{4.21}$$

Also, (4.21) is valid only at nodal points. Plugging (4.13) into (4.21) yields

$$\begin{aligned}
&(H_h^{xy} u)(\boldsymbol{z}) = (G_h^y G_h^x u)(\boldsymbol{z}) \\
=&(D_y G_h^x u)(\boldsymbol{z}) + h^{k+2}(\boldsymbol{b}^y \cdot D^{k+3} G_h^x u)(\boldsymbol{z}) + O(h^{k+4}) \\
=&D_y(D_x u + h^{k+1}\boldsymbol{a}^x \cdot D^{k+2} u + h^{k+2}\boldsymbol{b}^x \cdot D^{k+3} u + h^{k+3}\boldsymbol{c}^x \cdot D^{k+4} u \\
&+ \cdots)(\boldsymbol{z}) + h^{k+2}(\boldsymbol{b}^y \cdot D^{k+3} D_x u)(\boldsymbol{z}) + O(h^{k+4}) \\
=&(D_y D_x u)(\boldsymbol{z}) + h^{k+2}(\boldsymbol{b}^x \cdot D_y D^{k+3} u + \boldsymbol{b}^y \cdot D^{k+3} D_x u)(\boldsymbol{z}) + O(h^{k+4}).
\end{aligned}$$

In the last identity we have used (4.19) and (4.20).

The argument for the other three entries of recovered Hessian matrix are similar. We conclude that the Hessian recovery operator H_h is exact for polynomials of degree up to $k+3$ when k is even and the mesh is translation invariant and symmetric with respect to x and y.

The above results can be summarized as the following theorem:

Theorem 4.1. *The Hessian recovery operator H_h preserves polynomials of degree $k+1$ for an arbitrary mesh. If z is a node of a translation invariant mesh, then H_h preserves polynomials of degree $k+2$. If we further suppose z is local symmetry center for all sampling points involved and k is a even number, then H_h preserves polynomials of degree $k+3$. Moreover, if the sampling points are symmetric with respect to z, then H_h is symmetric.*

Remark. According to [94], the best Hessian recovery method in the literature preserves polynomial of degree 2 for linear element. Our method preserves polynomial of degree 2 on general unstructured meshes and preserves polynomials of degree 3 on translation invariant meshes for linear element.

Theorem 4.2. *Let $u \in W_\infty^{k+2}(\mathcal{K}_z)$; then*

$$\|Hu - H_h u\|_{0,\infty,\mathcal{K}_z} \lesssim h^k |u|_{k+2,\infty,\mathcal{K}_z}.$$

If z is a node of translation invariant mesh and $u \in W_\infty^{k+3}(\mathcal{K}_z)$, then

$$|(Hu - H_h u)(z)| \lesssim h^{k+1} |u|_{k+3,\infty,\mathcal{K}_z}.$$

Furthermore, if z is a symmetric node of translation invariant mesh and $u \in W_\infty^{k+4}(\mathcal{K}_z)$ with

k an even number, then

$$|(Hu - H_h u)(z)| \lesssim h^{k+2} |u|_{k+4,\infty,\mathcal{K}_z}.$$

Proof. It is a direct result of Theorem 4.1 and application of the Hilbert-Bramble Lemma. $\square$

4.4 Superconvergence analysis

In this section, we first use the supercloseness between the gradient of the finite element solution u_h and the gradient of the interpolation $I_h u$ [12, 28, 56, 57, 98, 101], and properties of the PPR operator [107, 79] to establish the superconvergence property of our Hessian recovery operator on mildly structured mesh. Then we utilize the tool of superconvergence by difference quotients from [97] to prove the proposed Hessian recovery method is ultraconvergent for translation invariant finite element space of any order.

4.4.1 Linear element

Linear finite element space $S^{h,1}$ on quasi-uniform mesh $\mathcal{T}_h$ is considered in this subsection. In order to discuss superconvergent result, we need some condition on the mesh. We firstly talk about mesh condition.

Definition 4.3. *The triangulation $\mathcal{T}_h$ is said to satisfy Condition (σ, α) if there exist a partition $\mathcal{T}_{h,1} \cup \mathcal{T}_{h,2}$ of $\mathcal{T}_h$ and positive constants α and σ such that every two adjacent triangles in $\mathcal{T}_{h,1}$ form an $O(h^{1+\alpha})$ parallelogram and*

$$\sum_{T \in \mathcal{T}_{h,2}} |T| = O(h^\sigma).$$

An $O(h^{1+\alpha})$ parallelogram is a quadrilateral shifted from a parallelogram by $O(h^{1+\alpha})$.

For general α and σ, Xu and Zhang [101] proved the following theorem.

Theorem 4.4. *Let u be the solution of (2.2), $u_h \in S^{h,1}$ be the finite element solution of (2.8), and $I_h u \in S^{h,1}$ be the linear interpolation of u. If the triangulation $\mathcal{T}_h$ satisfies Condition (σ, α) and $u \in H^3(\Omega) \cap W^2_\infty(\Omega)$, then*

$$|u_h - I_h u|_{1,\Omega} \lesssim h^{1+\rho}(|u|_{3,\Omega} + |u|_{2,\infty,\Omega}),$$

where $\rho = \min(\alpha, \sigma/2, 1/2)$.

Using the above result, we are able to obtain a convergent result for our Hessian recovery operator.

Theorem 4.5. *Under the same condition as Theorem 4.4, we have*

$$\|Hu - H_h u_h\|_{0,\Omega} \leq h^\rho \|u\|_{3,\infty,\Omega}.$$

Proof. We decompose $Hu - H_h u_h$ as $(Hu - H_h u) + H_h(I_h u - u_h)$, since $H_h u = H_h(I_h u)$. Using the triangle inequality and the definition of H_h, we obtain

$$\begin{aligned}
\|Hu - H_h u_h\|_{0,\Omega} &\leq \|Hu - H_h u\|_{0,\Omega} + \|H_h(I_h u - u_h)\|_{0,\Omega} \\
&= \|Hu - H_h u\|_{0,\Omega} + \|G_h(G_h(I_h u - u_h))\|_{0,\Omega}.
\end{aligned}$$

The first term in the above expression is bounded by $h|u|_{3,\infty,\Omega}$ according to Theorem 4.2.

Since G_h is a bounded linear operator [80], it follows that

$$\|H_h(I_hu - u_h)\|_{0,\Omega} \lesssim \|\nabla(G_h(I_hu - u_h))\|_{0,\Omega}$$

Notice that $G_h(I_hu - u_h)$ is a function in S_h and hence the inverse estimate [35, 25] can be applied. Thus,

$$\|H_h(I_hu - u_h)\|_{0,\Omega} \lesssim h^{-1}\|G_h(I_hu - u_h)\|_{0,\Omega} \lesssim h^{-1}\|I_hu - u_h\|_{1,\Omega}$$

and hence Theorem 4.4 implies that

$$\|H_h(I_hu - u_h)\|_{0,\Omega} \lesssim h^\rho\|u\|_{3,\infty,\Omega}.$$

Combining the above two estimates completes our proof. □

4.4.2 Quadratic element

We proceed to quadratic finite element space $S^{h,2}$. According to [57], a triangulation $\mathcal{T}_h$ is strongly regular if any two adjacent triangles in $\mathcal{T}_h$ form an $O(h^2)$ approximate parallelogram. Huang and Xu proved the following superconvergence results in [57].

Theorem 4.6. *et u be the solution of* (2.2), $u_h \in S^{h,2}$ *be the finite element solution of* (2.8), *and $I_hu \in S^{h,2}$ be the quadratic interpolation of u. If the triangulation $\mathcal{T}_h$ is uniform or strongly regular and $u \in H^4(\Omega)$, then*

$$|u_h - I_hu|_{1,\Omega} \lesssim h^3|u|_{4,\Omega}.$$

Based on the above theorem, we obtain the following superconvergent result.

Theorem 4.7. *Under the same assumption as in Theorem 4.6, we have*

$$\|Hu - H_h u_h\|_{0,\Omega} \leq h^2 \|u\|_{4,\Omega}.$$

Proof. The proof is similar to the proof of Theorem 4.5 by using Theorem 4.6 and the inverse estimate. □

Remark. Theorem 4.7 can be generalized to mildly structured meshes as in [57].

4.4.3 Translation invariant element of any order

First, we observe that the Hessian recovery operator results in a difference quotient. It is due to the fact that G_h is a difference quotient [107] and the composition of two difference quotients is still a difference quotient. Let us take linear element on uniform triangular mesh of the regular pattern as an example, see Figure 24(a). The recovered second order derivative at a nodal point z is

$$\begin{aligned}(H_h^{xx} u_h)(z) = \frac{1}{36h^2}\big(&- 12u_0 + 2u_1 - 4u_2 - 4u_3 + 2u_4 - 4u_5 - 4u_6 + 4u_7 + 4u_8 + u_9 \\ &- 2u_{10} + u_{11} + 4u_{12} + 4u_{13} + 4u_{14} + u_{15} - 2u_{16} + u_{17} + 4u_{18}\big).\end{aligned}$$

Let ϕ_j be the nodal shape functions. Since $\phi_z(z') = \delta_{zz'}$, it follows that

$$
\begin{aligned}
&(H_h^{xx}u_h)\phi_0(x,y)\\
=&\frac{1}{36h^2}[-12u_0\phi_0(x,y) + 2u_1\phi_1(x+h,y) - 4u_2\phi_2(x+h,y+h)\\
&- 4u_3\phi_3(x,y+h) + 2u_4\phi_4(x-h,y) - 4u_5\phi_5(x-h,y-h)\\
&- 4u_6\phi_6(x,y-h) + 4u_7\phi_7(x+2h,y) + 4u_8\phi_8(x+2h,y+h)\\
&+ u_9\phi_9(x+2h,y+2h) - 2u_{10}\phi_{10}(x+h,y+2h) + u_{11}\phi_{11}(x,y+2h)\\
&+ 4u_{12}\phi_{12}(x-h,y+h) + 4u_{13}\phi_{13}(x-2h,y) + 4u_{14}\phi_{14}(x-2h,y-h)\\
&+ u_{15}\phi_{15}(x-2h,y-2h) - 2u_{16}\phi_{16}(x-h,y-2h) + u_{17}\phi_{17}(x,y-2h)\\
&+ 4u_{18}\phi_{18}(x+h,y-h)].
\end{aligned}
$$

The translations are in the directions of $\ell_1 = (1,0)$, $\ell_2 = (0,1)$, $\ell_3 = (\frac{\sqrt{2}}{2}, \frac{\sqrt{2}}{2})$, $\ell_4 = (\frac{\sqrt{2}}{2}, -\frac{\sqrt{2}}{2})$, $\ell_5 = (\frac{\sqrt{5}}{5}, \frac{2\sqrt{5}}{5})$, and $\ell_6 = (\frac{2\sqrt{5}}{5}, \frac{\sqrt{5}}{5})$. Therefore, we can express the recovered second order derivative as

$$(H_h^{xx}u_h)(z) = \sum_{|\nu|\le M}\sum_{i=1}^{6} C_{\nu,h}^{i} u_h(z+\nu h\ell_i), \tag{4.22}$$

for some integer M.

Since u and u_h are the solution of variational problem (2.2) and (2.8), respectively. Then for any $v \in S_0^{h,r}$, we deduce that

$$\mathcal{B}(u-u_h, v) = 0. \tag{4.23}$$

In particular, (4.23) holds for any $v \in S_{00}^{h,r}$.

Let all coefficients in the bilinear form $\mathcal{B}(\cdot,\cdot)$ be constant. Then the orthogonal property

(4.23) impiles

$$\mathcal{B}(T^{\ell}_{\nu\tau}(u-u_h),v)=\mathcal{B}(u-u_h,T^{\ell}_{-\nu\tau}v)=\mathcal{B}(u-u_h,(T^{\ell}_{\nu\tau})^{*}v)=0.$$

for any $v\in S^{h,r}_{00}$.

Therefore, Theorem 5.5.2 of [97] (with $F\equiv 0$) implies that

$$\begin{aligned}\|H^{xx}_h(u-u_h)\|_{0,\infty,\Omega_0}\lesssim\left(\ln\frac{d}{h}\right)^{\bar r}&\min_{v\in S_h}\|H^{xx}_h u-v\|_{0,\infty,\Omega_1}\\&+d^{-s-\frac{2}{q}}\|H^{xx}_h(u-u_h)\|_{-s,q,\Omega_1}.\end{aligned}\tag{4.24}$$

Here $\bar r=1$ for linear element and $\bar r=0$ for higher order element. Note that $H^{xx}_h u\in S^{h,r}$ and hence the first term on the right hand side of (4.24) can be estimated by standard approximation theory under the assumption that the finite element space includes piecewise polynomial of degree k:

$$\min_{v\in S_h}\|H^{xx}_h u-v\|_{0,\infty,\Omega_1}\lesssim h^{k+1}|u|_{k+3,\infty,\Omega_1},\tag{4.25}$$

provided $u\in W^{k+3}_{\infty}(\Omega)$, see [25, 35]. It remains to attack the second term on the right hand side of (4.24). Note that

$$\|H^{xx}_h(u-u_h)\|_{-s,q,\Omega_1}=\sup_{\phi\in C^{\infty}_0(\Omega_1),\|\phi\|_{s,q',\Omega_1}=1}(H^{xx}_h(u-u_h),\phi).\tag{4.26}$$

Here $\frac{1}{q} + \frac{1}{q'} = 1$ and

$$\begin{aligned}(H_h^{xx}(u-u_h), \phi) &= (u-u_h, (H_h^{xx})^*\phi) \\ &\lesssim \|u-u_h\|_{0,\infty,\Omega_2}\|(H_h^{xx})^*\phi\|_{0,1,\Omega_2} \\ &\lesssim \|u-u_h\|_{0,\infty,\Omega_2},\end{aligned} \tag{4.27}$$

where we use the fact that $\|(H_h^{xx})^*\phi\|_{0,1,\Omega_2}$ is bounded uniformly with respect to h when $s \geq 1$. We now once again apply Theorem 5.5.1 from [97] to $\|u-u_h\|_{0,\infty,\Omega_2}$ with $\Omega_2 \subset\subset \Omega$ separated by d, then

$$\begin{aligned}\|u-u_h\|_{0,\infty,\Omega_2} \lesssim &\left(\ln\frac{d}{h}\right)^{\bar{r}} \min_{v\in S_h}\|u-v\|_{0,\infty,\Omega} \\ &+ d^{-s-\frac{2}{q}}\|u-u_h\|_{-s,q,\Omega}.\end{aligned} \tag{4.28}$$

If the separation parameter $d = O(1)$, then we combine (4.24), (4.25) and (5.13) to obtain

$$\|H_h^{xx}(u-u_h)\|_{0,\infty,\Omega_0} \lesssim \left(\ln\frac{1}{h}\right)^{\bar{r}} h^{k+1}\|u\|_{k+3,\infty,\Omega} + \|u-u_h\|_{-s,q,\Omega}. \tag{4.29}$$

Following the same argument, we can establish the same result for H_h^{xy}, H_h^{yx}, and H_h^{yy}. Therefore, (4.29) is satisfied by replacing H_h^{xx} with H_h:

$$\|H_h(u-u_h)\|_{0,\infty,\Omega_0} \lesssim \left(\ln\frac{1}{h}\right)^{\bar{r}} h^{k+1}\|u\|_{k+3,\infty,\Omega} + \|u-u_h\|_{-s,q,\Omega}. \tag{4.30}$$

Now we are in a perfect position to prove our main result for translation invariant finite element space of any order.

Theorem 4.8. *Let all the coefficients in the bilinear operator $B(\cdot,\cdot)$ be constant; let $\Omega_0 \subset\subset \Omega_2 \subset\subset \Omega$ be separated by $d = O(1)$; let the finite element space $S^{h,r}$, which includes piecewise polynomials of degree r, be translation invariant in the directions required by the Hessian recovery operator H_h on Ω_2; and let $u \in W_\infty^{k+3}(\Omega)$. Assume that Theorem 5.2.2 from [97] is applicable. Then*

$$\|Hu - H_h u_h\|_{0,\infty,\Omega_0} \lesssim \left(\ln \frac{1}{h}\right)^{\bar{r}} h^{k+1}\|u\|_{k+3,\infty,\Omega} + \|u - u_h\|_{-s,q,\Omega}. \tag{4.31}$$

for some $s \geq 0$ and $q \geq 1$.

Proof. We decompose

$$Hu - H_h u_h = (Hu - I_h(Hu)) + (I_h(Hu) - H_h u) + H_h(u - u_h), \tag{4.32}$$

where $I_h(Hu) \in \prod_{i=1}^{2} S^{h,r} \times \prod_{i=1}^{2} S^{h,r}$ is the standard Lagrange interpolation of Hu in the finite element space $S^{h,r}$. By the standard approximation theory, we obtain

$$\|Hu - I_h(Hu)\|_{0,\infty,\Omega} \lesssim h^{k+1}|Hu|_{k+1,\infty,\Omega} \lesssim h^{k+1}|u|_{k+3,\infty,\Omega}. \tag{4.33}$$

For the second term, using Theorem 4.2, we have

$$\begin{aligned}
\|I_h(Hu) - H_h u\|_{0,\infty,\Omega_0} =& \|\sum_{z\in\mathcal{N}_h}((Hu)(z) - (H_h u)(z))\phi_z\|_{0,\infty,\Omega_0} \\
&\lesssim \max_{z\in\mathcal{N}_h\cap\Omega_0} |(Hu)(z) - (H_h u)(z)| \\
&\lesssim h^{k+1}|u|_{k+3,\infty,\Omega}.
\end{aligned} \tag{4.34}$$

The last term in (4.32) is bounded by (4.30). The conclusion follows by combining (4.30), (4.33) and (4.34). □

Remark. Theorem 4.8 is a ultraconvergence result under the condition

$$\|u - u_h\|_{-s,q,\Omega} \lesssim h^{k+\sigma}, \quad \sigma > 0.$$

The reader is referred to [85] for negative norm estimates.

4.5 Numerical tests

In this section, two numerical examples are provided to illustrate our Hessian recovery method. The first one is designed to demonstrate the polynomial preserving property of the proposed Hessian recovery method. The second one is devoted to a comparison of our method with some existing Hessian recovery methods in the literature on both uniform and unstructured meshes.

In order to evaluate the performance of Hessian recovery methods, we split mesh nodes $\mathcal{N}_h$ into $\mathcal{N}_{h,1}$ and $\mathcal{N}_{h,2}$, where $\mathcal{N}_{h,2} = \{z \in \mathcal{N}_h : \operatorname{dist}(z, \partial\Omega) \leq L\}$ denotes the set of nodes near boundary and $\mathcal{N}_{h,1} = \mathcal{N}_h \setminus \mathcal{N}_{h,2}$ denotes rest interior nodes. Now, we can define

$$\Omega_{h,1} = \bigcup\{\tau \in \mathcal{T}_h : \tau \text{ has all of its vertices in } \mathcal{N}_{h,1}\},$$

and $\Omega_{h,2} = \Omega \setminus \Omega_{h,1}$. In the following examples we choose $L = 0.1$.

Let $\widetilde{G}_h$ be the weighted average recovery operator. Then we define

$$H_h^{ZZ}u_h = \left(\widetilde{G}_h(\widetilde{G}_h^x u_h), \quad \widetilde{G}_h(\widetilde{G}_h^y u_h)\right),$$

and

$$H_h^{LS}u_h = \left(\widetilde{G}_h(G_h^{x_1} u_h), \quad \widetilde{G}_h(G_h^{x_2} u_h)\right).$$

For any nodal point z, fit a quadratic polynomial p_z at z as PPR. Then H_h^{QF} is defined as

$$H_h^{QF}u_h(z) = \begin{pmatrix} \frac{\partial^2 p_z}{\partial x_1^2}(0,0) & \frac{\partial^2 p_z}{\partial x_1 \partial x_2}(0,0) \\ \frac{\partial^2 p_z}{\partial x_2 \partial x_1}(0,0) & \frac{\partial^2 p_z}{\partial x_2^2}(0,0) \end{pmatrix}.$$

H_h^{ZZ}, H_h^{LS}, and H_h^{QF} are the first three Hessian recovery methods in [89]. To compare them, define

$$De = \|H_h u_h - Hu\|_{L^2(\Omega_{1,h})}, \quad De^{ZZ} = \|H_h^{ZZ}u_h - Hu\|_{L^2(\Omega_{1,h})},$$

$$De^{LS} = \|H_h^{LS}u_h - Hu\|_{L^2(\Omega_{1,h})}, \quad De^{QF} = \|H_h^{QF}u_h - Hu\|_{L^2(\Omega_{1,h})}.$$

where u_h is the finite element solution.

Example 4.3. Consider the following function

$$u(x,y) = sin(\pi x)sin(\pi y), \quad (x,y) \in \Omega = (0,1) \times (0,1). \tag{4.35}$$

Let $I_h u$ be the standard Lagrangian interpolation of u in the finite element space. To validate Theorem 4.2, we apply the Hessian recovery operator H_h to $I_h u$ and consider the discrete maximum error of $H_h(I_h u) - Hu$ at all vertices in $N_{1,h}$. First, linear element on uniform meshes are taken into account. Figure 25 display the numerical results on the uniform meshes. The numerical errors decrease at a rate of $O(h^2)$ for four different pattern uniform meshes. It means the proposed Hessian recovery method preserves polynomial of degree 3 for linear element on uniform meshes.

Next, we consider unstructured meshes. We start from an initial mesh generated by EasyMesh[84] as shown in Figure 26(a), followed by four levels of refinement using bisection. Figure 26(b) shows that the recovered Hessian $H_h(I_h u)$ converges to the exact Hessian at rate $O(h)$. This coincides with the result in Theorem 4.1 that H_h only preserves polynomials of degree 2 on general unstructured meshes

Then we turn to quadratic element. We test the discrete error of recovered Hessian $H_h(I_h u)$ and the exact Hessian Hu using uniform meshes of regular pattern and the same Delaunay meshes. Similarly, we define $\|\cdot\|_{\infty,h}$ as a discrete maximum norm at all vertices and edge centers in an interior region $\Omega_{1,h}$. The result of uniform mesh of regular pattern is reported in Figure 27(a). As predicted by Theorem 4.2, $H_h u_I$ converges to Hu at rate of $O(h^4)$ which implies H_h preserves polynomials of degree 5 for quadratic element on uniform triangulation. For unstructured mesh, we observe that $H_h u_I$ approximates Hu at a rate of $O(h^2)$ from Figure 27(b).

Example 3.5.2. We consider the following elliptic equation

$$\begin{cases} -\Delta u = 2\pi^2 \sin \pi x \sin \pi y, & \text{in } \Omega = [0,1]\times[0,1], \\ u = 0, & \text{on } \partial\Omega. \end{cases} \tag{4.36}$$

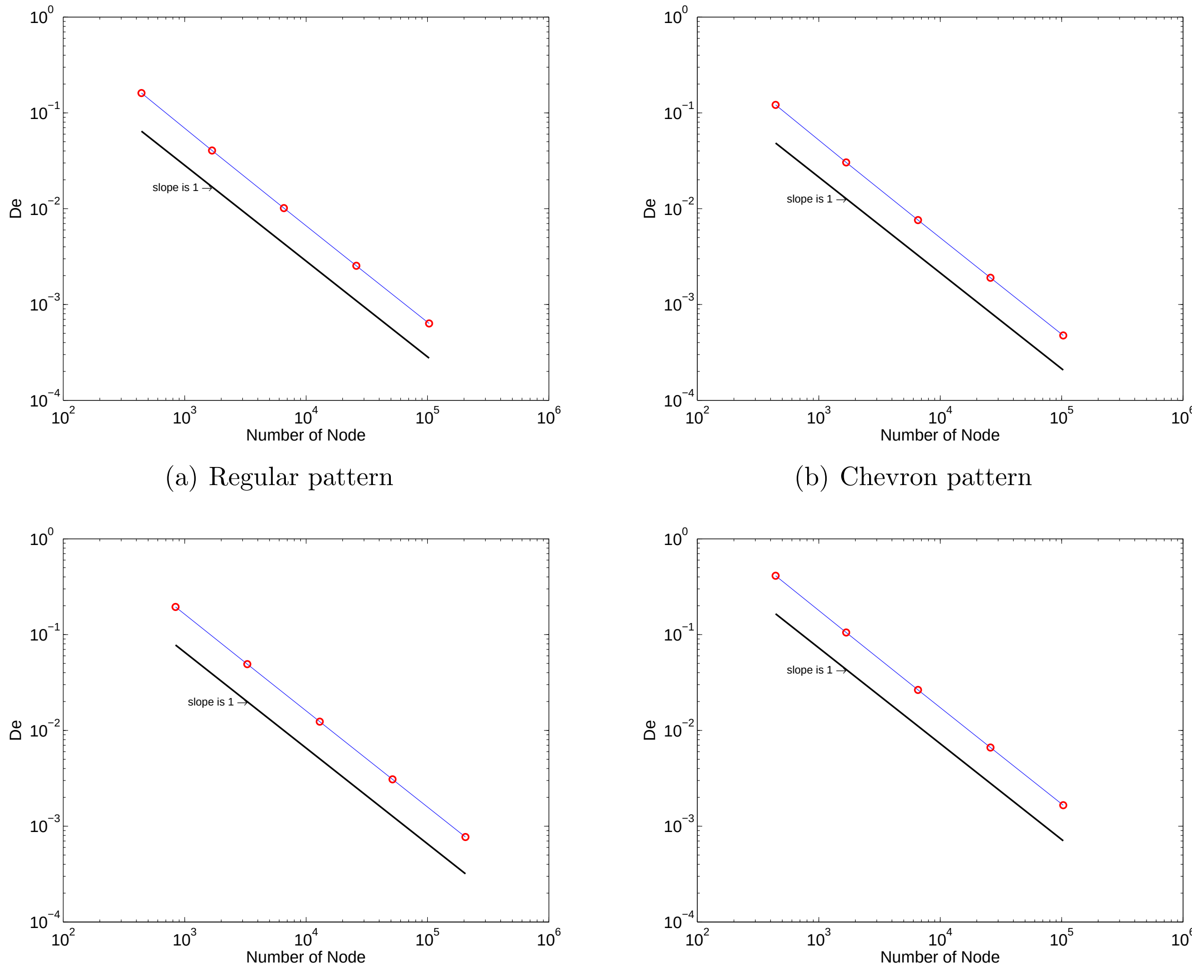

(a) Regular pattern

(b) Chevron pattern

(c) Crisscross pattern

(d) Unionjack pattern

Figure 25: Polynomial preserving property of Hessian recovery for linear element on 2D uniform mesh

The exact solution is $u(x,y) = \sin(\pi x)\sin(\pi y)$. First, linear element is considered. In Table 1, we report the numerical results for regular pattern meshes. All four methods ultraconverge at a rate of $O(h^2)$ in the interior subdomain. It is not a surprise that H_h^{LS} and H_h^{ZZ} perform as good as H_h since it is well known that the polynomial preserving recovery is the same as weighted average for uniform triangular mesh of the regular pattern.

The results of the Chevron pattern is shown in Table 2. $H_h u_h$ approximates Hu at rate $O(h^2)$ while $H_h^{LS} u_h$, $H_h^{ZZ} u_h$ and $H_h^{QF} u_h$ approximate Hu at rate $O(h)$. It is observed that

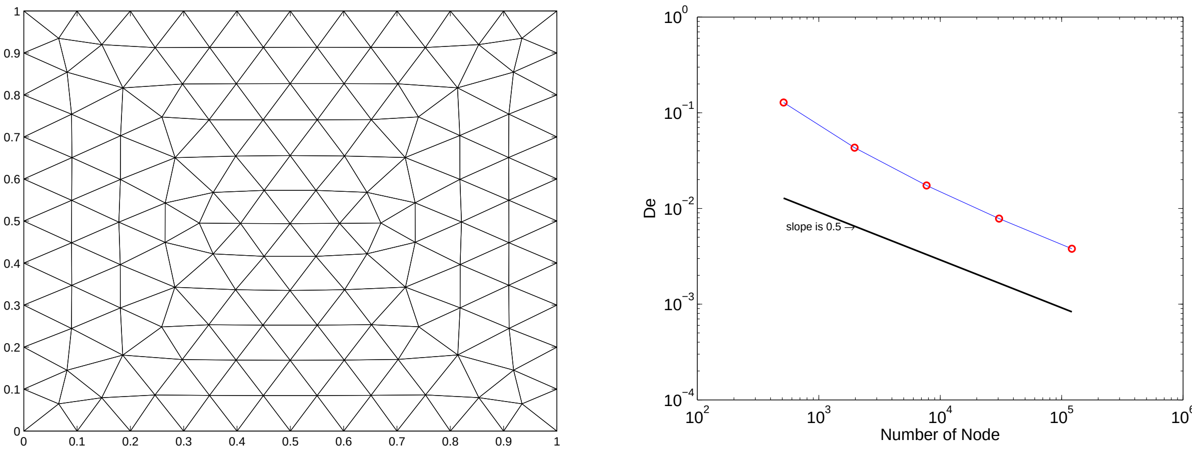

(a) Delaunay mesh (b) Numerical Result

Figure 26: Polynomial preserving property of Hessian recovery for linear element on 2D unstructured mesh

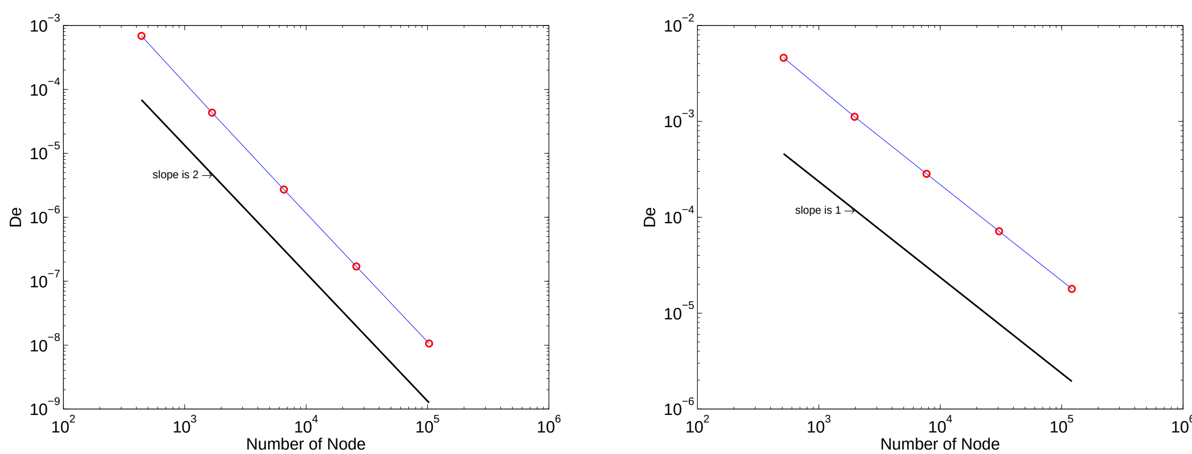

(a) Uniform mesh (b) Delaunay mesh

Figure 27: Polynomial preserving property of Hessian recovery for 2D quadratic element

our method out-performs other three Hessian recovery methods on the Chevron pattern uniform meshes. To the best of our knowledge, the proposed PPR-PPR Hessian recovery is the only method to achieve $O(h^2)$ superconvergence for linear element under the Chevron pattern triangular mesh.

Then the Criss-cross pattern mesh is considered and results are displayed in Table 3. An $O(h^2)$ convergence rate is observed for our recovery method, H_h^{LS} and H_h^{ZZ} while no

Table 1: Comparative results for linear element on 2D regular pattern mesh

Dof	De	order	$De^{ZZ}e$	order	De^{LS}	order	De^{QF}	order
121	7.93e-001		9.73e-001		7.93e-001		4.01e-001	
441	2.02e-001	1.06	2.02e-001	1.22	2.02e-001	1.06	1.03e-001	1.05
1681	5.10e-002	1.03	5.10e-002	1.03	5.10e-002	1.03	2.61e-002	1.03
6561	1.28e-002	1.02	1.28e-002	1.02	1.28e-002	1.02	6.53e-003	1.02
25921	3.20e-003	1.01	3.20e-003	1.01	3.20e-003	1.01	1.63e-003	1.01
103041	8.00e-004	1.00	8.00e-004	1.00	8.00e-004	1.00	4.08e-004	1.00

Table 2: Comparative results for linear element on 2D chevron pattern mesh

Dof	De	order	$De^{ZZ}e$	order	De^{LS}	order	De^{QF}	order
121	6.51e-001		7.98e-001		7.82e-001		9.03e-001	
441	1.34e-001	1.22	2.12e-001	1.03	2.34e-001	0.93	4.30e-001	0.57
1681	3.38e-002	1.03	7.96e-002	0.73	9.87e-002	0.64	2.11e-001	0.53
6561	8.46e-003	1.02	3.57e-002	0.59	4.68e-002	0.55	1.05e-001	0.51
25921	2.11e-003	1.01	1.73e-002	0.53	2.30e-002	0.52	5.23e-002	0.51
103041	5.29e-004	1.00	8.57e-003	0.51	1.15e-002	0.50	2.62e-002	0.50

Table 3: Comparative results for linear element on 2D crisscross pattern mesh

Dof	De	order	$De^{ZZ}e$	order	De^{LS}	order	De^{QF}	order
221	5.49e-001		3.57e-001		4.40e-001		7.14e-001	
841	1.28e-001	1.09	8.03e-002	1.12	1.04e-001	1.08	6.17e-001	0.11
3281	3.22e-002	1.01	2.01e-002	1.02	2.62e-002	1.01	5.95e-001	0.03
12961	8.06e-003	1.01	5.04e-003	1.01	6.55e-003	1.01	5.90e-001	0.01
51521	2.02e-003	1.00	1.26e-003	1.00	1.64e-003	1.00	5.89e-001	0.00
205441	5.04e-004	1.00	3.15e-004	1.00	4.09e-004	1.00	5.88e-001	0.00

Table 4: Comparative results for linear element on 2D unionjack pattern mesh

Dof	De	order	$De^{ZZ}e$	order	De^{LS}	order	De^{QF}	order
121	1.25e+000		8.40e-001		9.87e-001		1.05e+000	
441	3.16e-001	1.06	1.77e-001	1.20	2.48e-001	1.07	6.95e-001	0.32
1681	7.96e-002	1.03	4.46e-002	1.03	6.24e-002	1.03	6.14e-001	0.09
6561	2.00e-002	1.02	1.12e-002	1.02	1.56e-002	1.02	5.95e-001	0.02
25921	5.00e-003	1.01	2.80e-003	1.01	3.91e-003	1.01	5.90e-001	0.01
103041	1.25e-003	1.00	6.99e-004	1.00	9.78e-004	1.00	5.89e-001	0.00

Table 5: Comparative results for linear element on 2D unstructured mesh

Dof	De	order	$De^{ZZ}e$	order	De^{LS}	order	De^{QF}	order
139	4.31e-001		4.38e-001		4.40e-001		3.26e-001	
513	1.38e-001	0.87	2.20e-001	0.53	1.49e-001	0.83	1.79e-001	0.46
1969	5.39e-002	0.70	2.36e-001	-0.05	5.85e-002	0.69	8.88e-002	0.52
7713	2.38e-002	0.60	1.62e-001	0.28	2.55e-002	0.61	4.35e-002	0.52
30529	1.14e-002	0.54	1.13e-001	0.26	1.19e-002	0.56	2.15e-002	0.51
121473	5.59e-003	0.51	7.97e-002	0.25	5.73e-003	0.53	1.07e-002	0.51

convergence rate is observed for H_h^{QF}. The results for the Union-Jack pattern mesh is very similar to the Criss-cross pattern mesh except that our recovery method superconverges at rate $O(h^2)$ as shown in Table 4.

Now, we turn to unstructured mesh generated by EasyMesh [84] as in the previous examples. Numerical data are listed in Table 5. H_h, H_h^{LS} and H_h^{QF} converge at a rate of $O(h^2)$ while H_h^{ZZ} only converges at a rate of $O(h)$.

The results above indicate clearly that our Hessian recovery method converges at rate $O(h)$ on general Delaunay meshes, which is predicted by Theorem 4.5. On uniform meshes, we can obtain $O(h^2)$ ultraconvergence on an interior sub-domain as predicted by Theorem 4.8.

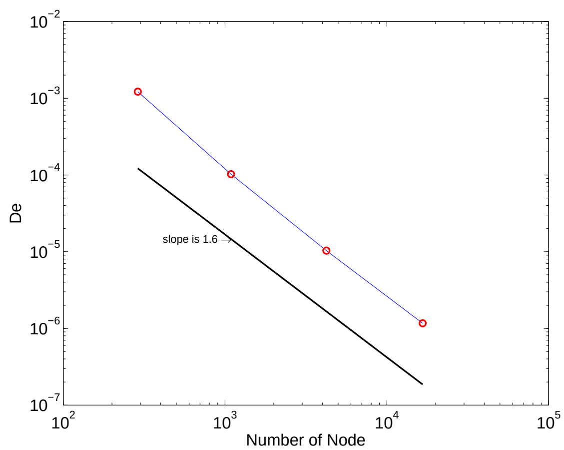

(a) Uniform mesh

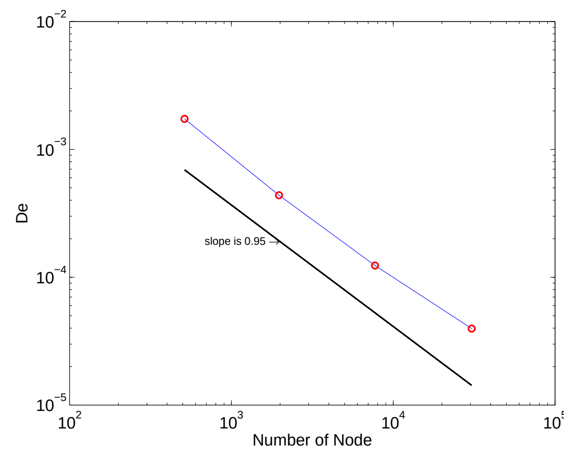

(b) Delaunay mesh

Figure 28: Numerical result of Hessian recovery for 2D quadratic element

Now, we consider quadratic element. Note that our Hessian recovery method is well defined for arbitrary order elements. However, the extension of the other three methods to quadratic element is not straightforward or even impossible and hence only our method is implemented here. We report the numerical results in Figure 28(a) for regular pattern uniform mesh. About $O(h^{3.2})$ order convergence is observed, which is a bit better than the theoretical result predicted by Theorem 4.8. Figure 28(b) shows the result for Delaunay mesh generated by EasyMesh [84]. About $O(h^{1.9})$ superconvergence is observed.

4.6 Conclusion

In this chapter, we introduced a Hessian recovery method for arbitrary order Lagrange finite elements. Theoretically, we proved that the PPR-PPR Hessian recovery operator H_h preserves polynomials of degree $k+1$ on general unstructured meshes and preserves polynomials of degree $k+2$ on translation invariant meshes. This polynomial preserving property, combined with the supercloseness property of the finite element method, enables us to prove convergence and superconvergence results for our Hessian recovery method on mildly structured meshes. Moreover, we proved the ultraconvergence result for translation invariant finite element space of any order by using the argument of superconvergence by difference quotient from [97].

CHAPTER 5 Superconvergent two-grid schemes for elliptic eigenvalue problems

A tremendous variety of science and engineering applications, e.g. the buckling of columns and shells and the vibration of elastic bodies, contain models of eigenvalue problems of partial differential equations. A recent survey article [46] of SIAM Review listed 515 references on theory and application of the Laplacian eigenvalue problem.

In this chapter, we apply PPR gradient recovery to efficient computation of eigenvalue. We combine ideas of the two-grid method[102, 34, 62, 72, 108], two-space method[5, 91], shifted-inverse power method[55, 103], and PPR recovery enhancement [82, 78, 81] to design our new algorithms. The first purpose is to introduce two superconvergent two-grid methods for eigenvalue problems. The new proposed methods enjoy all advantages of the above methods : low computational cost and superconvergence.

In addition, we apply PPR gradient recovery for adaptive finite element method of eigenvalue problems. In the context of adaptive finite element method for elliptic eigenvalue problems, residual type a posteriori error estimators are analyzed in [40, 53, 67] and recovery type a posteriori error estimators are investigated by [75, 99, 73]. For all adaptive methods mentioned above, an algebraic eigenvalue problem has to be solved during every iteration, which is very time consuming. This cost dominates the computational cost of AFEM and usually is ignored. To reduce computational cost, Mehrmann and Miedlar [77] introduced a new adaptive method which only requires an inexact solution of algebraic eigenvalue equation on each iteration by only performing a few iterations of Krylov subspace solver. Recently, Li and Yang [68] proposed an adaptive finite element method based on multi-scale discretization for eigenvalue problems and Xie [100] introduced a type of adaptive finite element method based on the multilevel correction scheme. Both methods only solve an eigenvalue problem on the coarsest mesh and solve boundary value problems on adaptive refined meshes.

The second purpose of this chapter is to propose two multilevel adaptive methods. Using our methods, solving an eigenvalue problem by AFEM will not be more difficult than solving a boundary value problem by AFEM. The most important feature which makes them distinguishing from the methods in [68, 100] is that superconvergence of eigenfunction approximation and ultraconvergence (two order higher) of eigenvalue approximation can be numerically observed.

In Section 5.1, we introduce the model eigenvalue problem and its conforming finite element discretization. Section 5.2 is devoted to presenting two superconvergent two-grid methods and their error estimates. In Section 5.3, we propose two multilevel adaptive methods. Section 5.4 gives some numerical examples to demonstrate efficiency of our new methods and finally some conclusions are drawn in Section 5.5.

5.1 A PDE eigenvalue problem and its conforming finite element discretization

Consider the following second order self adjoint elliptic eigenvalue problem:

$$\begin{cases} -\nabla(\mathcal{D}\nabla u) + cu = \lambda u, & \text{in } \Omega, \\ u = 0, & \text{on } \partial\Omega; \end{cases} \tag{5.1}$$

where $\mathcal{D}$ is a 2×2 symmetric positive definite matrix and $c \in L^{\infty}(\Omega)$. Define a bilinear form $\mathcal{B}(\cdot, \cdot) : H^1(\Omega) \times H^1(\Omega) \to \mathbb{R}$ by

$$\mathcal{B}(u, v) = \int_{\Omega} (\mathcal{D}\nabla u \cdot \nabla v + cuv) dx.$$

Without loss of generality, we may assume that $c \geq 0$. It is easy to see that

$$\mathcal{B}(u, v) \leq C\|u\|_{1,\Omega}\|v\|_{1,\Omega}, \quad \forall u, v \in H_0^1(\Omega),$$

and

$$\mathcal{B}(u, u) \geq \alpha\|u\|_{1,\Omega}^2, \quad \forall u \in H_0^1(\Omega).$$

Define $|||\cdot|||_{\Omega} = \sqrt{\mathcal{B}(\cdot, \cdot)}$. Then $|||\cdot|||_{\Omega}$ and $\|\cdot\|_{1,\Omega}$ are two equivalent norms in $H_0^1(\Omega)$.

The variational formulation of (5.1) reads as: Find $(\lambda, u) \in \mathbb{R} \times H_0^1(\Omega)$ with $u \neq 0$ such that

$$\mathcal{B}(u, v) = \lambda(u, v), \quad \forall v \in H_0^1(\Omega). \tag{5.2}$$

It is well known that (5.2) has a countable sequence of real eigenvalues $0 < \lambda_1 \leq \lambda_2 \leq \lambda_3 \leq \cdots \to \infty$ and corresponding eigenfunctions $u_1, u_2, u_3, \cdots$ which can be assumed to satisfy $\mathcal{B}(u_i, u_j) = \lambda_i(u_i, u_j) = \delta_{ij}$. In the sequence $\{\lambda_j\}$, the λ_i are repeated according to geometric multiplicity.

The finite element discretization of (5.1) is : Find $(\lambda_h, u_h) \in \mathbb{R} \times S_0^{h,r}$ with $u_h \neq 0$ such that

$$\mathcal{B}(u_h, v_h) = \lambda_h(u_h, v_h), \quad \forall v_h \in S_0^{h,r}. \tag{5.3}$$

Similarly, (5.3) has a finite sequence of eigenvalues $0 < \lambda_{1,h} \leq \lambda_{2,h} \leq \cdots \leq \lambda_{n_h,h}$ and corresponding eigenfunctions $u_{1,h}, u_{2,h}, \cdots, u_{n_h,h}$ which can be chosen to satisfy $\mathcal{B}(u_{i,h}, u_{j,h}) = \lambda_{i,h}(u_{i,h}, u_{j,h}) = \delta_{ij}$ with $i, j = 1, 2, \cdots, n_h$ and $n_h = \dim S_0^{h,r}$.

Suppose that the algebraic multicity of λ_i is equal to q, i.e. $\lambda_i = \lambda_{i+1} = \cdots = \lambda_{i+q-1}$. Let $M(\lambda_i)$ be the space spanned by all eigenfunctions corresponding to λ_i. Also, let $M_h(\lambda_h)$ be the direct sum of eigenspaces corresponding to all eigenvalue $\lambda_{i,h}$ that convergences to λ_i.

For the above conforming finite element discretization, the following result has been established by many authors [7, 8, 31, 92, 102, 103].

Theorem 5.1. *Suppose $M(\lambda_i) \subset H_0^1(\Omega) \cap H^{r+1}(\Omega)$. Let $\lambda_{i,h}$ and λ_i be the ith eigenvalue of* (5.3) *and* (5.2)*, respectively. Then*

$$\lambda_i \leq \lambda_{i,h} \leq \lambda_i + Ch^{2r}. \tag{5.4}$$

For any eigenfunction $u_{i,h}$ corresponding to $\lambda_{i,h}$ satisfying $\|u_{i,h}\|_{a,\Omega} = 1$, there exists $u_i \in M(\lambda_i)$ such that

$$|||u_i - u_{i,h}|||_\Omega \leq Ch^r. \tag{5.5}$$

Before ending this subsection, we present an important identity [8] of eigenvalue and eigenfunction approximation.

Lemma 5.2. *Let (λ, u) be the solution of* (5.2)*. Then for any $w \in H_0^1(\Omega)\backslash\{0\}$, there holds*

$$\frac{\mathcal{B}(w,w)}{(w,w)} - \lambda = \frac{\mathcal{B}(w-u, w-u)}{(w,w)} - \lambda\frac{(w-u, w-u)}{(w,w)}. \tag{5.6}$$

This identity will play an important role in our superconvergence analysis.

According to [82], two adjacent triangles (sharing a common edge) form an $O(h^{1+\alpha})$ ($\alpha > 0$) approximate parallelogram if the lengths of any two opposite edges differ by only $O(h^{1+\alpha})$.

Definition 5.3. *The triangulation $\mathcal{T}_h$ is said to satisfy Condition α if any two adjacent triangles form an $O(h^{1+\alpha})$ parallelogram.*

Let G_h be the PPR gradient recovery operator as defined in section 4.2. Using the same methods [107, 93], we can prove the following superconvergence result:

Theorem 5.4. *Suppose $M(\lambda_i) \subset H_0^1(\Omega) \cap W^{3,\infty}(\Omega)$. Further, suppose $\mathcal{T}_h$ satisfies Condition α. Let G_h be the polynomial preserving recovery operator and $r = 1$. Then for any eigenfunction of (5.3) corresponding to $\lambda_{i,h}$, there exists an eigenfunction $u_i \in M(\lambda_i)$ corresponding to λ_i such that*

$$\|\mathcal{D}^{\frac{1}{2}}\nabla u_i - \mathcal{D}^{\frac{1}{2}}G_h u_{i,h}\|_{0,\Omega} \lesssim h^{1+\rho}\|u_i\|_{3,\infty,\Omega}, \tag{5.7}$$

where $\rho = \min(\alpha, 1)$.

As pointed out in [82], $\alpha = \infty$ if $\mathcal{T}_h$ is generated using regular refinement. Fortunately, the fine grid $\mathcal{T}_h$ is always a regular refinement of some coarse grid $\mathcal{T}_H$ for two-grid method. When we introduce two-grid methods in Section 5.2, we only perform gradient recovery on fine grid $\mathcal{T}_h$. Thus we assume $\alpha = \infty$ and hence $\rho = 1$ in section 5.2.

5.2 Superconvergent two-grid methods

In the literature, two-grid methods [102, 103, 55, 108] were proposed to reduce the cost of eigenvalue computations. To further improve the accuracy, two different approaches: gradient recovery enhancement [82, 93, 78, 99] and two-space methods [5, 91] can be used. Individually, those tools are useful in certain circumstances. Combined them properly, we are able to design much effective and superconvergence algorithms, which we shall describe below.

5.2.1 Gradient recovery enhanced shifted inverse power two-grid scheme

In this scheme, we first use the shifted inverse power based two-grid scheme [103, 55] and then apply the gradient recovery enhancing technique [82].

Algorithm 1

---

1. Solve the eigenvalue problem on a coarse grid $\mathcal{T}_H$: Find $(\lambda_{i,H}, u_{i,H}) \in \mathbb{R} \times S_0^{H,1}$ and $\|u_{i,H}\|_a = 1$ satisfying

$$\mathcal{B}(u_{i,H}, v_H) = \lambda_{i,H}(u_{i,H}, v_H), \quad \forall v_H \in S_0^{H,1}. \tag{5.8}$$

2. Solve a source problem on the fine grid $\mathcal{T}_h$: Find $u_h^i \in S_0^{h,1}$ such that

$$\mathcal{B}(u_h^i, v_h) - \lambda_{i,H}(u_h^i, v_h) = (u_{i,H}, v_h), \quad \forall v_h \in S_0^{h,1}, \tag{5.9}$$

   and set $u^{i,h} = \frac{u_h^i}{\|u_h^i\|_a}$.

3. Apply the gradient recovery operator G_h on $u^{i,h}$ to get $G_h u^{i,h}$.

4. Set

$$\lambda^{i,h} = \frac{\mathcal{B}(u^{i,h}, u^{i,h})}{(u^{i,h}, u^{i,h})} - \frac{\|\mathcal{D}^{\frac{1}{2}}\nabla u^{i,h} - \mathcal{D}^{\frac{1}{2}} G_h u^{i,h}\|_{0,\Omega}^2}{(u^{i,h}, u^{i,h})}. \tag{5.10}$$

To prove our main superconvergence result, we need the following Lemma, which was proved in [103, Theorem 4.1].

Lemma 5.5. *Suppose that* $M(\lambda_i) \subset H_0^1(\Omega) \cap W^{3,\infty}(\Omega)$. *Let* $(\lambda^{i,h}, u^{i,h})$ *be an approximate eigenpair of* (5.2) *obtained by Algorithm 1 and let* H *be properly small. Then*

$$dist(u^{i,h}, M_h(\lambda_i)) \lesssim H^4 + h^2, \tag{5.11}$$

where $dist(u^{i,h}, M_h(\lambda_i)) = \inf_{v \in M_h(\lambda_i)} |||u^{i,h} - v|||_\Omega$.

Based on the above Lemma, we can establish the superconvergence result for eigenfunctions.

Theorem 5.6. *Suppose that* $M(\lambda_i) \subset H_0^1(\Omega) \cap W^{3,\infty}(\Omega)$. *Let* $(\lambda^{i,h}, u^{i,h})$ *be an approximate eigenpair of* (5.2) *obtained by Algorithm 1 and let* H *be properly small. Then there exists* $u_i \in M(\lambda_i)$ *such that*

$$\|\mathcal{D}^{\frac{1}{2}} G_h u^{i,h} - \mathcal{D}^{\frac{1}{2}} \nabla u_i\|_{0,\Omega} \lesssim (H^4 + h^2). \tag{5.12}$$

Proof. Let the eigenfunctions $\{u_{j,h}\}_{j=i}^{i+q-1}$ be an orthonormal basis of $M_h(\lambda_i)$. Note that

$$\mathrm{dist}(u^{i,h}, M_h(\lambda_i)) = |||u^{i,h} - \sum_{j=i}^{j=i+q-1} \mathcal{B}(u^{i,h}, u_{j,h}) u_{j,h}|||_\Omega.$$

Let $\widetilde{u}_h = \sum_{j=i}^{j=i+q-1} \mathcal{B}(u^{i,h}, u_{j,h}) u_{j,h}$. According to Theorem 5.4, there exist $\{\widetilde{u}_j\}_{j=i}^{i+q-1} \subset M(\lambda_i)$ such that

$$\|\mathcal{D}^{\frac{1}{2}} G_h u^{j,h} - \mathcal{D}^{\frac{1}{2}} \nabla \widetilde{u}_j\|_{0,\Omega} \lesssim h^2. \tag{5.13}$$

Let $u_i = \sum_{j=i}^{j=i+q-1} \mathcal{B}(u^{i,h}, u_{j,h})\widetilde{u}_j$; then $u_i \in M(\lambda_i)$. Using (5.13), we can derive that

$$
\begin{aligned}
&\|\mathcal{D}^{\frac{1}{2}} G_h \widetilde{u}^h - \mathcal{D}^{\frac{1}{2}} \nabla u_i\|_{0,\Omega} \\
=&\|\sum_{j=i}^{j=i+q-1} \mathcal{B}(u^{i,h}, u_{j,h})(\mathcal{D}^{\frac{1}{2}} G_h u_{j,h} - \mathcal{D}^{\frac{1}{2}} \nabla \widetilde{u}_j)\|_{0,\Omega} \\
\lesssim&\left(\sum_{j=i}^{j=i+q-1} \|(\mathcal{D}^{\frac{1}{2}} G_h u_{j,h} - \mathcal{D}^{\frac{1}{2}} \nabla \widetilde{u}_j)\|_{0,\Omega}^2\right)^{\frac{1}{2}} \\
\lesssim&h^2.
\end{aligned}
$$

Thus, we have

$$
\begin{aligned}
&\|\mathcal{D}^{\frac{1}{2}} G_h u^{i,h} - \mathcal{D}^{\frac{1}{2}} \nabla u_i\|_{0,\Omega} \\
\leq&\|\mathcal{D}^{\frac{1}{2}} G_h(u^{i,h} - \widetilde{u}_h)\|_{0,\Omega} + \|\mathcal{D}^{\frac{1}{2}} G_h \widetilde{u}_h - \mathcal{D}^{\frac{1}{2}} \nabla u_i\|_{0,\Omega} \\
\lesssim&\|G_h(u^{i,h} - \widetilde{u}_h)\|_{0,\Omega} + h^2 \\
\lesssim&\|\nabla(u^{i,h} - \widetilde{u}_h)\|_{0,\Omega} + h^2 \\
\lesssim&|||u^{i,h} - \widetilde{u}_h|||_{\Omega} + h^2 \\
\lesssim&(H^4 + h^2) + h^2 \\
\lesssim&H^4 + h^2;
\end{aligned}
$$

where we use Lemma 5.5 to bound $\|u^{i,h} - \widetilde{u}_h\|_{a,\Omega}$.

The following Lemma is needed in the proof of a superconvergence property of our eigenvalue approximation.

Lemma 5.7. *Suppose that $M(\lambda_i) \subset H_0^1(\Omega) \cap W^{3,\infty}(\Omega)$. Let $(\lambda^{i,h}, u^{i,h})$ be an approximate* *eigenpair of* (5.2) *obtained by Algorithm 1 and let H be properly small. Then*

$$\|\mathcal{D}^{\frac{1}{2}}G_h u^{i,h} - \mathcal{D}^{\frac{1}{2}}\nabla u^{i,h}\|_{0,\Omega} \lesssim (H^2 + h). \tag{5.14}$$

Proof. Let $\widetilde{u}_h$ be defined as in Theorem 5.6. Then we have

$$\begin{aligned}
&\|\mathcal{D}^{\frac{1}{2}}G_h u^{i,h} - \mathcal{D}^{\frac{1}{2}}\nabla u^{i,h}\|_{0,\Omega} \\
\leq&\|\mathcal{D}^{\frac{1}{2}}G_h u^{i,h} - \mathcal{D}^{\frac{1}{2}}G_h \widetilde{u}_h\|_{0,\Omega} + \|\mathcal{D}^{\frac{1}{2}}G_h \widetilde{u}_h - \mathcal{D}^{\frac{1}{2}}\nabla \widetilde{u}_h\|_{0,\Omega} + \|\mathcal{D}^{\frac{1}{2}}\nabla \widetilde{u}_h - \mathcal{D}^{\frac{1}{2}}\nabla u^{i,h}\|_{0,\Omega} \\
\lesssim&\|G_h u^{i,h} - G_h \widetilde{u}_h\|_{0,\Omega} + \|\mathcal{D}^{\frac{1}{2}}G_h \widetilde{u}_h - \mathcal{D}^{\frac{1}{2}}\nabla \widetilde{u}_h\|_{0,\Omega} + \|\mathcal{D}^{\frac{1}{2}}\nabla \widetilde{u}_h - \mathcal{D}^{\frac{1}{2}}\nabla u^{i,h}\|_{0,\Omega} \\
\lesssim&\|\nabla u_{i,h} - \nabla \widetilde{u}_h\|_{0,\Omega} + \|\mathcal{D}^{\frac{1}{2}}G_h \widetilde{u}_h - \mathcal{D}^{\frac{1}{2}}\nabla \widetilde{u}_h\|_{0,\Omega} \\
\lesssim&|||u_{i,h} - \widetilde{u}_h|||_{\Omega} + \|\mathcal{D}^{\frac{1}{2}}G_h \widetilde{u}_h - \mathcal{D}^{\frac{1}{2}}\nabla \widetilde{u}_h\|_{0,\Omega} \\
\lesssim&(H^4 + h^2) + h \\
\lesssim&(H^2 + h).
\end{aligned}$$

Here we use the fact that $|||\cdot|||_{\Omega}$ and $\|\cdot\|_{1,\Omega}$ are two equivalent norms on $H_0^1(\Omega)$.

Now we are in a perfect position to prove our main superconvergence result for eigenvalue approximation.

Theorem 5.8. *Suppose that* $M(\lambda_i) \subset H_0^1(\Omega) \cap W^{3,\infty}(\Omega)$. *Let* $(\lambda^{i,h}, u^{i,h})$ *be an approximate eigenpair of* (5.2) *obtained by Algorithm 1 and let H be properly small.*

$$|\lambda^{i,h} - \lambda_i| \lesssim H^6 + h^3. \tag{5.15}$$

Proof. It follows from (5.6) and (5.10) that

$$
\begin{aligned}
&\lambda^{i,h} - \lambda_i \\
=&\frac{\mathcal{B}(u^{i,h}, u^{i,h})}{(u^{i,h}, u^{i,h})} - \frac{\|\mathcal{D}^{\frac{1}{2}}\nabla u^{i,h} - \mathcal{D}^{\frac{1}{2}}G_h u^{i,h}\|_{0,\Omega}^2}{(u^{i,h}, u^{i,h})} - \lambda_i \\
=&\frac{\mathcal{B}(u^{i,h} - u_i, u^{i,h} - u_i)}{(u^{i,h}, u^{i,h})} - \frac{\|\mathcal{D}^{\frac{1}{2}}\nabla u^{i,h} - \mathcal{D}^{\frac{1}{2}}G_h u^{i,h}\|_{0,\Omega}^2}{(u^{i,h}, u^{i,h})} - \frac{\lambda_i(u^{i,h} - u_i, u^{i,h} - u_i)}{(u^{i,h}, u^{i,h})} \\
=&\frac{(\mathcal{D}^{\frac{1}{2}}(u^{i,h} - u_i), \mathcal{D}^{\frac{1}{2}}(u^{i,h} - u_i))}{(u^{i,h}, u^{i,h})} - \frac{\|\mathcal{D}^{\frac{1}{2}}\nabla u^{i,h} - \mathcal{D}^{\frac{1}{2}}G_h u^{i,h}\|_{0,\Omega}^2}{(u^{i,h}, u^{i,h})} + \\
&\frac{(c(u^{i,h} - u_i), u^{i,h} - u_i) - \lambda_i(u^{i,h} - u_i, u^{i,h} - u_i)}{(u^{i,h}, u^{i,h})} \\
=&\frac{\|\mathcal{D}^{\frac{1}{2}}\nabla G_h u^{i,h} - \mathcal{D}^{\frac{1}{2}}\nabla u_i\|_{0,\Omega}^2}{(u^{i,h}, u^{i,h})} + \frac{2(\mathcal{D}^{\frac{1}{2}}G_h u^{i,h} - \mathcal{D}^{\frac{1}{2}}\nabla u_i, \mathcal{D}^{\frac{1}{2}}\nabla u^{i,h} - \mathcal{D}^{\frac{1}{2}}G_h u^{i,h})}{(u^{i,h}, u^{i,h})} + \\
&\frac{(c(u^{i,h} - u_i), u^{i,h} - u_i) - \lambda_i(u^{i,h} - u_i, u^{i,h} - u_i)}{(u^{i,h}, u^{i,h})}.
\end{aligned}
$$

From Theorem 4.1 in [103], we know that $\|u^{i,h} - u_i\|_{0,\Omega} \lesssim (H^4 + h^2)$ and hence the last term in the above equation is bounded by $O((H^4 + h^2)^2)$. Theorem 5.6 implies that the first term is also bounded by $O((H^4 + h^2)^2)$. Using the Hölder inequality, we obtain

$$
\begin{aligned}
& |(\mathcal{D}^{\frac{1}{2}}G_h u^{i,h} - \mathcal{D}^{\frac{1}{2}}\nabla u_i, \mathcal{D}^{\frac{1}{2}}\nabla u^{i,h} - \mathcal{D}^{\frac{1}{2}}G_h u^{i,h})| \\
\leq\ & \|\mathcal{D}^{\frac{1}{2}}G_h u^{i,h} - \mathcal{D}^{\frac{1}{2}}\nabla u_i\|_{0,\Omega}\|\mathcal{D}^{\frac{1}{2}}\nabla u^{i,h} - \mathcal{D}^{\frac{1}{2}}G_h u^{i,h})\|_{0,\Omega} \\
\lesssim\ & (H^4 + h^2)(H^2 + h) \lesssim H^6 + h^3 \qquad (5.16)
\end{aligned}
$$

and hence

$$|\lambda^{i,h} - \lambda_i| \lesssim H^6 + h^3.$$

This completes our proof.

Taking $H = O(\sqrt{h})$, Theorem 5.6 and 5.8 implies that we can get $O(h^2)$ superconvergence and $O(h^3)$ superconvergence for eigenfunction and eigenvalue approximation, respectively.

Remark. Using the Hölder inequality to estimate (5.16) does not take into account the cancellation in the integral. Similar as [82], numerical experiments show that the actual bound is

$$|(\mathcal{D}^{\frac{1}{2}} G_h u^{i,h} - \mathcal{D}^{\frac{1}{2}} \nabla u_i, \mathcal{D}^{\frac{1}{2}} \nabla u^{i,h} - \mathcal{D}^{\frac{1}{2}} G_h u^{i,h})| \lesssim (H^4 + h^2)^2,$$

which says that we have "double"-order gain by applying recovery.

Remark. Algorithm 1 is a combination of the shifted inverse power two-grid method [103, 55] and gradient recovery enhancement [82]. It inherits all excellent properties of both methods: low computational cost and superconvergence. We will demonstrate in our numerical tests that Algorithm 1 outperforms shifted inverse power two-grid method in [103, 55].

Remark. If we firstly use classical two-grid methods as in [102] and then apply gradient recovery, we can prove $\|\mathcal{D}^{\frac{1}{2}} G_h u^{i,h} - \mathcal{D}^{\frac{1}{2}} \nabla u_i\|_{0,\Omega} \lesssim (H^2 + h^2)$ and $|\lambda^{i,h} - \lambda_i| \lesssim H^3 + h^3$. It means we can only get optimal convergence rate insteading of superconvergent convergence rate when $H = O(\sqrt{h})$.

5.2.2 Higher order space based superconvergent two-grid scheme

Our second scheme can be viewed as a combination of the two-grid scheme proposed by Yang and Bi [103] or Hu and Cheng [55] and the two-space method introduced by Racheva and Andreev [91].

Note that we use linear finite element space $S_0^{H,1}$ on coarse grid $\mathcal{T}_H$ and quadratic finite element space $S_0^{h,2}$ on fine grid $\mathcal{T}_h$. Compared with the two-grid scheme [103, 55], the main

Algorithm 2

1. Solve an eigenvalue problem on a coarse grid $\mathcal{T}_H$: Find $(\lambda_{i,H}, u_{i,H}) \in \mathbb{R} \times S_0^{H,1}$ and $\|u_{i,H}\|_a = 1$ satisfying

$$\mathcal{B}(u_{i,H}, v_H) = \lambda_{i,H}(u_{i,H}, v_H), \quad \forall v_H \in S_0^{H,1}. \tag{5.17}$$

2. Solve a source problem on the fine grid $\mathcal{T}_h$: Find $u_h^i \in S_0^{h,2}$ such that

$$\mathcal{B}(u^{i,h}, v_h) - \lambda_{i,H}(u^{i,h}, v_h) = (u_{i,H}, v_h), \quad \forall v_h \in S_0^{h,2}. \tag{5.18}$$

3. Compute the Rayleigh quotient

$$\lambda^{i,h} = \frac{\mathcal{B}(u^{i,h}, u^{i,h})}{(u^{i,h}, u^{i,h})}. \tag{5.19}$$

---

difference is that Algorithm 2 uses linear element on coarse grid $\mathcal{T}_H$ and quadratic element on fine grid $\mathcal{T}_h$ while the two-grid uses linear element on both coarse grid $\mathcal{T}_H$ and $\mathcal{T}_h$. Compared with the two-space method [91], the main difference is that Algorithm 2 uses a coarse grid $\mathcal{T}_H$ and a fine grid $\mathcal{T}_h$ whereas the two-space method only uses a grid $\mathcal{T}_h$. Algorithm 2 shares the advantages of both methods: low computational cost and high accuracy. Thus, we would expect Algorithm 2 performs much better than both methods.

For Algorithm 2, we have the following Theorem:

Theorem 5.9. *Suppose that $M(\lambda_i) \subset H_0^1(\Omega) \cap H^3(\Omega)$. Let $(\lambda^{i,h}, u^{i,h})$ be an approximate eigenpair of* (5.2) *by Algorithm 1 and let H be properly small. Then there exists $u_i \in M(\lambda_i)$ such that*

$$|||u^{i,h} - u_i|||_\Omega \lesssim (H^4 + h^2); \tag{5.20}$$

$$\lambda^{i,h} - \lambda_i \lesssim (H^8 + h^4). \tag{5.21}$$

Proof. By Theorem 4.1 in [103], we have

$$|||u^{i,h} - u_i|||_\Omega \lesssim \eta_a(H)\delta_H^3(\lambda_i) + \delta_h(\lambda_i); \tag{5.22}$$

and

$$\lambda^{i,h} - \lambda_i \lesssim \eta_a^2(H)\delta_H^6(\lambda_i) + \delta_h^2(\lambda_i). \tag{5.23}$$

Since we use linear element on $\mathcal{T}_H$ and quadratic element on $\mathcal{T}_h$, it follows from the interpolation error estimate [25, 35] that

$$\eta_a(H) \lesssim H, \quad \delta_H(\lambda_i) \lesssim H, \quad \delta_h(\lambda_i) \lesssim h^2.$$

Substituting the above three estimate into (5.22) and (5.23), we get (5.20) and (5.21).

Comparing Algorithm 1 and 2, the main difference is that Algorithm 1 solves a source problem on fine grid $\mathcal{T}_h$ using linear element and hence perform gradient recovery while Algorithm 2 solves a source problem on fine grid $\mathcal{T}_h$ using quadratic element. Both Algorithm 1 and 2 lead to $O(h^2)$ superconvergence for eigenfunction approximation and $O(h^4)$ ultraconvergence for eigenvalue approximation by taking $H = O(\sqrt{h})$. The message we would like to deliver here is that polynomial preserving recovery plays a similar role as quadratic element, but with much lower computational cost.

Remark. In order to get higher order convergence, we require higher regualrity such as $M(\lambda_i) \subset H_0^1(\Omega) \cap W^{3,\infty}(\Omega)$ for Algorithm 1 and $M(\lambda_i) \subset H_0^1(\Omega) \cap H^3(\Omega)$ for Algorithm 2, in the proof. However, we can use Algorithm 1 and 2 to get high accuracy approximation even with low regularity.

5.3 Multilevel adaptive methods

Algorithm 3 Given a tolerance $\epsilon > 0$ and a parameter $0 \leq \theta < 1$.

1. Generate an initial mesh $\mathcal{T}_{h_0}$.
2. Solve (5.2) on $\mathcal{T}_{h_0}$ to get a discrete eigenpair $(\bar{\lambda}^{h_0}, u^{h_0})$.
3. Set $\ell = 0$.
4. Compute $\eta(u^{h_\ell}, T)$ and $\eta(u^{h_\ell}, \Omega)$, then let
$$\lambda^{h_\ell} = \bar{\lambda}^{h_\ell} - \eta(u^{h_\ell}, \Omega)^2.$$
5. If $\eta(u^{h_\ell}, \Omega)^2 < \epsilon$, stop; else go to 6.
6. Choose a minimal subset of elements $\widehat{\mathcal{T}}_{h_\ell} \subset \mathcal{T}_{h_\ell}$ such that
$$\sum_{T \in \widehat{\mathcal{T}}_{h_\ell}} \eta^2(u_h, T) \geq \theta \eta^2(u_h, \Omega);$$
then refine the elements in $\widehat{\mathcal{T}}_{h_\ell}$ and necessary elements to get a new conforming mesh $\mathcal{T}_{h_{\ell+1}}$.
7. Find $u \in S_0^{h_{\ell+1},1}$ such that
$$\mathcal{B}(u, v) = \lambda_{h_\ell}(u^{h_\ell}, v), \quad v \in S_0^{h_{\ell+1},1},$$
and set $u^{h_{\ell+1}} = \frac{u}{\|u\|_{0,\Omega}}$. Define
$$\bar{\lambda}^{h_{\ell+1}} = \frac{\mathcal{B}(u^{h_{\ell+1}}, u^{h_{\ell+1}})}{(u^{h_{\ell+1}}, u^{h_{\ell+1}})}. \tag{5.24}$$
8. Let $\ell = \ell + 1$ and go to 4.

In this section, we incorporate two-grid methods and gradient recovery enhancing technique into the framework of adaptive finite element method and propose two multilevel adaptive methods. Both methods only need to solve an eigenvalue problem on initial mesh and solve an associated boundary value problem on adaptive refined mesh during every iteration.

Algorithm 4 Given a tolerance $\epsilon > 0$ and a parameter $0 \leq \theta < 1$.

1. Generate an initial mesh $\mathcal{T}_{h_0}$.
2. Solve (5.2) on $\mathcal{T}_{h_0}$ to get a discrete eigenpair $(\bar{\lambda}^{h_0}, u^{h_0})$.
3. Set $\ell = 0$.
4. Compute $\eta(u^{h_\ell}, T)$ and $\eta(u^{h_\ell}, \Omega)$, then let
$$\lambda^{h_\ell} = \bar{\lambda}^{h_\ell} - \eta(u^{h_\ell}, \Omega)^2.$$
5. If $\eta(u^{h_\ell}, \Omega)^2 < \epsilon$, stop; else go to 6.
6. Choose a minimal subset of elements $\widehat{\mathcal{T}}_{h_\ell} \subset \mathcal{T}_{h_\ell}$ such that
$$\sum_{T \in \widehat{\mathcal{T}}_{h_\ell}} \eta^2(u_h, T) \geq \theta \eta^2(u_h, \Omega);$$
then refine the elements in $\widehat{\mathcal{T}}_{h_\ell}$ and necessary elements to get a new conforming mesh $\mathcal{T}_{h_{\ell+1}}$.
7. Find $u \in S_0^{h_{\ell+1},1}$ such that
$$\mathcal{B}(u, v) - \lambda_{h_\ell}(u, v) = (u^{h_\ell}, v), \quad v \in S_0^{h_{\ell+1},1}, \tag{5.25}$$
and set $u^{h_{\ell+1}} = \frac{u}{\|u\|_{0,\Omega}}$. Define
$$\bar{\lambda}^{h_{\ell+1}} = \frac{\mathcal{B}(u^{h_{\ell+1}}, u^{h_{\ell+1}})}{(u^{h_{\ell+1}}, u^{h_{\ell+1}})}.$$
8. Let $\ell = \ell + 1$ and go to 4.

Let u_h be a finite element solution in $S^{h,1}$ and G_h be PPR recovery operator. Define a local a posteriori error estimator on the element T as

$$\eta(u_h, T) = \|\mathcal{D}^{\frac{1}{2}} G_h u_h - \mathcal{D}^{\frac{1}{2}} \nabla u_h\|_{0,T}, \tag{5.26}$$

and a global error estimator as

$$\eta(u_h, \Omega) = \left(\sum_{T \in \mathcal{T}_h} \eta(u_h, T)^2 \right)^{\frac{1}{2}}. \tag{5.27}$$

Given a tolerance ϵ and a parameter θ, we describe our multilevel adaptive methods in Algorithm 3 and 4. Here we use Dörfler marking strategy [38] in step 6.

Note that the only difference between Algorithm 3 and 4 is that they solve different boundary value problems on step 7. Algorithm 3 solves boundary value problem (5.24) like two-grid scheme in [102] while Algorithm 4 solves boundary value problem (5.25) similar to two-grid scheme in [103, 55]. Boundary value problem (5.25) would lead to a near singular linear system. Although there are many efficient iterative methods, like multigrid methods, as pointed out in [55], the computational cost of solving (5.24) should be higher than (5.25). Numerical results of both methods are almost the same as indicated by examples in next section. Thus, Algorithm 3 is highly recommended.

Compared to methods in [68, 100], Algorithm 3 and 4 use recovery based a posteriori error estimator. The propose of gradient recovery in the above two algorithms is twofold. The first one is to provide an asymptotically exact a posteriori error estimator. The other is to greatly improve the accuracy of eigenvalue and eigenfunction approximations. Superconvergence result $O(N^{-1})$ and ultraconvergence $O(N^{-2})$ are numerically observed for eigenfunction and eigenvalue approximation respectively. However, methods in [68, 100] can only numerically give asymptotically optimal results. We would like to emphasize that the new algorithms can get superconvergence or ultraconvergence results with no more or even less computational cost compared to the methods proposed in [68, 100].

5.4 Numerical Experiment

In this section, we present several numerical examples to demonstrate the effectiveness and superconconvergence of the proposed algorithms and validity our theoretical results.

The first example is designed to demonstrate superconvergence property of Algorithm 1 and 2 and make some comparison with the two-grid scheme in [103, 55]. Let the ith eigenpairs obtained by Algorithm 1 and 2 be denoted by $(\lambda^{i,\mathrm{A1}}, u^{i,\mathrm{A1}})$ and $(\lambda^{i,\mathrm{A2}}, u^{i,\mathrm{A2}})$. Also, let $(\lambda^{i,\mathrm{TG}}, u^{i,\mathrm{TG}})$ be the ith eigenpair produced by the shift inverse based two-grid scheme in [103, 55].

The presentation of other examples is used to illustrate the effectiveness and sueprconvergence of Algorithm 3 and 4. In these examples, we focus on the first eigenpair. Let $\bar{\lambda}_{\mathrm{A3}}$ and λ_{A3} be the eigenvalue generated by Algorithm 3 without and with gradient recovery enhancing, respectively. Define $\bar{\lambda}_{\mathrm{A4}}$, λ_{A4}, u_{A3}, and u_{A4} in a similar way.

Example 5.1. Consider the following Laplace eigenvalue problem

$$\begin{cases} -\Delta u = \lambda u, \quad \text{in } \Omega, \\ u = 0, \quad \text{on } \partial\Omega, \end{cases} \tag{5.28}$$

where $\Omega = (0,1)\times(0,1)$. The eigenvalue of (5.28) are $\lambda_{k,l} = (k^2+l^2)\pi^2$ and the corresponding eigenfunctions are $u_{k,l} = \sin(k\pi x)\sin(l\pi y)$ with $k, l = 1, 2, \cdots$. It is easy to see the first three eigenvalues are $\lambda_1 = 2\pi^2$ and $\lambda_2 = \lambda_3 = 5\pi^2$.

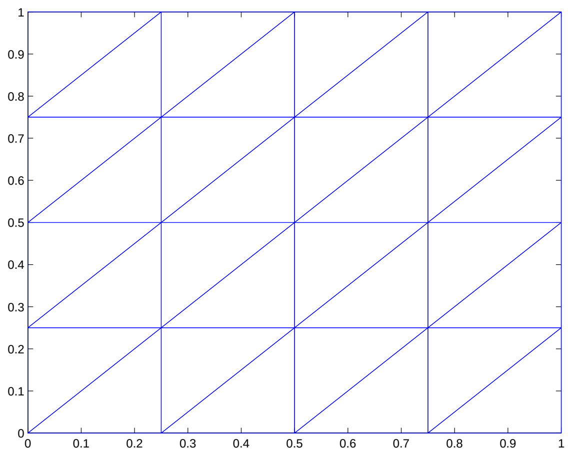

Figure 29: Uniform Mesh

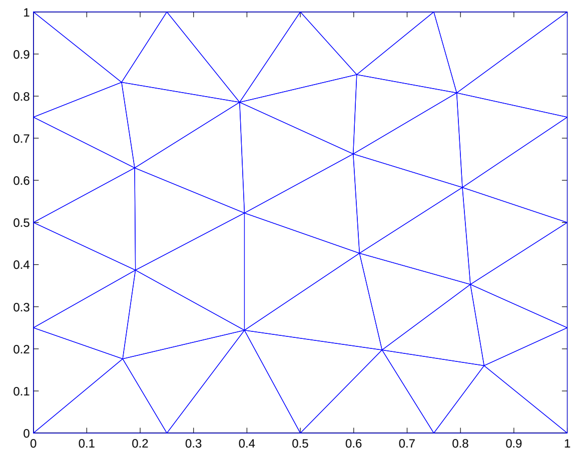

Figure 30: Delaunay Mesh

Table 6: Eigenpair errors of Algorithm 1 for Example 1 on Uniform Mesh

i	H	h	$\lambda^{i,\mathrm{A1}}$	$\lambda^{i,\mathrm{A1}} - \lambda_i$	*Order*	$\|G_h u^{i,\mathrm{A1}} - \nabla u_i\|_{0,\Omega}$	*Order*
1	1/4	1/16	19.733813512912	-5.40e-03		7.059395e-02	
1	1/8	1/64	19.739186935311	-2.19e-05	3.97	4.387700e-03	2.00
1	1/16	1/256	19.739208716241	-8.59e-08	4.00	2.734342e-04	2.00
1	1/32	1/1024	19.739208801843	-3.36e-10	4.00	1.707544e-05	2.00
2	1/4	1/16	49.311524605286	-3.65e-02	0.00	———	
2	1/8	1/64	49.347897768530	-1.24e-04	4.10	———	
2	1/16	1/256	49.348021565420	-4.40e-07	4.07	———	
2	1/32	1/1024	49.348022003783	-1.66e-09	4.02	———	
3	1/4	1/16	49.311750580349	-3.63e-02	0.00	———	
3	1/8	1/64	49.347802761238	-2.19e-04	3.69	———	
3	1/16	1/256	49.348021182216	-8.23e-07	4.03	———	
3	1/32	1/1024	49.348022002296	-3.15e-09	4.01	———	

First, uniform mesh as in Fig 29 is considered. The fine meshes $\mathcal{T}_h$ are of sizes $h = 2^{-j}$ ($j = 4, 6, 8, 10$) and the corresponding coarse meshes $\mathcal{T}_H$ of size $H = \sqrt{h}$. Table 6 lists the numerical results for Algorithm 1. $\|G_h u^{i,\mathrm{A1}} - \nabla u_i\|_{0,\Omega}$ (i = 1) superconverges at rate of $O(h^2)$ which consists with our theoretical analysis. However, $|\lambda^{\mathrm{i,A1}} - \lambda_i|$ (i = 1, 2, 3) ultraconverges at rate of $O(h^4)$ which is better than the results predicted by Theorem 5.8. In particular, it verifies the statement in Remark 5.2.1. Since λ_2 and λ_2 are multiples eigenvalues, the error of

Table 7: Eigenpair errors of Algorithm 2 for Example 1 on Uniform Mesh

i	H	h	$\lambda^{i,\mathrm{A2}}$	$\lambda^{i,\mathrm{A2}} - \lambda_i$	*Order*	$\|\nabla u^{i,\mathrm{A2}} - \nabla u_i\|_{0,\Omega}$	*Order*
1	1/4	1/16	19.740140941323	9.32e-04		3.344371e-02	
1	1/8	1/64	19.739212357340	3.56e-06	4.02	2.076378e-03	2.00
1	1/16	1/256	19.739208816236	1.41e-08	3.99	1.308168e-04	1.99
1	1/32	1/1024	19.739208802235	5.59e-11	3.99	8.198527e-06	2.00
2	1/4	1/16	49.399143348018	5.11e-02	0.00	———	
2	1/8	1/64	49.348217238157	1.95e-04	4.02	———	
2	1/16	1/256	49.348022827362	8.22e-07	3.95	———	
2	1/32	1/1024	49.348022008741	3.29e-09	3.98	———	
3	1/4	1/16	49.573605264596	2.26e-01	0.00	———	
3	1/8	1/64	49.348559514553	5.38e-04	4.36	———	
3	1/16	1/256	49.348024046492	2.04e-06	4.02	———	
3	1/32	1/1024	49.348022013418	7.97e-09	4.00	———	

Table 8: Eigenpair errors of shift-inverse Two-grid scheme for Example 1 on Uniform Mesh

i	H	h	$\lambda^{i,\mathrm{TG}}$	$\lambda^{i,\mathrm{TG}} - \lambda_i$	*Order*	$\|\nabla u^{i,\mathrm{TG}} - \nabla u_i\|_{0,\Omega}$	*Order*
1	1/4	1/16	19.930259632276	1.91e-01		4.375101e-01	
1	1/8	1/64	19.751103117985	1.19e-02	2.00	1.090672e-01	1.00
1	1/16	1/256	19.739951989101	7.43e-04	2.00	2.726155e-02	1.00
1	1/32	1/1024	19.739255250511	4.64e-05	2.00	6.815303e-03	1.00
2	1/4	1/16	50.199210624678	8.51e-01	0.00	———	
2	1/8	1/64	49.399315353599	5.13e-02	2.03	———	
2	1/16	1/256	49.351217793553	3.20e-03	2.00	———	
2	1/32	1/1024	49.348221696982	2.00e-04	2.00	———	
3	1/4	1/16	50.779973345337	1.43e+00	0.00	———	
3	1/8	1/64	49.428220994371	8.02e-02	2.08	———	
3	1/16	1/256	49.353003975409	4.98e-03	2.00	———	
3	1/32	1/1024	49.348333256327	3.11e-04	2.00	———	

eigenfunctions approximation are not available and it is represented by "−" in Tables 6-12. One important thing we want to point out is that we observe numerically that λ_{A1} obtained by Algorithm 1 approximates the exact eigenvalue from below; see column 4 in Table 6. Similar phenomenon was observed in [44] where they use a local high-order interpolation recovery. We want to remark that lower bound of eigenvalue is very important in practice and there are many efforts for obtaining eigenvalue approximation from below. The readers are referred to [6, 70, 104, 105] for other ways to approximate eigenvalue from below. In Table 7, we report the numerical result of Algorithm 2. As expected, $O(h^4)$ convergence of eigenvalue approximation and $O(h^2)$ convergence of eigenfunction approximation are observed which validate our Theorem 5.9. The shift-inverse power method based two-grid scheme in [103, 55] is then considered, the result being displayed in Table 8. $\lambda^{i,\mathrm{TG}}$ approximates λ_i (i = 1, 2, 3) at a rate $O(h^2)$ and $\|u^{i,\mathrm{TG}} - u_i\|_{a,\Omega}$ (i=1) converges at a rate of $O(h)$.

Comparing Tables 6 to 8, huge advantages of Algorithm 1 and 2 are demonstrated. For instance, on the fine grid with size $h = 1/1024$ and corresponding coarse grid with size $H = 1/32$, the approximate first eigenvalues produced by Algorithm 1 and 2 are exact up to 10 digits while one can only trust the first five digits of the first eigenvalue generated by the two-grid scheme in [103, 55].

Table 9: Comparison of Three Algorithms for Example 1 on Uniform mesh

i	H	h	i, λ^{A1}	$\lambda^{\mathrm{i,A1}} - \lambda_i$	$\lambda^{i,\mathrm{A2}}$	$\lambda^{i,\mathrm{A2}} - \lambda_i$	$\lambda^{i,\mathrm{TG}}$	$\lambda^{i,\mathrm{TG}} - \lambda_i$
1	1/2	1/16	20.1083669	3.69e-01	20.2080796	4.69e-01	20.3504780	6.11e-01
1	1/4	1/256	19.7398503	6.41e-04	19.7398588	6.50e-04	19.7406011	1.39e-03

Then we consider the case $H = O(\sqrt[4]{h})$ for the first eigenvalue. We use the fine meshes of mesh size $h = 2^{-j}$ with $j = 4, 8$ and corresponding coarse meshes satisfying $H = \sqrt[4]{h}$. The numerical results are shown in Table 9. We can see that the two proposed Algorithms give better approximate eigenvalues. Thus Algorithm 1 and 2 outperforms the two-grid scheme even in the case $H = \sqrt[4]{h}$. One interesting thing that we would like to mention is that $\lambda^{i,\mathrm{A1}}$ approximates λ_i from above in this case, see column 4 in Table 9.

Table 10: Eigenpair errors of Algorithm 1 for Example 1 on Delaunay Mesh

i	H	h	$\lambda^{i,\mathrm{A1}}$	$\lambda^{i,\mathrm{A1}} - \lambda_i$	*Order*	$\|G_h u^{i,\mathrm{A1}} - \nabla u_i\|_{0,\Omega}$	*Order*
1	31	385	19.735647110619	-3.56e-03		5.338236e-02	
1	105	5761	19.739198229599	-1.06e-05	2.15	2.835582e-03	1.08
1	385	90625	19.739208765246	-3.69e-08	2.05	1.686396e-04	1.02
1	1473	1443841	19.739208802041	-1.38e-10	2.02	1.049196e-05	1.00
2	31	385	49.307472112236	-4.05e-02	0.00	————	
2	105	5761	49.347888708818	-1.33e-04	2.11	————	
2	385	90625	49.348021524994	-4.80e-07	2.04	————	
2	1473	1443841	49.348022003630	-1.82e-09	2.01	————	
3	31	385	49.301142920140	-4.69e-02	0.00	————	
3	105	5761	49.347856273486	-1.66e-04	2.09	————	
3	385	90625	49.348021393237	-6.12e-07	2.03	————	
3	1473	1443841	49.348022003123	-2.32e-09	2.01	————	

Table 11: Eigenpair errors of Algorithm 2 for Example 1 on Delaunay Mesh

i	H	h	$\lambda^{i,\mathrm{A2}}$	$\lambda^{i,\mathrm{A2}}-\lambda_i$	*Order*	$\|\nabla u^{i,\mathrm{A2}}-\nabla u_i\|_{0,\Omega}$	*Order*
1	31	385	19.739293668773	8.49e-05		9.258930e-03	
1	105	5761	19.739209125443	3.23e-07	2.06	5.705799e-04	1.03
1	385	90625	19.739208803434	1.26e-09	2.01	3.555028e-05	1.01
1	1473	1443841	19.739208802184	5.33e-12	1.97	2.220103e-06	1.00
2	31	385	49.350648806465	2.63e-03	0.00	———	
2	105	5761	49.348029138391	7.13e-06	2.18	———	
2	385	90625	49.348022031328	2.59e-08	2.04	———	
2	1473	1443841	49.348022005547	1.00e-10	2.01	———	
3	31	385	49.351570779092	3.55e-03	0.00	———	
3	105	5761	49.348029733509	7.73e-06	2.27	———	
3	385	90625	49.348022033250	2.78e-08	2.04	———	
3	1473	1443841	49.348022005554	1.07e-10	2.01	———	

Table 12: Eigenpair errors of shift-inverse Two-grid scheme for Example 1 on Delaunay Mesh

i	H	h	$\lambda^{i,\mathrm{TG}}$	$\lambda^{i,\mathrm{TG}}-\lambda_i$	*Order*	$\|\nabla u^{i,\mathrm{TG}}-\nabla u_i\|_{0,\Omega}$	*Order*
1	31	385	19.821235920927	8.20e-02		2.865766e-01	
1	105	5761	19.744334806708	5.13e-03	1.02	7.159881e-02	0.51
1	385	90625	19.739529185236	3.20e-04	1.01	1.789929e-02	0.50
1	1473	1443841	19.739228826191	2.00e-05	1.00	4.474820e-03	0.50
2	31	385	49.828430094852	4.80e-01	0.00	———	
2	105	5761	49.377951127988	2.99e-02	1.03	———	
2	385	90625	49.349892261888	1.87e-03	1.01	———	
2	1473	1443841	49.348138895061	1.17e-04	1.00	———	
3	31	385	49.893495693695	5.45e-01	0.00	———	
3	105	5761	49.381970792689	3.39e-02	1.03	———	
3	385	90625	49.350143791388	2.12e-03	1.01	———	
3	1473	1443841	49.348154618353	1.33e-04	1.00	———	

Now, we turn to unstructured meshes. First we generate a coarse mesh $\mathcal{T}_H$ and repeat regular refinement on $\mathcal{T}_H$ until $H = O(\sqrt{h})$ to get the corresponding fine mesh $\mathcal{T}_h$. The first level coarse mesh is generated by EasyMesh [84] and the other three level coarse mesh are generated by regular refinement. The numerical results are provided in Tables 10 to 12. Note that N_H and N_h denote the number of vertices on coarse mesh $\mathcal{T}_H$ and fine mesh $\mathcal{T}_h$, respectively. Concerning the convergence of eigenvalue, Algorithm 1 and 2 ultraconverge at rate $O(h^4)$ while the two-grid scheme converges at rate $O(h^2)$. Note that in Tables 5.5–5.7, $N_H \approx H^{-2}$ and $N_h \approx h^{-2}$. Therefore, convergent rates for H and h "double" the rates for N_H and N_h, respectively. As for eigenfunction, $\|G_h u^{i,\mathrm{A1}} - \nabla u_i\|_{0,\Omega}$ and $\|\nabla u^{i,\mathrm{A2}} - \nabla u_i\|_{0,\Omega}$ are about $O(h^2)$ while $\|\nabla u^{\mathrm{i,TG}} - \nabla u_i\|_{0,\Omega} \approx O(h)$.

Example 5.2. In the previous example, the eigenfunctions u are analytic. Here we consider Laplace eigenvalue value problem on the L-shaped domain $\Omega = (-1,1)\times(-1,1)/[0,1)\times(-1,0]$. The first eigenfunction has a singularity at the origin. To capture this singularity, multilevel adaptive algorithms 3 and 4 are used with $\theta = 0.4$. Since the first exact eigenvalue is not available, we choose an approximation $\lambda = 9.6397238440219$ obtained by Betcke and Trefethen in [14], which is correct up to 14 digits.

Fig 31 shows the initial uniform mesh while Fig 32 is the mesh after 18 adaptive iterations. Fig 33 reports numerical results of the first eigenvalue approximation. It indicates clearly $\bar{\lambda}_{\mathrm{A3}}$ and $\bar{\lambda}_{\mathrm{A4}}$ approximate λ at a rate of $O(N^{-1})$ while λ_{A3} and λ_{A4} approximate λ at a rate of $O(N^{-2})$. The numerical results for Algorithms 3 and 4 are almost the same. Furthermore, we notice that λ_{A3} and λ_{A4} approximate the exact eigenvalue from below. It is well known that $\bar{\lambda}_{\mathrm{A3}}$ and $\bar{\lambda}_{\mathrm{A4}}$ are upper bounds for the exact eigenvalue. In actual computation, we use $\bar{\lambda}_{\mathrm{A3}} - \lambda_{\mathrm{A3}} \leq \epsilon$ as stop criteria for adaptive Algorithm 3 where ϵ is the given tolerance. A similar procedure is applied to Algorithm 4.

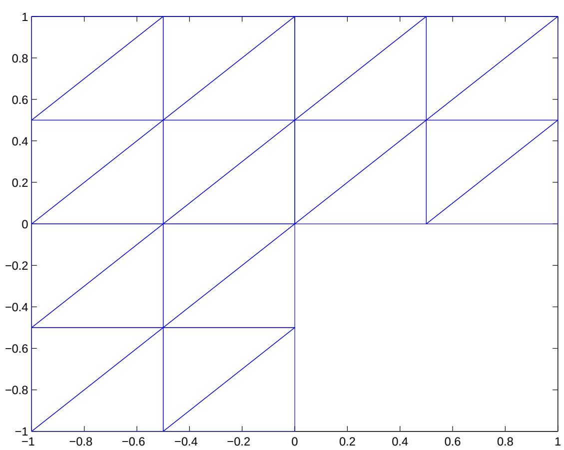

Figure 31: Initial Mesh for Example 5.2

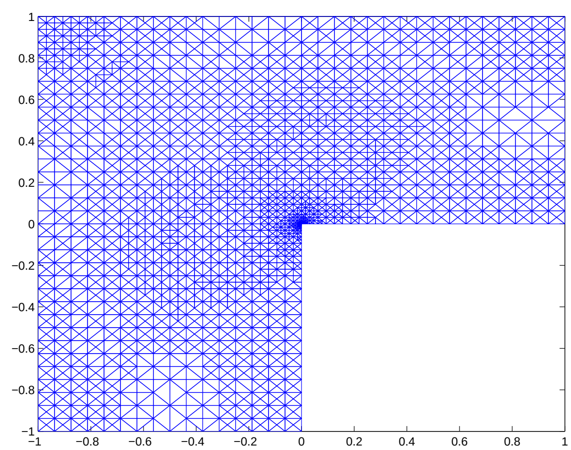

Figure 32: Adaptive Mesh for Example 5.2

In the context of adaptive finite element method for boundary value problems, the ef-

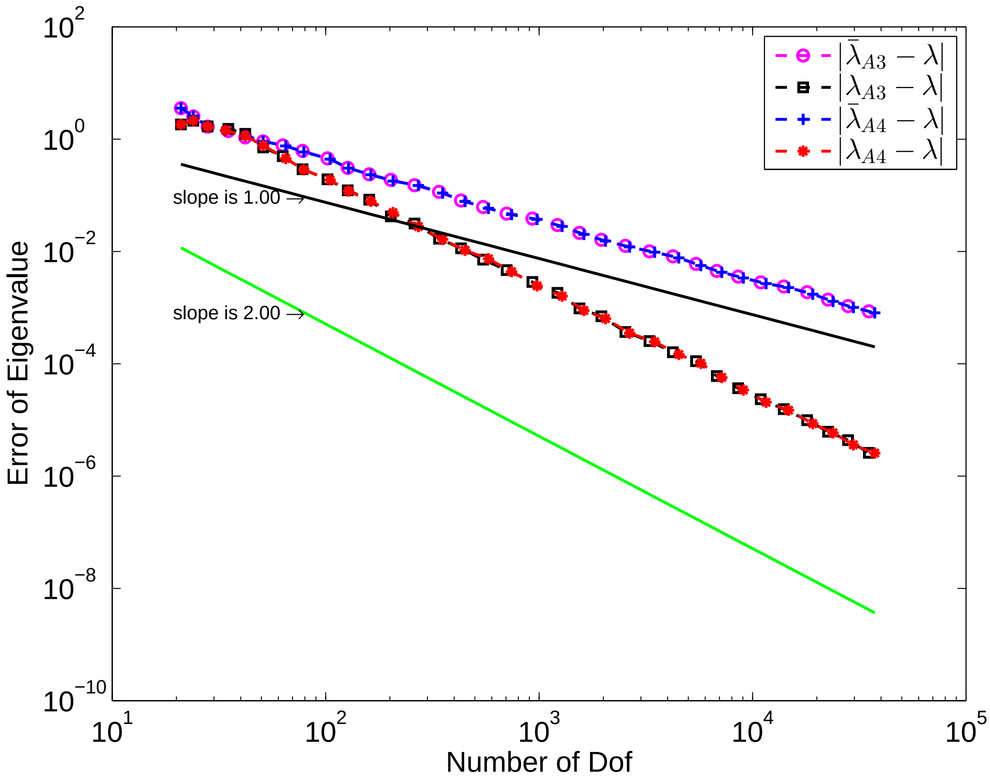

Figure 33: Eigenvalue Approximation Error for Example 5.2

fectivity index κ is used to measure the quality of an error estimator [4, 11]. For eigenvalue problem, it is better to consider eigenvalue effectivity index insteading of traditional effectivity index in [4, 11]. In the article, we consider a similiar eigenvalue effective index as in [48]

$$\kappa = \frac{\|\mathcal{D}^{\frac{1}{2}} G_h u_h - \mathcal{D}^{\frac{1}{2}} \nabla u_h\|_{0,\Omega}^2}{|\lambda - \lambda_h|}, \tag{5.29}$$

where u_h is either u_{A3} or u_{A4} and λ_h is either λ_{A3} or λ_{A4}. The effectivity index for the two proposed multilevel adaptive algorithms are reported in Figs 34 and 35. We see that κ converges to 1 quickly after the first few iterations, which indicates that the posteriori error estimator (5.26) or (5.27) is asymptotically exact.

Example 5.3. Consider the following harmonic oscillator equation [47], which is a simple

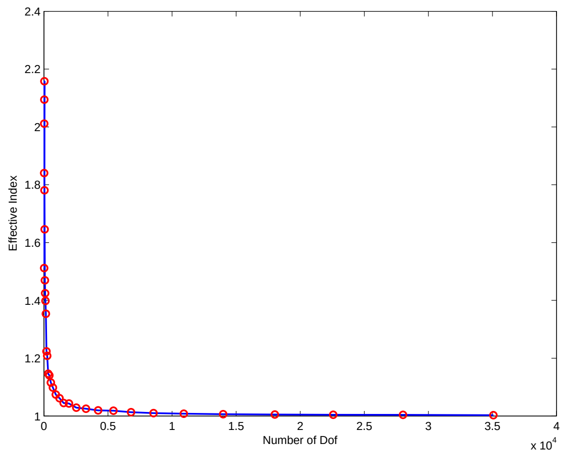

Figure 34: Effective index of Algorithm 3 for Example 5.2

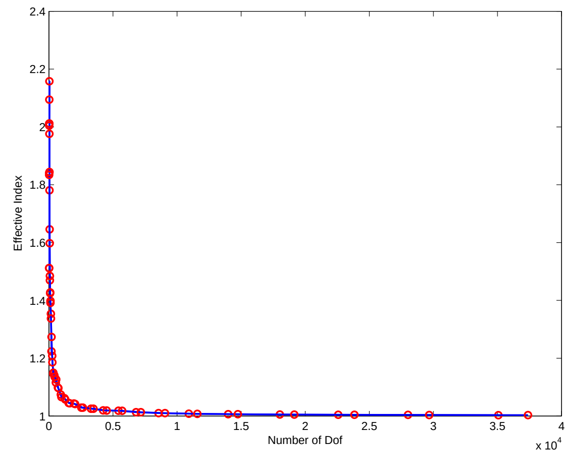

Figure 35: Effective index of Algorithm 4 for Example 5.2

model in quantum mechanics,

$$-\frac{1}{2}\Delta u + \frac{1}{2}|x|^2 u = \lambda u, \quad \text{in } \mathbb{R}^2, \tag{5.30}$$

where $|x| = \sqrt{|x_1|^2 + |x_2|^2}$. The first eigenvalue of (5.30) is $\lambda = 1$ and the corresponding eigenfunction is $u = \gamma e^{-|x|^2/2}$ with any nonzero constant γ.

We solve this eigenvalue problem with $\Omega = (-5, 5) \times (-5, 5)$ and zero boundary condition as in [100]. The initial mesh is shown in Fig 36 and the adaptive mesh after 20 iterations is displayed in Fig 37. The parameter θ is chosen as 0.4. Numerical results are presented in Figs 38 and 39. For eigenvalue approximation, $O(N^{-1})$ convergence rate is observed for $|\bar{\lambda}_{\mathrm{A3}} - \lambda|$ while $O(N^{-2})$ ultraconvergence rate is observed for $|\lambda_{\mathrm{A3}} - \lambda|$. For eigenfunction approximation, $\|\mathcal{D}^{\frac{1}{2}}\nabla u_{\mathrm{A3}} - \mathcal{D}^{\frac{1}{2}}\nabla u\|_{0,\Omega} \approx O(N^{-0.5})$ and $\|\mathcal{D}^{\frac{1}{2}}G_h u_{\mathrm{A3}} - \mathcal{D}^{\frac{1}{2}}\nabla u\|_{0,\Omega} \approx O(N^{-1})$. The numerical result of Algorithm 4 is similar.

Figs 40 and 41 graph the eigenvalue effectivity index for the two proposed multilevel adaptive algorithms. They also indicate that the posteriori error estimator (5.26) or (5.27) is asymptotically exact for problem (5.30).

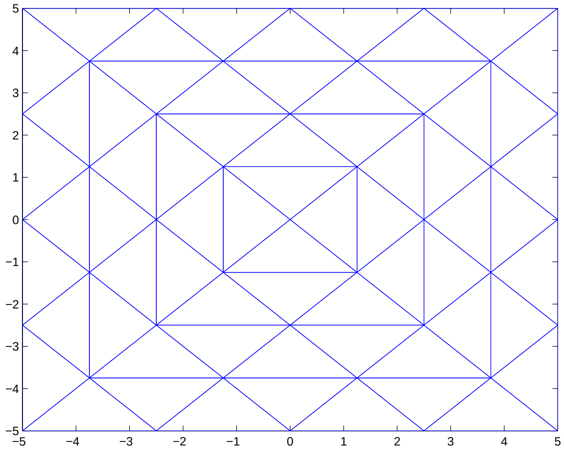

Figure 36: Initial Mesh for Example 5.3

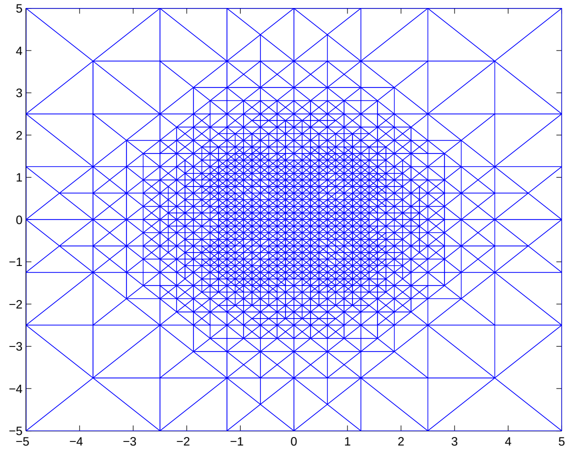

Figure 37: Adaptive Mesh for Example 5.3

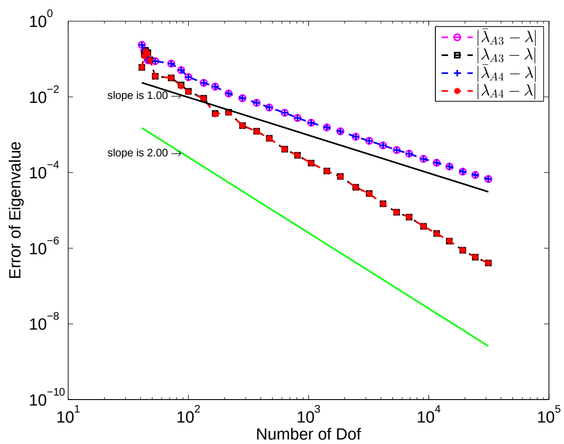

Figure 38: Eigenvalue approximatio Error for Example 5.3

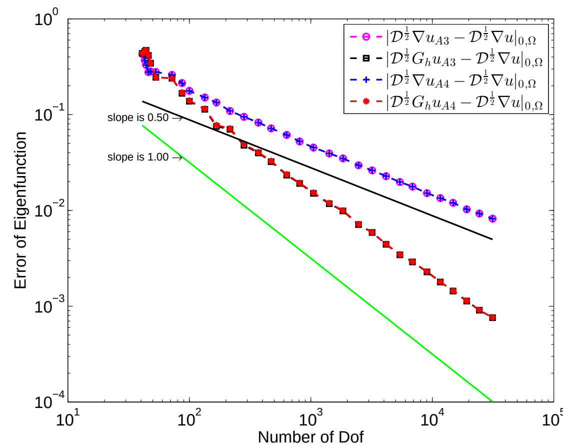

Figure 39: Eigenfunction approximatio Error for Example 5.3

5.5 Conclusion

When eigenfunctions are relatively smooth, two-space method (using higher-order elements in the second stage) is superior to two-grid methods (using the same element at finer grids in the second stage). They have the comparable accuracy. However, at the last stage, the degrees of freedom of the two-space method is much smaller than that of the two-grid method.

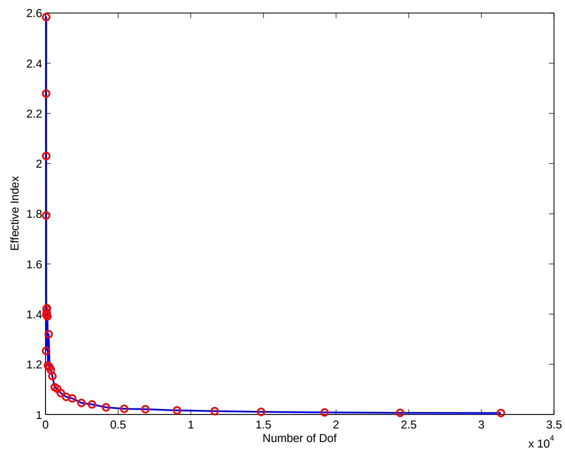

Figure 40: Effective index of Algorithm 3 for Example 5.3

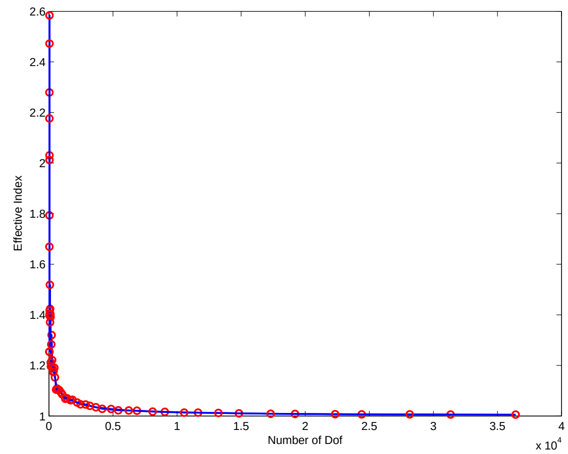

Figure 41: Effective index of Algorithm 4 for Example 5.3

For linear element on structured meshes, using gradient recovery at the last stage achieves similar accuracy as the quadratic element on the same mesh. Therefore, with much reduced cost, the gradient recovery is comparable with the two-stage method on the same mesh.

Algorithms 3 and 4 use recovery type error estimators to adapt the mesh, and have two advantages comparing with the residual based adaptive algorithms. 1) Cost effective. In fact, the recovery based error estimator plays two roles: one is to measure the error, and another is to enhance the eigenvalue approximation. 2) Higher accuracy. Indeed, after recovery enhancement, the approximation error is further reduced.

REFERENCES

[1] R. A. Adams and J. J. F. Fournier, *Sobolev spaces*, Second edition, Elsevier/Academic Press, Amsterdam, 2003.

[2] A. Agouzal and Y. Vassilevski, *On a discrete Hessian recovery for P1 finite elements*, J. Numer. Math., 10 (2002), 1–12.

[3] M. Ainsworth, *Robust a posteriori error estimation for nonconforming finite element approximation*, SIAM J. Numer. Anal., 42 (2005), 2320–2341.

[4] M. Ainsworth and J. T. Oden, *A posteriori error estimation in finite element analysis*, Wiley-Interscience [John Wiley & Sons], New York, 2000.

[5] A. B. Andreev, R. D. Lazarov, and M. R. Racheva, *Postprocessing and higher order convergence of the mixed finite element approximations of biharmonic eigenvalue problems*, J. Comput. Appl. Math., 182 (2005), 333–349.

[6] M. G. Armentano and R. G. Durán, *Asymptotic lower bounds for eigenvalues by nonconforming finite element methods*, Electron. Trans. Numer. Anal., 17 (2004), 93–101.

[7] I. Babuška and J. Osborn, *Finite element-Galerkin approximation of the eigenvalues and eigenvectors of selfadjoint problems*, Math. Comp., 52 (1989), 275–297.

[8] I. Babuška and J. Osborn, *Eigenvalue problems*, Handbook of numerical analysis, Vol. II, 641–787, Handb. Numer. Anal., II, North-Holland, Amsterdam, 1991.

[9] I. Babuška and W. C. Rheinboldt, *Error estimates for adaptive finite element computations*, SIAM J. Numer. Anal., 15 (1978), 736–754.

[10] I. Babuška and W. C. Rheinboldt, *A-posteriori error estimates for the finite element method*, Int. J. Numer. Meth. Engng., 12 (1978), 1597–1615.

[11] I. Babuška and T. Strouboulis, *The finite element method and its reliability*, University Press, New York, 2001.

[12] R. E. Bank and J. Xu, *Asymptotically exact a posteriori error estimators. I. Grids with superconvergence*, SIAM J. Numer. Anal., 41 (2003), 2294–2312.

[13] R. E. Bank, J. Xu, and B. Zheng, *Superconvergent derivative recovery for Lagrange triangular elements of degree p on unstructured grids*, SIAM J. Numer. Anal., 45 (2007), 2032–2046.

[14] T. Betcke, L. N. Trefethen, *Reviving the method of particular solutions*, SIAM Rev., 47 (2005), 469–491.

[15] P. Binev, W. Dahmen, and R. DeVore, *Adaptive finite element methods with convergence rates*, Numer. Math., 97 (2004), 219–268.

[16] D. Boffi, F. Brezzi, and M. Fortin, *Mixed finite element methods and applications*, Springer, Heidelberg, 2013.

[17] D. Braess, *Finite elements. Theory, fast solvers, and applications in elasticity theory*, Third edition, Cambridge University Press, Cambridge, 2007.

[18] J. H. Bramble, *A proof of the inf-sup condition for the Stokes equations on Lipschitz domains*, Math. Models Methods Appl. Sci., 13 (2003), 361–371.

[19] J. H. Bramble and A. H. Schatz, *Higher order local accuracy by averaging in the finite element method*, Math. Comp., 31 (1977), 94–111.

[20] J. H. Brandts, *Superconvergence and a posteriori error estimation for triangular mixed finite elements*, Numer. Math., 68 (1994), 311?324.

[21] S. C. Brenner, *Forty Years of the Crouzeix-Raviart element*, Numer. Methods Partial Differential Eq., 31 (2015), 367–396.

[22] S. C. Brenner, F. Li, and L.-Y. Sung, *A locally divergence-free nonconforming finite element method for the time-harmonic Maxwell equations*, Math. Comp., 76 (2007), 573–595.

[23] S. C. Brenner, F. Li, and L.-Y. Sung, *Nonconforming Maxwell eigensolvers*, J. Sci. Comput., 40 (2009), 51–85.

[24] S. C. Brenner and L.-Y. Sung, *Linear finite element methods for planar linear elasticity*, Math. Comp., 59 (1992), 321–338.

[25] S. C. Brenner and L. R. Scott, *The mathematical theory of finite element methods*, Third edition, Springer, New York, 2008.

[26] F. Brezzi and M. Fortin, *Mixed and hybrid finite element methods*, Springer-Verlag, New York, 1991.

[27] Z. Cai and S. Zhang, *Recovery-based error estimators for interface problems: mixed and nonconforming finite elements*, SIAM J. Numer. Anal. 48 (2010), 30–52.

[28] W. Cao, *Superconvergence analysis of the linear finite element method and a gradient recovery postprocessing on anisotropic meshes*, Math. Comp., 84 (2015), 89–117.

[29] C. Carstensen and S. Bartels, *Each averaging technique yields reliable a posteriori error control in FEM on unstructured grids. I. Low order conforming, nonconforming, and mixed FEM*, Math. Comp., 71 (2002), 945–969.

[30] C. Carstensen and C. Merdon, *Computational survey on a posteriori error estimators for nonconforming finite element methods for the Poisson problem*, J. Comput. Appl. Math., 249 (2013), 74–94.

[31] F. Chatelin, *Spectral approximation of linear operators*, Academic Press, New York, 1983.

[32] C. Chen and Y. Huang, *High accuracy theory of finite element methods*(Chinese), Hunan Science Press, Hunan, China, 1995.

[33] Z. Chen and H. Wu, *Selected Topics in Finite Element Methods*, Science Press, Beijing, 2010.

[34] C.-S Chien and B.-W Jeng, *A two-grid discretization scheme for semilinear elliptic eigenvalue problems*, SIAM J. Sci. Comput., 27 (2006), 1287–1304.

[35] P. G. Ciarlet, *The finite element method for elliptic problems*, North-Holland, Amsterdam-New York-Oxford, 1978.

[36] V. Girault and P.-A. Raviart, *Finite element methods for Navier-Stokes equations*, Springer-Verlag, Berlin, 1986.

[37] M. Crouzeix, and P.-A. Raviart, *Conforming and nonconforming finite element methods for solving the stationary Stokes equations. I.*, Rev. Francaise Automat. Informat. Recherche Opérationnelle Sér. Rouge, 7 (1973), 33–75.

[38] W. Dörfler, *A convergent adaptive algorithm for Poisson's equation*, SIAM J. Numer. Anal., 33 (1996), 1106–1124.

[39] W. Dörfler and M. Ainsworth, *Reliable a posteriori error control for nonconformal finite element approximation of Stokes flow*, Math. Comp., 74 (2005), 1599–1619.

[40] R. G. Durán, C. Padra and R. Rodríguez, *A posteriori error estimates for the finite element approximation of eigenvalue problems*, Math. Models Methods Appl. Sci., 13 (2003), no. 8, 1219–1229.

[41] H. C. Elman, D. J. Silvester, and A. J. Wathen, *Finite elements and fast iterative solvers: with applications in incompressible fluid dynamics*, Second edition, Oxford University Press, Oxford, 2014.

[42] A. Ern and M. Vohralk, *Four closely related equilibrated flux reconstructions for nonconforming finite elements*, C. R. Math. Acad. Sci. Paris, 351 (2013), 77–80.

[43] R. S. Falk, *Nonconforming finite element methods for the equations of linear elasticity*, Math. Comp., 57 (1991), 529–550.

[44] J. Fang, X. Gao, and A. Zhou, *A finite element recovery approach to eigenvalue approximations with applications to electronic structure calculations*, J. Sci. Comput., 55 (2013), 432–454.

[45] X. Gan and J. E. Akin, *Superconvergent second order derivative recovery technique and its application in a nonlocal damage mechanics model*, Finite Elements in Analysis and Design, 35 (2014), 118-127.

[46] D. S. Grebenkov and B.-T Nguyen, *Geometrical structure of Laplacian eigenfunctions*, SIAM Rev., 55 (2013), 601–667.

[47] W. Greiner, *Quantum Mechanics*, 3rd edition, Springer, Berlin, 1994.

[48] S. Giani, L Grubišić, and J. Ovall, *Benchmark results for testing adaptive finite element eigenvalue procedures*, Appl. Numer. Math., 62 (2012), 121–140.

[49] H. Guo and Z. Zhang, *Gradient Recovery for the Crouzeix-Raviart Element*, accepted by J. Sci. Comput.

[50] H. Guo, Z. Zhang, and R. Zhao, *Hessian Recovery for Finite Element Methods*, arXiv:1406.3108, submitted.

[51] H. Guo, Z. Zhang and R. Zhao, *Superconvergent two-grid schemes for Elliptic eigenvalue problems*, arXiv:1405.4641, submitted.

[52] B. Heimsund, X. Tai, and J. Wang, *Superconvergence for the gradient of finite element approximations by L2 projections*, SIAM J. Numer. Anal., 40 (2002), 1263–1280.

[53] R. H. W. Hoppe, H. Wu, and Z. Zhang, *Adaptive finite element methods for the Laplace eigenvalue problem*, J. Numer. Math., 18 (2010), 281–302.

[54] J. Hu and R. Ma, *Superconvergence of both the Crouzeix-Raviart and Morley elements* , arXiv:1408.1286.

[55] X. Hu, and X. Cheng, *Acceleration of a two-grid method for eigenvalue problems*, Math. Comp., 80 (2011), 1287–1301.

[56] C. Huang and Z. Zhang, *Polynomial preserving recovery for quadratic elements on anisotropic meshes*, Numer. Methods Partial Differential Equations 28 (2012), 966–983.

[57] Y. Huang and J. Xu, *Superconvergence of quadratic finite elements on mildly structured grids*, Math. Comp., 77 (2008), 1253–1268.

[58] Y Huang and N. Yi, *The superconvergent cluster recovery method*, J. Sci. Comput., 44 (2010), 301–322.

[59] W. Huang and R. D. Russell, *Adaptive moving mesh methods*, Springer, New York, 2011.

[60] L. Kamenski, *Anisotropic Mesh Adaptation Based on Hessian Recovery and A Posteriori Error Estimates*, Dissertation, Technische Universität Darmstadt, 2009.

[61] L. Kamenski and W. Huang, *How a nonconvergent recovered Hessian works in mesh adaptation*, SIAM J. Numer. Anal., 52 (2014), 692–1708.

[62] K. Kolman, *A two-level method for nonsymmetric eigenvalue problems*, Acta Math. Appl. Sin. Engl. Ser., 21 (2005), 1–12.

[63] M. Křížek and P. Neittaanmäki, *Superconvergence phenomenon in the finite element method arising from averaging gradients*, Numer. Math., 45 (1984), 105–116.

[64] A. M. Lakhany and J. R. Whiteman, *Superconvergent recovery operators: derivative recovery techniques*, Finite element methods, 195–215, Lecture Notes in Pure and Appl. Math., 196, Dekker, New York, 1998.

[65] O. Lakkis and T. Pryer, *A finite element method for second order nonvariational elliptic problems* SIAM J. Sci. Comput., 33 (2011), 786–801.

[66] O. Lakkis and T. Pryer, *A finite element method for nonlinear elliptic problems*, SIAM J. Sci. Comput., 35 (2013), A2025–A2045.

[67] M. G. Larson, *A posteriori and a priori error analysis for finite element approximations of self-adjoint elliptic eigenvalue problems*, SIAM J. Numer. Anal., 38 (2000), 608–625.

[68] H. Li and Y. Yang, *The adaptive finite element method based on multi-scale discretizations for eigenvalue problems*, Comput. Math. Appl., 65 (2013), 1086–1102.

[69] M. Li, S. Mao, and Z. Zhang, *Superconvergence analysis of nonconforming Crouzeix-Raviart finite element method*, preprint.

[70] Q. Lin, H. Xie, and J. Xu, *Lower bounds of the discretization error for piecewise polynomials*, Math. Comp., 83 (2014), 1–13.

[71] Q. Lin and N. Yan, *The Construction and Analysis of High Efficiency Finite Elements*, Hebei University Press, Hebei, China, 1996.

[72] F. Liu, M. Stynes, and A. Zhou, *Postprocessed two-scale finite element discretizations, Part I*, SIAM J. Numer. Anal., 49 (2011), 1947–1971.

[73] H. Liu and N. Yan, *Enhancing finite element approximation for eigenvalue problems by projection method*, Comput. Methods Appl. Mech. Engrg., 233-236 (2012), 81–91.

[74] R. Luce, and B. I. Wohlmuth, *A local a posteriori error estimator based on equilibrated fluxes*, SIAM J. Numer. Anal., 42 (2004), 1394–1414.

[75] D. Mao, L. Shen, and A. Zhou, Aihui, *Adaptive finite element algorithms for eigenvalue problems based on local averaging type a posteriori error estimates*, Adv. Comput. Math., 25 (2006), 135–160.

[76] L. D. Marini, *An inexpensive method for the evaluation of the solution of the lowest order Raviart-Thomas mixed method*, SIAM J. Numer. Anal., 22 (1985), 493–496.

[77] V. Mehrmann and A. Miedlar, *Adaptive computation of smallest eigenvalues of self-adjoint elliptic partial differential equations*, Numer. Linear Algebra Appl., 18 (2011), 387–409.

[78] L. Meng and Z. Zhang, *The ultraconvergence of eigenvalues for bi-quadratic finite elements*, J. Comput. Math., 30 (2012), 555–564.

[79] A. Naga and Z. Zhang, *A posteriori error estimates based on the polynomial preserving recovery*, SIAM J. Numer. Anal., 42 (2004), 1780–1800.

[80] A. Naga and Z. Zhang, *The polynomial-preserving recovery for higher order finite element methods in 2D and 3D*, Discrete Contin. Dyn. Syst. Ser. B, 5 (2005), 769–798.

[81] A. Naga and Z. Zhang, *Function value recovery and its application in eigenvalue problems*, SIAM J. Numer. Anal., 50 (2012), 272–286.

[82] A. Naga, Z. Zhang, and A. Zhou, *Enhancing eigenvalue approximation by gradient recovery*, SIAM J. Sci. Comput., 28 (2006), 1289–1300.

[83] M. Neilan, Michael, *Finite element methods for fully nonlinear second order PDEs based on a discrete Hessian with applications to the Monge-Ampre equation*, J. Comput. Appl. Math., 263 (2014), 351–369.

[84] B. Niceno, *EasyMesh: A Two-Dimensional Quality Mesh Generator*, `http://www-dinma.univ.trieste.it/nirftc/research/easymesh/easymesh.html`.

[85] J. A. Nitsche and A. H. Schatz, *Interior estimates for Ritz-Galerkin methods*, Math. Comp., 28 (1974), 937–958.

[86] , R. H. Nochetto, K. G. Siebert, and A. Veeser, *Theory of adaptive finite element methods: an introduction*, Multiscale, nonlinear and adaptive approximation, 409–542, Springer, Berlin, 2009.

[87] , R. H. Nochetto, A. Veeser, *Primer of adaptive finite element methods*, Multiscale and adaptivity: modeling, numerics and applications, 125–225, Springer, Heidelberg, 2012.

[88] J. Ovall, *Function, gradient, and Hessian recovery using quadratic edge-bump functions*, SIAM J. Numer. Anal., 45 (2007), 1064–1080.

[89] M. Picasso, F. Alauzet, H. Borouchaki, P.-L. George, *A numerical study of some Hessian recovery techniques on isotropic and anisotropic meshes*, SIAM J. Sci. Comput., 33 (2011), 1058–1076.

[90] B. Pouliot, M. Fortin, A. Fortin, É Chamberland, *On a new edge-based gradient recovery technique*, Internat. J. Numer. Methods Engrg., 93 (2013), 52–65.

[91] M. R. Racheva and A. B. Andreev, *Superconvergence postprocessing for eigenvalues*, Comput. Methods Appl. Math., 2 (2002), 171–185.

[92] G. Strang and G. Fix, *An analysis of the finite element method*, Second edition, Wellesley-Cambridge Press, Wellesley, 2008.

[93] L. Shen and A. Zhou, *A defect correction scheme for finite element eigenvalues with applications to quantum chemistry*, SIAM J. Sci. Comput., 28 (2006), 321–338.

[94] M.-G. Vallet, C.-M. Manole, J. Dompierre, S. Dufour, and F. Guibault, *Numerical comparison of some Hessian recovery techniques*, Internat. J. Numer. Methods Engrg., 72 (2007), 987–1007.

[95] R. Verfürth, *A review of a posteriori error estimation and adaptive mesh-refinement techniques*, Wiley and Teubner, New York, 1996.

[96] R. Verfürth, *A posteriori error estimation techniques for finite element methods*, Oxford University Press, Oxford, 2013.

[97] L. B. Wahlbin, *Superconvergence in Galerkin finite element methods*, 1605. Springer-Verlag, Berlin, 1995.

[98] H. Wu and Z. Zhang, *Can we have superconvergent gradient recovery under adaptive meshes?*, SIAM J. Numer. Anal., 45 (2007), 1701–1722.

[99] H. Wu and Z. Zhang, *Enhancing eigenvalue approximation by gradient recovery on adaptive meshes*, IMA J. Numer. Anal. 29 (2009), 1008–1022.

[100] H. Xie, *A multilevel correction type of adaptive finite element method for eigenvalue problems*, arXiv1201.2308v1 [math.NA].

[101] J. Xu and Z. Zhang, *Analysis of recovery type a posteriori error estimators for mildly structured grids*, Math. Comp., 73 (2004), 1139–1152.

[102] J. Xu and A. Zhou, *A two-grid discretization scheme for eigenvalue problems*, Math. Comp., 70 (2001), 17–25.

[103] Y. Yang and H. Bi, *Two-grid finite element discretization schemes based on shifted-inverse power method for elliptic eigenvalue problems*, SIAM J. Numer. Anal., 49 (2011), 1602–1624.

[104] Y. Yang, Z. Zhang, and F. Lin, *Eigenvalue approximation from below using non-conforming finite elements*, Sci. China Math. 53 (2010), 137–150.

[105] Z. Zhang, Y. Yang, and Z. Chen, *Eigenvalue approximation from below by Wilson's element* (Chinese), Math. Numer. Sin., 29 (2007), 319–321.

[106] Z. Zhang, *Polynomial preserving recovery for meshes from Delaunay triangulation or with high aspect ratio*, Numer. Methods Partial Differential Equations, 24 (2008), 960–971.

[107] Z. Zhang and A. Naga, *A new finite element gradient recovery method: superconvergence property*, SIAM J. Sci. Comput., 26 (2005), 192–1213.

[108] J. Zhou, X. Hu, L. Zhong, S. Shu, and L. Chen, *Two-grid methods for Maxwell eigenvalue problems*, SIAM J. Numer. Anal., 52 (2014), 2027–2047.

[109] Q. Zhu and Q. Lin, *Superconvergence theory of the finite element method* (Chinese), Hunan Science Press, Hunan, China, 1989.

[110] J. Z. Zhu and O. C. Zienkiewicz, *Superconvergence recovery technique and a posteriori error estimators*, Internat. J. Numer. Methods Engrg., 30 (1990), 1321–1339.

[111] O. C. Zienkiewicz and J. Z. Zhu, *The superconvergent patch recovery and a posteriori error estimates. I. The recovery technique*, Internat. J. Numer. Methods Engrg., 33 (1992), 1331–1364.

[112] O. C. Zienkiewicz and J. Z. Zhu, *The superconvergent patch recovery and a posteriori error estimates. II. Error estimates and adaptivity*, Internat. J. Numer. Methods Engrg., 33 (1992), 1365–1382.

ABSTRACT

RECOVERY TECHNIQUES FOR FINITE ELEMENT METHODS AND THEIR APPLICATIONS

by

HAILONG GUO

August 2015

Advisor: Dr. Zhimin Zhang

Major: Mathematics

Degree: Doctor of Philosophy

Recovery techniques are important post-processing methods to obtain improved approximate solutions from primary data with reasonable cost. The practical usage of recovery techniques is not only to improve the quality of approximation, but also to provide an asymptotically exact posteriori error estimators for adaptive methods. This dissertation presents recovery techniques for nonconforming finite element methods and high order derivative as well as applications of gradient recovery.

Our first target is to develop a systematic gradient recovery technique for Crouzeix-Raviart element. The proposed method uses finite element solution to build a better approximation of the exact gradient based on local least square fittings. Due to polynomial preserving property of least square fitting, it is easy to show that the new proposed method preserves quadratic polynomials. In addition, the proposed gradient recovery is linearly bounded. Numerical tests indicate the recovered gradient is superconvergent to the exact gradient for both second order elliptic equation and Stokes equation. The gradient recovery technique can be used in a posteriori error estimates for Crouzeix-Raviart element, which is relatively simple to implement and problem independent.

Our second target is to propose and analyze a new effective Hessian recovery for continuous finite element of arbitrary order. The proposed Hessian recovery is based on polynomial preserving recovery. The proposed method preserves polynomials of degree $(k+1)$ on general unstructured meshes and polynomials of degree $(k+2)$ on translation invariant meshes. Based on it polynomial preserving property, we can able to prove superconvergence of the proposed method on mildly structured meshes. In addition, we establish the ultraconvergence result for the new Hessian recovery technique on translation invariant finite element space of arbitrary order.

Our third target is to demonstrate application of gradient recovery in eigenvalue computation. We propose two superconvergent two-grid methods for elliptic eigenvalue problems by taking advantage of two-gird method, two-space method, shifted-inverse power method, and gradient recovery enhancement. Theoretical and numerical results reveal that the proposed methods provide superconvergent eigenfunction approximation and ultraconvergent eigenvalue approximation. In addition, two multilevel adaptive methods based recovery type a posterior error estimate are proposed.

AUTOBIOGRAPHICAL STATEMENT

Hailong Guo

Education

- Ph.D. in Mathematics, 2015
  Wayne State University, Detroit, Michigan, USA
- M.A. in Statistics, 2014
  Wayne State University, Detroit, Michigan, USA
- M.S. in Computational Mathematics, 2010
  Peking University, China
- B.S. in Applied Mathematics, 2007
  Hunan Normal University, China

Selected List of Awards and Scholarships

1. The Maurich J. Zelonka Endowed Mathematics Scholarship, Department of Mathematics, Wayne State University, 2013.
2. Dr. Paul A. Catlin Award for outstanding achievement in the Master's Program, Wayne State University, 2014.
3. The Karl W. and Helen L. Folley Endowed Mathematics Scholarship, Department of Mathematics, Wayne State University, 2015.
4. Graduate Student Traveling Award, Department of Mathematics, Wayne State University, 2015.
5. The Alfred L. Nelson Award for outstanding achievement in the Ph.D. Program, Department of Mathematics, Wayne State University, 2015.

Selected List of Publications

1. C. Huang, H. Guo, and Z. Zhang, A spectral collocation method for eigenvalue problems of compact integral operators, J. Integral Equations Appl., 25(2013), 79-101.
2. H. Guo, C. Huang, and Z. Zhang, Superconvergece of conforming finite element for fourth order singularly perturbed problems of reaction diffusion type in 1D, Numer. Methods Partial Differential Equations, 30(2014), 550-566.
3. H. Guo and Z. Zhang, Gradient Recovery for the Crouzeix-Raviart Element, accepted by J. Sci. Comput.
4. H. Guo, Z. Zhang, and R. Zhao, Hessian Recovery for Finite Element Methods, arXiv: 1406.3108, submitted.
5. H. Guo, Z. Zhang and R. Zhao, Superconvergent two-grid schemes for Elliptic eigenvalue problems, arXiv:1405.4641, submitted.